SIMULATING EVOLUTION OF POROELASTICITY AND DEFORMATION OF GREEN RIVER OIL SHALE UNDER *IN SITU* PYROLYSIS

by

Walter Joseph Glauser

A thesis submitted to the faculty of
The University of Utah
in partial fulfillment of the requirements for the degree of

Master of Science

Department of Chemical Engineering

The University of Utah

August 2016

The University of Utah Graduate School

STATEMENT OF THESIS APPROVAL

The thesis of Walter Joseph Glauser

has been approved by the following supervisory committee members:

John David McLennan	, Chair	September 11, 2015 Date Approved
Milind Deo	, Member	September 10, 2015 Date Approved
Geoffrey Silcox	, Member	September 10, 2015 Date Approved

and by Milind Deo , Chair of

the Department of Chemical Engineering

and by David B. Kieda, Dean of The Graduate School.

ABSTRACT

Simulating *in situ* pyrolysis requires an understanding of rock mechanics, reservoir engineering, thermodynamics, heat transfer, reaction kinetics, and mass transfer. In order to account for the possibility of subsidence, a model of poroelasticity is also required for oil shale. Poroelastic models couple deformation of porous media with fluid flow in and out of pores, while accounting for stress-response of the fluid. When pyrolyzed, kerogen in oil shale decomposes into lighter molecular weight organic compounds, such as bitumen, oil, gas, and char. Pyrolization greatly reduces the mechanical capability of oil shale, while producing oil and gas. A simulation which accounts for the mechanical transformation and deformation of oil shale during *in situ* pyrolysis was implemented using Itasca Consulting Group's FLAC3D™.

While a weakening, increasingly porous rock matrix might be expected to collapse, the compression is counteracted by growing pore fluid pressure. Due to its large residence time, a significant fraction of the oil produced *in situ* is likely to be lost through decomposition. In this simulation, the stresses of pore pressure and confining pressure mostly cancelled each other out. The analysis results may reflect the complexity of the problem more than they shed light on the true nature of *in situ* pyrolysis. In principle, increasing pore pressures could cause fractures to open during pyrolysis, but the simulation is not equipped to represent flow from zone to zone via fracture. Should fracturing be predicted, a module has been developed to relieve excess pressure by

bleeding fluid into noncommunicated fractures for each zone. Alternatively, if tensile pressure is predicted, and fluid has been stored in the simulated fractures, the module will release fluid back into the geometry, thus preserving mass balance in the system.

For Marian,

TABLE OF CONTENTS

Appendices

LIST OF FIGURES

Figures

LIST OF NOMENCLATURE

A	activity
API	API gravity
CH	hydrogen to carbon ratio (given in subscript)
C_p	bulk heat capacity [$\mathrm{J/(kg \cdot K)}$]
c	cohesion [Pa]
E	Young's modulus of elasticity [Pa]
E_1, E_2	activation energy
F_o	Fourier number of heat transfer
FA	Fisher assay yield [$\mathrm{gal/ton}$]
f_i	fraction of chemical kinetic rate.
f^s	shear failure criterion [Pa]
f^t	tensile failure criterion [Pa]
G_B	shear modulus of bulk system [Pa]
G	shear modulus [Pa]
g_v	fluid volume source/sink term $[\mathrm{m^3/m^3}]$
$\Delta H_{R1}, \Delta H_{R2}$	reaction enthalpy [$\mathrm{kJ/kg}$]
$\hbar$	Planck's constant [6.626×10^{-34} J·s]
h_f	potential failure surface
K_B	bulk modulus [Pa]
k_{Ri}	reaction rate coefficients $[\mathrm{s^{-1}}]$
M	Biot modulus [Pa]
M_g	molecular weight of gas [$\mathrm{kg/mol}$]
N_A	Avogadro's number 6.022×10^{23}
N_ψ	function of dilation angle.
O_c	organic content [Unitless]
P	pore pressure [Pa]
q	flow rate $[\mathrm{kg/m^3}]$
$\vec{q}$	volume average velocity [$\mathrm{m/s}$]
$\overrightarrow{q_w}$	mass average velocity [m/s]
R	gas constant
$R_x( )$	reaction rate of a given species
r	radius from heater well [m] $\left(\sqrt{x^2 + y^2}\right)$
S	saturation
S^C	compressive strength [Pa]
S^T	tensile strength [Pa]
S_x, S_z	stress level.

T	temperature [K]
T_F	temperature [°F]
T_R	temperature [R]
t	time [s]
w_i	mass fraction is species i [kg/kg]
x, y	horizontal coordinates
z	vertical coordinate
α	Biot coefficient
β	thermal coefficient of expansion
γ_g	gas specific gravity
δ_{ij}	Kronecker delta
ϵ_{ij}	strain
τ_{ij}	shear stress component
κ	permeability $[\mathrm{m}^2]$
λ	thermal conductivity $[\mathrm{W}/(\mathrm{m} \cdot \mathrm{K})]$
μ	viscosity $[\mathrm{Pa} \cdot \mathrm{s}]$
ν	Poisson's ratio
ξ	zone extra (software symbol)
ϕ	porosity
$\phi°$	friction angle
ρ	density
$\sigma_1, \sigma_2, \sigma_3$	principle stresses
σ_{ii}	normal stress
σ_i^I	principle stress predicted for plastic deformation.
σ_i^N	net stress
σ_{ux}, σ_{uz}	unconfined compressive strength [Pa]
χ	volume fraction $[\mathrm{m}^3/\mathrm{m}^3]$
ψ	dilation angle

LIST OF SUBSCRIPT NOMENCLATURE

0	initial value
1	oil property
2	gas property
3	coke property
4	kerogen property
5	mineral fraction
B	bulk properties
f	fluid phase
G	geometric mean
H	horizontal
h	heater well property
p	production well property
R	reaction modified property
s	solid phase
V	vertical
w	mass property

ACKNOWLEDGEMENTS

A special thanks to the support of Dr. John McLennan, and to the rest of the staff and faculty at the University of Utah, Department of Chemical Engineering. The author would also like to acknowledge the support of the Department of Energy and the Energy and Geoscience Institute, without which none of this would be possible.

CHAPTER 1

INTRODUCTION

1.1 Background

Pyrolysis in oil shale, literally "heat destruction," is a complex family of endothermic, anaerobic reactions whereby kerogen and bitumen decompose into oil, gas, and coke under raised temperatures. Over geologic time, this phenomenon is responsible for generating most of the world's oil resources [1]. Theoretically, pyrolysis has no minimum temperature to operate, but moderate temperatures are required for these reactions to occur even in geologic timescales.

Oil shale is not shale, and contains very little oil. Green river oil shale is a sedimentary rock consisting of very fine alternating kerogen-rich and -poor laminae. This layering of organic material results in orthotropic properties. Permeability and porosity are very low. When heated to pyrolysis, the kerogen in oil shale produces oil, gas, and coke. Unless it is removed, shale oil can further break down into lighter gases and coke at these elevated temperatures.

Deposits of oil shale exist in many parts of the world. The most abundant resources identified to date occur in the United States in the Green River formation. The Green River formation is found in the Uintah Basin, in Utah; the Green River and Washakie basins, in Wyoming; and the Piceance Creek basin, near White River, Colorado. The

Piceance Creek setting is the most studied of these deposits. The Mahogany zone oil shale from the Green River formation is composed primarily of kerogen, dolomite, calcite, plagioclase, and quartz. Near Rifle Colorado, it is buried approximately 300 m (~1000 ft) below the surface. Estimates on recoverable oil volumes in Piceance Creek vary between 300 and 750 million barrels, depending on the investigator and minimum organic content cut-off [2]. This constitutes approximately two-thirds of the potential petroleum fluids in the Green River Formation. An excellent review of oil shale development history was compiled by Dyni [3].

Numerous *in situ* and *ex situ* production strategies have been reviewed by Crawford et al. [4] While various production strategies have been tried, all essentially involve heating the rock to temperatures in the range of 350-800 °C to generate oil in a commercially acceptable timeframe. *Ex situ* strategies consist of mining oil shale and pyrolyzing it at the surface using retorts. *In situ* strategies heat oil shale while it's still underground and subsequently produce petroleum like a conventional well.

Ex situ methods have proven to be marginally economical in Estonia and China, where oil shale outcrops are easy to mine and other petroleum resources are not easily available [4]. Several pilot mining operations have been attempted in the area of Rifle Colorado [5]. Additionally, the Red Leaf process [6] or open pit mining would allow the largest fraction of oil shale to be recovered, but would require altering the surface landscape and subsequent remediation. Room and pillar mining has also been proposed, but this leaves approximately 45% of the oil shale behind, due to structural requirements for supporting the mine roof [7]. Regardless of the mining method, surface retorting may also manifest a number of environmental problems, such as release of carcinogens into

the atmosphere and spent shale disposal.

To try to avoid many of these problems, numerous *in situ* pilot operations have been attempted [2] but the capital costs are tremendous. In the United States, most pilot facilities, along with their sponsoring organizations, have come and gone with changes in U.S. government policy and fluctuations in the energy market. Groundwater contamination is one of the primary environmental concerns with *in situ* operations.

1.2 Research History

In the United States, oil shale has yet to be proven to be an economic resource. This is due to more significant capital and operating costs than are incurred in conventional or unconventional hydrocarbon exploitation. Almost from the beginning, oil shale has been viewed as a contingency fuel source, rather than a primary one [8]. During World Wars I and II, Europe and the United States both heavily invested in research when it was feared that they could lose access to energy [3]. Another large spike in research correlates to the 1970s' oil crises.

Processing does not end with retorting or pyrolysis. Products that one could theoretically produce from the Green River shale are more appropriate for diesel fuel and jet fuel than naphtha. In addition to pyrolysis, hydrotreating and hydrocracking are necessary for conversion into common gasoline. Currently, most existing refineries are only designed to handle gasoline-type crude. Since the distillates from oil shale lack the variety of structures necessary for good gasoline, current technology would lead to jet fuel, diesel and kerosene. Existing refineries will require extensive renovation to process this resource.

1.3 Research Objectives

The purpose of this study is to explore subsidence or heave potential of oil shale undergoing *in situ* pyrolysis by accounting for changing mechanical properties of the Mahogany zone in the Piceance Creek basin. Subsidence is the local "sinking" of the surface associated with compaction occurring at depth due to removal of fluids. Heave is the local "rising" of the surface associated with expansion at depth, potentially due to an increase in fluid or temperature. There is potential for either compaction or subsidence or both, sequentially or spatially, to occur.

Whether heave or subsidence dominates *in situ* oil shale production depends on the relative rates of fluid generation and drainage. Petroleum fluids are generated *in situ* by pyrolysis, while the reservoir oil shale is converted from a low permeability, low porosity, extremely rigid medium to a porous, permeable and weak formation sensitive to collapse under existing geologic stress regimes. Numerical simulation can provide significant insight into the interplay of mass, energy and momentum during pyrolysis and subsequent drainage of the Mahogany zone. If drainage keeps up with oil-range fluid generation, subsidence may be expected to dominate. Conversely, if drainage is too slow, relative to petroleum fluid generation, gas will dominate and could potentially cause heave. The intent has been to consider the feasibility of *in situ* oil shale pyrolysis, rather than assessing the economics of any particular recovery scheme.

In situ fracturing due to heating is considered a possibility, but it is beyond the scope of this study to explicitly examine it. In FLAC3D™, discontinuities must be assigned to the geometry prior to running the simulation. Also, convergence requirements in the software hinder the implementation of significant permeability gradients.

Porosity, permeability, and pore pressure are generated during pyrolysis of kerogen into oil and gas. Complex changes to fluid and mechanical properties of a pyrolyzing formation could lead to significant subsidence or heave.

In a series reaction scheme, oil is an intermediate product of pyrolysis. A large portion of oil-range fluids may be lost in an *in situ* operation if the oil produced cannot be drained quickly enough. Petroleum fluid quality and production are highly dependent on the relative rates of creation, destruction, and transport of oil and gas in a given volume. All of these are dependent on the heating rate of oil shale. If oil shale is heated quickly, fluid flow may increase, but at a cost to the amount of oil that is finally extracted [1].

To account for the effect of pore fluid on mechanical deformation, an elastic model was combined with a Mohr-Coulomb failure criterion and Biot's linear consolidation model. The overall model is poroelastic because it accounts for rock deforming by considering the response of the bulk system and the pore fluids it contains. Biot's linear model mechanisms whereby pore fluid volume can change in a system, including stress-strain interactions between pores and the bulk material. Additionally, the model captures the distinction between fluid and solid matrix compression, and describes how bulk deformation is affected by fluid drainage. The fluid response to changing stress is affected by changes in pore pressure, while the bulk material response to effective stress changes.

To the author's knowledge, this is the first attempt to apply poroelastic theory to oil shale. A reasonable poroelastic model will determine how much the oil shale swells or collapses under pyrolysis, and may assist in developing an understanding of drainage behavior.

The theory section is divided into physics modules. In each module, the models for each relevant parameter are introduced. Additionally, the strengths and weaknesses of each model are described. Given the paucity of available data and the high cost of developing even pilot scale *in situ* projects, this study intends to shed light on the development of oil shale in the Mahogany zone of the Green River formation using numerical simulation.

Due to the heterogeneous nature of oil shale and other petroleum sources, and the complexity of pyrolysis in general, a universal model of pyrolysis simply does not exist. Most investigators have adapted relatively simple empirical models while capturing one or two pieces of this complex phenomenon. This study followed a similar philosophy.

CHAPTER 2

THEORY

Previous studies have tried to capture many of the phenomena involved in *in situ* pyrolysis with the aid of simulation [9], [10]. Many investigators have tried to determine appropriate models for pyrolysis. A few researchers have attempted to determine the properties of oil shale, and how these change due to pyrolysis. It is appropriate to include changes in porosity and compaction in simulation while including thermal and fluid effects.

To capture all of these effects, a number of theoretical and empirical models were employed in FLAC3D™, a rock-mechanics software package produced by Itasca Consulting Group. The basic capabilities of FLAC3D™ have been supplemented by customized algorithms for the simulation package.

To assist future investigations, the empirical equations used in this simulation are presented in the units provided by their original authors. Completed calculations were then converted into SI units.

This chapter is divided into several sections. The first introduces governing equations for mass balance, energy balance, and methods of handling volume change. Subsequent sections introduce the constitutive models used for rock mechanics and poroelasticity, heat transfer and chemical reactions, explaining the reasons for choosing each model. The software implementation of these models in FLAC3D™ is covered in Appendix A.

2.1 Governing Equations

A complete continuum model of oil shale pyrolysis requires a mass balance, energy balance, volume balance, momentum balance, and constitutive stress-strain relationships.

2.1.1 Mass Balance

If a volume of oil shale is considered small enough to be considered infinitesimal, but still large enough to be considered continuous in poroelastic properties and homogeneous in composition, the mass balance becomes

$$\frac{\partial \rho_B}{\partial t} + \nabla \cdot (\rho_B \, \overrightarrow{q_w})_{\mathrm{f}} = 0 \tag{1}$$

where ρ_B is bulk density, and $\overrightarrow{q_w}$ represents mass average velocity. The subscript f is used to designate fluids, since solid components do not flow from cell to cell.

Bulk density is defined in FLAC3D™ as a combination of fluid and solid phase densities in the expression

$$\rho_B = \rho_s + \phi \, S \, \rho_f \tag{2}$$

where ρ_s is the solid phase, ϕ is porosity, S is saturation, and ρ_f is fluid density. The software package implicity assumes that the solid density includes empty pores in this calculation. In this model, the mass is divided into solid and fluid phases. The solid phase comprises kerogen, coke and the mineral fractions of the oil shale. This model combines the gas and oil components into a single fluid phase because the version of FLAC3D™ available is currently not equipped to handle multiphase fluids. Saturation is always considered unity for this model, because the FLAC3D™ assumes that gas is infinitely compressible. Additionally, gas drainage could not be tracked separately as its own phase. Comprehensive phase thermodynamics are beyond the scope of this study.

Other than conversion from solids to fluids via pyrolysis, previous work by Burnham and Braun [1] suggests that little phase change is expected between *in situ* oil and gas phases.

The mass balance for a single species can be expressed as

$$\frac{\partial(\rho_B w_i)}{\partial t} = -\nabla \cdot (w_i \rho_B \, \vec{q}_w)_{\mathrm{f}} + \rho_B R_x(w_i) \tag{3}$$

where w_i is the mass fraction of species i (kg/kg), $\overrightarrow{q_w}$ is the specific mass flow rate (m/s), and R_x is the reaction term for a given species. To track oil and gas flow separately, the specific mass flow rate $\overrightarrow{q_w}$ was derived from Darcy's flow equation. The following derivation demonstrates the formulation of the specific mass flow rate. On a per volume basis, Darcy's law may be expressed as

$$\vec{q} = \frac{\kappa}{\mu} \nabla \mathrm{P} \tag{4}$$

where κ is absolute permeability (m^2), μ is fluid viscosity (Pa·s) and ∇P is the pressure gradient ($\mathrm{Pa/m}$). $\vec{q}$ has units of $\mathrm{m/s}$, bulk fluid volumetric velocity. The volumetric flow rate is converted to a mass specific flow rate by dividing by fluid volume fraction. This is equivalent to porosity in a fully saturated porous system.

$$\overrightarrow{q_w} = \frac{\kappa}{\mu \phi} \nabla P \tag{5}$$

At complete saturation, the fluid volume fraction of a given zone is equivalent to its porosity. The relationship between mass fraction and volume fraction, assuming volume is conserved, is

$$\chi_i \rho_i / \rho_B = w_i, \qquad \chi_1 + \chi_2 = \phi; \quad i = 1,2. \tag{6}$$

Consider χ_1 as the volumetric fraction of oil, and χ_2 as the gas volumetric fraction. Going back to Equation 3, one can expand the derivatives and rearrange to get the following relation.

$$\underbrace{w_i\left[\frac{\partial \rho_B}{\partial t}+\nabla\cdot(\rho_B\,\overrightarrow{q_w})_{\mathrm{f}}\right]}_{=0}+\rho_B\frac{\partial w_i}{\partial t}=-\rho_B\nabla\cdot(\overrightarrow{q_w}\,w_i)_{\mathrm{f}}+\rho_B R_x(w_i) \tag{7}$$

The overall mass balance was derived on the left hand side. Since it equals zero by definition, it can be dropped. Bulk density can then be divided through Equation 7 to yield the species mass fraction balance.

$$\frac{\partial w_i}{\partial t}=-\nabla\cdot(\overrightarrow{q_w}\,w_i)_{\mathrm{f}}+R_x(w_i) \tag{8}$$

2.1.2 Heat Balance

The heat balance for oil shale can be represented by

$$\rho_B C_p\left(\frac{\partial T}{\partial t}+\vec{q}\cdot\nabla T\right)=\lambda\nabla^2 T+\rho_B[w_4\mathrm{k_{R1}(T)}\Delta H_{R1}+w_1 k_{R2}\Delta H_{R2}] \tag{9}$$

where ρ_B is bulk density, C_p is bulk heat capacity, λ is thermal conductivity, w_1 and w_4 are mass fractions of oil and kerogen, respectively. k_{R1}, k_{R2} are reaction rate coefficients, and ΔH_{R1}, ΔH_{R2} are the reaction enthalpies for the first and second reactions, respectively. While flow is extremely slow in the system, thermal diffusivity is so small that even a miniscule Darcy flow would convect significant heat. Since FLAC3D™ cannot model thermal convection and fluid flow simultaneously, some simplification was required. The species mass balance can only be correctly calculated if fluid dynamics and heat transfer are accounted for simultaneously. Convective heat transfer was relaxed to allow the code to reach a tractable solution. The simplified heat equation is thus

$$\rho_B C_p\left(\frac{\partial T}{\partial t}\right)=\lambda\nabla^2 T-\rho_B[w_4\mathrm{k_{R1}(T)}\Delta H_{R1}+w_1 k_{R2}\Delta H_{R2}] \tag{10}$$

Available empirical models [11], [12] justify assuming that all components of the oil

shale have the same heat transfer properties because empirical tests have only focused on bulk oil shale properties.

2.1.3 Volume Balance

Although volume is not a conserved property, it is essential to account for volume changes in each cell of the numerical simulation. In FLAC3D™, one cannot directly alter the volumes of each zone so the following workaround was used. First, relative volume fractions (χ_i) of each component are recalculated using the mass balance. Next, the volume fractions of all components are used to determine overall properties for each phase and the bulk. Finally, the fluid, solid, and bulk moduli are assigned, so that the zone will expand or contract according to the prescribed stress-strain model.

$$\chi_i = \frac{\frac{w_i}{\rho_i}}{\sum\left(\frac{w_i}{\rho_i}\right)} \tag{11}$$

$$\frac{d\chi_i}{d_t} = \left[\frac{(dw_i/dt)}{\rho_i}\right] / \sum\left(\frac{w_i}{\rho_i}\right) \tag{12}$$

Overall volume changes from time step to time step are based on the net result of species reacting, flowing, expanding, or compressing.

This approach requires a number of simplifying assumptions to become tractable for a subsidence simulation. First, all mixtures are assumed ideal. Therefore, all volumes are additive. Second, aside from reactions, no phase changes occur. Third, all mixtures in each phase are considered homogeneous, as is required by the scale of zones in the model (on the order of 1 m). Computational cost and a lack of data make true thermodynamics impractical. It must be emphasized that the purpose of this simulation is to provide insight into stress-strain behavior of *in situ* oil shale undergoing pyrolysis, rather than an

exhaustive description of multiphase chemical properties in a porous medium.

FLAC3D™ 5.0 does not consider flow of more than one phase. Therefore, liquid (oil) and gas generated in the reactions are handled as a single "fluid" phase which fills all pore space. At a saturation of unity, the volume fraction of the fluid phase is equivalent (and, in this model, defines) porosity ϕ.

$$\phi = \chi_1 + \chi_2 \tag{13}$$

Consider χ_1 as the volumetric fraction of oil, and χ_2 as the gas volumetric fraction. Both are taken relative to the bulk zone (cell) volume.

Several methods were attempted to combine the bulk moduli of each component into phases and bulk properties. Of these, only Voight's estimate [13] was found to give numerical consistency and stability.

$$K_B = \sum \chi_i K_i, \qquad K_S = \frac{\sum(\chi_i K_i)_s}{1-\phi}, \qquad K_f = \frac{\sum(\chi_i K_i)_f}{\phi} \tag{14}$$

where K_B is bulk modulis, K_s is the solid matrix modulus, and K_f is the fluid modulus. The subscripts B, s, and f refer to the bulk, solid matrix, and fluid components, respectively. χ_i is the component volume fraction and K_i is the component modulus.

Phase density was assigned based on a similar scheme, using volumetric averages,

$$\rho_f = \frac{\left(\sum_f \chi_i \rho_i\right)}{\phi}, \qquad \rho_s = \sum_s \chi_i \rho_i \tag{15}$$

where χ_i is the component volume fraction and ρ_i is the component density. The subscripts s and f in the summations are for solid and fluid components, respectively. Fluid compressibility is averaged between the oil and gas phases. Stress-strain behavior is handled in the poroelastic model, described in section 2.2.

2.1.4 Deformation Model

A Mohr-Coulomb failure criteria was chosen for oil shale because many of the parameters used for more advanced models have not been experimentally determined for incorporation into FLAC3D™ at this time. Following FLAC3D™, this study adapts the convention that tensile stresses are positive, while compressive stresses are negative. They are numbered from most to least compressive, despite the sign convention. The most compressive stress, σ_1, is therefore technically the minimum principal stress, as follows

$$\sigma_3 \geq \sigma_2 \geq \sigma_1 \tag{16}$$

Mechanical deformation is defined for every grid point in the geometry in the following manner. First, the material is deformed using a given stress state and linear elasticity is initially assumed to hold.

$$\epsilon_i = \frac{3K_B + G_B}{9K_B G_B}\left[\sigma_i - \frac{3K_B - 2G_B}{6K_B + 2G_B}\left(\sigma_j + \sigma_k\right)\right], \qquad \epsilon_{ij} = \frac{\tau_{ij}}{2G_B} \tag{17}$$

K_B is the bulk modulus, G_B is the bulk shear, σ_{ii} are the principal stresses, τ_{ij} shear stresses, and ϵ is strain.

Second, the stress used to cause this elastic guess is compared against Mohr-Coulomb failure criterion. The Mohr-Coulomb failure criteria for tensile and shear failure are

$$f^t = \sigma_3 - S^T \tag{18}$$

$$f^s = \sigma_1 - \sigma_3 N_{\phi^0} + 2c\sqrt{N_{\phi^0}} \tag{19}$$

where f^t is the tensile failure criterion, S^T is tensile strength of the oil shale, f^s is the shear failure criterion, and c is cohesion. N_{ϕ^0} is a function of the friction angle ϕ^0. Failure occurs of the result of either Equation 18 or 19 is positive.

$$N_{\phi^0} = \frac{1 + \sin(\phi^0)}{1 - \sin(\phi^0)} \tag{20}$$

Since it is possible for the simulation to generate stresses that appear to fulfill both tensile and shear failure criteria, FLAC3D™ employs a potential failure surface.

$$\begin{aligned} h^f &= \sigma_3 - S^T + \left(\sqrt{1 + N_{\phi^0}} + N_{\phi^0}\right)\left[\sigma_1 - \left(S^T N_{\phi^0} - 2c\sqrt{N_{\phi^0}}\right)\right] \\ h^f &\begin{cases} h_f \le 0, & \text{correct stress using shear plastic correction.} \\ h_f > 0, & \text{correct stress using tensile plastic correction.} \end{cases} \end{aligned} \tag{21}$$

Finally, once the failure mode is determined, an appropriate plasticity correction is implemented. A "plastic tensile correction," as used by FLAC3D corrects the stress, not the strain. Let σ_i^I be a principal stress predicted for a purely elastic material and σ_i^N be a net stress, corrected for plastic deformation. Assuming a 0° dilatation angle for oil shale[1], the plastic correction becomes

$$\begin{aligned} \sigma_1^N &= \sigma_1^I - \frac{f^t\left(K_B - \frac{2}{3}G_B\right)}{K_B + \frac{4}{3}G_B} \\ \sigma_2^N &= \sigma_2^I \\ \sigma_3^N &= S^T \end{aligned} \quad . \tag{22}$$

For shear failure, the plastic correction is

$$\begin{aligned} \sigma_1^N &= \sigma_1^I - \frac{f^s}{1 - N_{\phi^0}} \\ \sigma_2^N &= \sigma_2^I \\ \sigma_3^N &= \sigma_3^I + \frac{f^s}{1 - N_{\phi^0}} \end{aligned} \quad . \tag{23}$$

Again, note that this simplification assumes that the oil shale's volume is conserved under plastic deformation so long as no reactions or drainage occur. Subsidence or heave therefore requires material to enter or leave the system. Consider also that the stress-

[1] Dilatation angle is used to describe how much volume is gained or lost as a result of failure. Assuming no volume change due to plastic deformation simplifies component density calculations.

strain curve will be affected by poroelasticity, considered in Section 2.2.5.

$$\Delta\sigma_{ij} = 2G_B\epsilon_{ij} + \left(K_B - \frac{2}{3}G_B\right)\epsilon_{kk}\delta_{ij} \tag{24}$$

2.2 Poroelastic Model of Oil Shale

To simulate the potential for subsidence, a stress-strain model for *in situ* pyrolysis must (at minimum) be able to break up bulk properties of oil shale into solid and fluid phases, define and modify properties for components in each phase, and account for changes in the properties of all components over a large range of temperatures and pressures. With conversion of kerogen to fluid (liquid and gas), and ultimately with drainage of the fluid to a producing wellbore, the weakened porous formation is subject to consolidation. The consolidation model must include pressure/volume interaction between the pore fluid and matrix of the shale, which is known as poroelasticity. Under pyrolysis, oil shale's evolving composition requires routinely recalculating the mechanical properties of each component. These, in turn, are used to update fluid, solid, and bulk parameters to determine deformation and drainage of each cell in the system.

Poroelastic response of *in situ* oil shale during pyrolysis is defined in the following manner:

1. A dry mechanical model describes oil shale constitutive characteristics prior to pyrolysis.
2. As mechanical properties and fluid volumes change during pyrolysis, the mechanical model is corrected with a consolidation model, in this case Biot's model for linear consolidation [14].
3. Models for mechanical properties of each component are defined as functions of

temperature and pressure, along with methods of combining and separating them for use in the numerical model.

Any complete description of the behavior of oil shale before, during, and after pyrolysis begins with a number of key mechanical relations. The chosen rock mechanics model must be able to account for changes in both plastic and elastic properties as the system is heated, pyrolyzed, and drained. Much of the challenge of developing an *in situ* oil shale simulation is based on the incompleteness of the mechanical model.

2.2.1 Dry Mechanical Model

Most studies of elastic behavior of oil shale assume transverse isotropy. Their complexity ranges from Chong and Smith's fit to Hooke's law [15] to a third-order relation developed by Cleary [16]. Chong and Smith's model allows for deriving nonlinear mechanical properties of oil shale at ambient temperature, but fails to account for temperature effects. Cleary's model includes temperature effects, but only 18 of the 35 required parameters have been mathematically defined for this rigorous and impractical approach. Alternatively, Closmann and Bradley [17] developed a robust model capturing changes of oil shale strength and Young's modulus as a function of temperature and oil shale richness. Unfortunately, Poisson's ratios were not reported for their triaxial tests and bulk moduli could not be determined.

The author found no single legacy oil shale model that considers all desired parameters, even prior to pyrolysis. Therefore, at least two empirical models must be combined to complete the prepyrolysis picture of oil shale and kerogen mechanics. Chong and Smith's model for ambient oil shale elasticity was combined with Closmann and Bradley's thermally dependent model.

2.2.2 Chong and Smith's Model of Oil Shale Elasticity

Elastic properties for oil shale are initialized using the following empirical correlations developed by Chong and Smith [15]. First, organic content of the shale is approximated based on a correlation for Green River Oil Shale by Smith, 1969 [18].

$$\chi_4 = O_C = \frac{164.9FA}{FA + 111.8} \tag{25}$$

where O_C is the percent organic volume of oil shale (assumed to be kerogen) and FA is the Fischer-Assay yield in gallons per ton (gal/ton).

Then, unconfined compressive strengths are calculated both parallel (*x*-*y*) and perpendicular (*z*) to the bedding, presuming transverse isotropy. For Colorado oil shale, these correlations are

$$\begin{aligned} \sigma_{ux} &= 127.73 - 1.125O_C \\ \sigma_{uz} &= 161.60 - 1.5415\ O_C \end{aligned} \tag{26}$$

where σ_{ux}, σ_{uz} are the unconfined compressive strengths (MPa) in the *x* and *z* directions, respectively.

Finally, Young's Moduli and Poisson ratios are expressed as functions of organic content and stress levels (S_x, S_z). For Colorado Oil Shale, these are

$$\begin{aligned} E_x &= 10.45 - 0.174\ O_C + 0.384\ S_x - 0.00519\ O_C S_x - 1.883 \times 10^{-7} S_x^4 \\ E_z &= 12.34 - 0.2196\ O_C + 0.7461\ S_z - 6.82 \times 10^{-5} O_C S_z - 9.869 \times 10^{-8} S_z^4 \\ \nu_{xz} &= -0.04419 + 0.00385\ O_C + 0.00645\ S_z \\ \nu_{xy} &= -0.03307 + 0.00333\ O_C + 0.00480\ S_x \end{aligned} \tag{27}$$

There is some ambiguity about the meaning of the stress level term used by Chong and Smith. While their other terms differentiate between perpendicular (z) and parallel (*x*-*y*) orientations relative to the shale bedding plane, it is unclear whether the stress levels are also distinguished this way. Based on correlations in the same model defining

separate ultimate strengths in both orientations, this author interpreted the stress levels as normalized ratios of unconfined stress as S_x and S_z, respectively.

$$S_x = \frac{\sigma_x}{\sigma_{ux}} \times 100, \qquad S_z = \frac{\sigma_z}{\sigma_{uz}} \times 100 \tag{28}$$

Shear moduli between the z-axis and the isotropic plane are estimated using an empirical correlation, also developed by Chong et al. [19]

$$G_{xz} = G_{yz} = \frac{E_x E_z}{E_z + E_x(1 + 2\nu_{zx})} \tag{29}$$

while the *x*-*y* shear modulus is calculated via Amadei's [20] correlation, remembering that $E_x = E_y$.

$$G_{xy} = \frac{E_x}{2\left(1 + \nu_{xy}\right)} \tag{30}$$

The existing poroelasticity model of FLAC3D™ requires that an isotropic mechanical model is maintained. Therefore an equivalent bulk modulus was derived from Chong and Smith's elastic model (see Appendix C). In the coordinates of interest for our problem, this relation becomes

$$K = \frac{E_x E_z}{2E_z\left(1 - \nu_{xy}\right) + E_x(1 - 4\nu_{xz})} \tag{31}$$

There is no known similar solution that allows us to develop an equivalent "average" shear modulus from basic equations. The way forward requires more detail about the process and the simulation plan. First, one should check the degree of anisotropy (G_{xy}/G_{xz}) in the material - as defined by Amadei [20]. Chong and Smith's empirical model for oil shale elastic properties is plotted in Fig. 1(A) for varying richness at 18.6 MPa (2698 psi) overburden stress and 13.2 MPa (1907 psi) lateral stress. The anisotropy between the two shear moduli is seen in panel (B) of the same figure. The failure

strength of the oil shale dips below the failure criteria at 75 gal/ton or above, leading to anomalous results.

Assuming that none of the oil shale is initially in a failure state, this empirical model limits the simulation to evaluating oil shale less than 70 gal/ton for expected initial stresses. While richer seams are known to exist, they are generally not found in the Mahogany zone [21]. This limitation should not seriously restrict the applicability of the simulation. Shear moduli anisotropy is actually fairly large even at 25 gal/ton; already at about 75%.

Geometry in the model is defined such that boundaries parallel to the z-axis are fixed due to balanced horizontal forces across planes of symmetry. The choice of geometry in this model (uniaxial strain) eliminates shear in the *x*-*y* direction, leaving one "active" shear term between lateral and axial directions. Consequently, only $G_{xz} = G_{yz}$ plays an active role in this model. G_{xz} was previously defined in Equation 29.

2.2.3 Closmann and Bradley

Several investigators have observed the effects of temperature on oil shale strength and elastic properties [17], [22]–[25]. Closmann and Bradley thoroughly investigated the thermal degradation of oil shale strength using Brazilian tensile testing [17]. They also carried out triaxial testing and developed the following empirical model for oil shale tensile and compressive strengths as a function of temperature and Fisher Assay yield.

$$\begin{aligned} \mathrm{S^C} &= 3.48 \times 10^5 T_F^{-0.615} \exp(2.99 \times 10^{-4} P - 0.0214 FA) \\ S_{\mathrm{V}}^{\mathrm{T}} &= \left(-288 + \frac{7.79 \times 10^8}{T_R^2} - 1.93 \times 10^4 \frac{FA}{T_R} + 0.229\, FA^2 \right) \\ S_{\mathrm{H}}^{\mathrm{T}} &= \left(-25.3 + \frac{6.48 \times 10^8}{T_R^2} - 2.93 \times 10^4 \frac{FA}{T_R} + 0.386\, FA^2 \right) \end{aligned} \tag{32}$$

In Equation 32, S^C is compressive strength, S_V^T and S_H^T are tensile strength in the vertical and horizontal directions. As it is heated, oil shale's ability to withstand stress declines substantially. Research on thermal-mechanical coupling in oil shale is sparse, but several investigators have developed correlations. Chu and Chang's correlations [25] show temperature dependence, but the link to oil shale richness is unclear. Closmann and Bradley's correlations were developed over a wider range of temperatures, and differentiated between compressive and tensile Young's moduli [17]. While this is more realistic than a truly elastic model, the underlying code was not designed to have separate extension and compression models.

While the associations between Chu and Chang's relations and sample organic content are ambiguous, they can still be used as a "measuring stick" to evaluate the work of Closmann and Bradley [17]. A quick comparison in Fig. 2 suggests that Closmann and Bradley's correlation for compressive Young's modulus would be the most appropriate for the simulation, based on its wider range of applicable experimental temperature.

$$E(T) = 0.1888E_0 \exp\left(\frac{492}{T}\right) \tag{33}$$

where $E(T)$ is the "new" Young's modulus at the current temperature $[K]$, and E_0 is the initial Young's modulus at 295 K (72°F). Until better correlations are developed, it is assumed that the same relationship will suffice in both the axial and longitudinal directions.

Assuming that Poisson's ratio is relatively constant,[2] the kerogen bulk modulus is

[2] This is more a matter of necessity than convenience or accuracy, since a model that includes changes in bulk modulus or Poisson's ratio with temperature was not available.

$$K_4(T_R) = 0.1888 K_{B,0} \exp\left(\frac{886}{T_R}\right) \tag{34}$$

Before pyrolysis begins, the kerogen and overall bulk modulus are the same. No conversion to SI units is required, because the expression automatically has the units of the initial bulk modulus. The shear modulus can be varied in the same way (Young's modulus is in the numerator for both relations).

2.2.4 Combining Chong and Smith with Closmann and Bradley

A marriage between Chong and Smith's relations and Closmann and Bradley's initially looks ideal, but there are some undesirable corollaries that must be accounted for. Closmann and Bradley developed their own empirical correlations for oil shale compressive strength, but didn't differentiate between parallel and perpendicular ultimate compressive strengths. Fig. 3 compares the two models at 70°F to determine whether it would be acceptable to combine them.

Probable causes for the weak correlation in Fig. 3 include differences in experimental procedure, sample geometries, and the presence of nahcolite[3] in Closmann and Bradley's samples. Additionally, a more quantitative comparison would require knowing the experimental temperature of Chong and Smiths' substantial work. The empirical models appear to correlate better near 300 K, but there is no evidence to justify this speculation. While more complete stress-strain models are desirable, completing a simulation requires compromise. Although a number of authors have observed that oil shale grade affects thermal strength degradation, only Closmann and Bradley explicitly model this coupling. As their correlations only cover isotropic elastic properties, this author was forced to find

[3] Soft, colorless, or white carbonate mineral ($NaHCO_3$).

equivalent isotropic properties for Chong and Smith's relationship.

Chong and Smith's empirical correlations are invalidated when temperatures change. As the shale is heated, its ultimate strength greatly declines; as noted by numerous authors [17], [23], [26]. Incompatibility of empirical correlations may be one of the greatest challenges to any complete multiphysics simulation of *in situ* pyrolysis. From a computational point-of-view, combining the two models risks jeopardizing numerical stability of the problem. To avoid shocking the iterative solution, initial strength is adapted from Closmann and Bradley's model, while Chong and Smith's concepts are used only to initialize the bulk and shear moduli.

Clearly, more thorough work is needed to complete the mechanical model of oil shale. Until the essential correlations are developed, a compromise must be made between Closmann and Bradley's thermal correlations and Chong and Smith's nonlinear models.

Combination of the two approaches requires several assumptions. If it can be assumed that Poisson's ratio does not change greatly for oil shale before it is heated to pyrolysis, the Young's modulus ratio calculated by Closmann and Bradley can be used with classic elastic relations to determine the bulk and shear modulus of oil shale. The shear modulus should also decrease.

Technically, these studies were for defining for bulk oil shale properties. For a reactive and poroelastic model, it is desirable to differentiate between the properties of each component. Since no appropriate studies differentiate the mechanical properties of pure kerogen, the Closmann and Bradley model was used as an approximation. The mineral and coke components (modeled as dolomite and graphite, respectively), are

considered constant. The current approach, therefore, is to overlay the best available studies of thermal effects with those for pressure- and organic content-dependence. Some useful correlations for thermal effects were developed by Closmann and Bradley [17], and were used to modify the initial elastic properties determined via Chong and Smith [15].

The Closmann and Bradley thermal model is used to calculate both the tensile and unconfined compressive strength, while Chong and Smith's model was used to initialize elastic properties of kerogen.

2.2.5 Biot's Consolidation Theory

The lack of previous studies on evolution of mechanical properties and internal fluids and pressure in oil shale is surprising, considering its critical implications to both oil shale rock mechanics and the economic feasibility of any true *in situ* operation. Pyrolysis drives the formation and destruction of pore pressure, permeability, and porosity. If the permeability is too low or pore pressure development is insufficient, most of the oil generated will be lost to further pyrolysis.

This complex interaction requires a model that can represent all possible interactions between pore fluids and the solid matrix containing them. Only a few known correlations accomplish this. The first is an extension of Biot's theory of consolidation [14], while the second is a careful formulation of mixing theory, such as that developed by Tong et al. [27]. The former was chosen because it was preprogrammed into FLAC3D™.

Biot's linear equation for consolidation of a fully saturated system may be expressed in differential form as

$$\frac{\partial P}{\partial t} = M\left(-\nabla \cdot \vec{q} + \nabla g_V - \alpha \frac{\partial \epsilon}{\partial t} + \beta \frac{\partial \mathrm{T}}{\partial \mathrm{t}}\right) \quad (35)$$

where M is the Biot modulus, P is pore pressure, t is time, $\vec{q}$ is the volumetric specific fluid velocity vector, g_v is the fluid volumetric source/sink, α is Biot's coefficient, ϵ is solid matrix strain, β is thermal expansion modulus of the bulk material and T is temperature. The left hand side of the equation is the change in pore pressure over time. The right hand side terms represent all of the ways that pore pressure can be changed in a poroelastic system. Respectively, they are the specific divergence of fluid flow, net generation of new pore fluid, pore strain due to bulk volume strain, and the thermal strain of the entire system.

It could be argued that a linear model is inappropriate, due to the nonlinearity of virtually every term in this equation. *In situ* pyrolysis is highly nonlinear, and there are major changes in everything from pressure and temperature to porosity and permeability. An analytical solution would demand that nonlinearity is accounted for, but this would also require defining nonlinear models for each contributing factor. Numerical simulation is not constrained by this rigor, as long as appropriate models are used to update the many contributing factors. Each of these terms will be defined for oil shale undergoing *in situ* pyrolysis, to allow for a complete simulation.

The Biot Coefficient, α , represents the ratio of the bulk modulus of the solid with pores to the bulk modulus of the solid alone. It's the relative compressibility of the bulk porous medium to that of the solid matrix, and represents the way stress is distributed between the two phases. Alternatively, it can be considered the relative change in pore volume for a change in bulk volume due to a pore pressure change.

$$\alpha = \max\left(1 - \frac{K_B}{K_s}, \quad \frac{3\phi}{2+\phi}\right) \tag{36}$$

First described by Biot as the "change in specific fluid content" [14], the specific volumetric flux $\vec{q}$ is simply the net velocity of fluid going in or out of a zone. Darcy's law was used to model the system, where κ is absolute permeability (m^2) and μ is dynamic viscosity (Pa·s).

$$\vec{q} = \frac{\kappa}{\mu}\nabla P \tag{37}$$

Dynamic viscosity and permeability are assumed constant for the fluid mixture as a matter of numerical necessity.[4] Appendix D contains a more complete discussion of models for these properties.

The Biot Modulus represents a linear relationship between changes in pore pressure, and the volume of the pores in a poroelastic medium. For a reversibly compressible system, it is

$$M = \frac{K_f}{\phi + (\alpha - \phi)(1-\alpha)\frac{K_f}{K_B}} \tag{38}$$

where K_f is the fluid bulk modulus, and other terms have been previously defined. If the solid matrix is assumed relatively incompressible, relative to the bulk system (such that $\alpha \cong 1$), then the Biot Modulus simplifies to

$$M = \frac{K_f}{\phi}. \tag{39}$$

[4] FLAC3D™ 5.0 is unable to converge if either viscosity or permeability are nonuniform in the geometry.

2.3 Thermal Model

Under true *in situ* pyrolysis conditions, heat transfer is dominated by conduction. The heating process is extremely slow for oil shale because kerogen is an excellent insulator [12], [28]. A proposed operation placing heating wells and production wells as close at 25 ft would require many months of heating before producing fluids. One could try to fracture shale to speed up heat transfer via convection. Unfortunately, oil shale also loses virtually all of its strength before 150 °C, so any fractures will almost certainly close up long before pyrolysis temperatures are reached. Alternatively, some have suggested combining pyrolysis with combustion to speed up the heating process, and maintain porosity. While this approach would save a significant amount of energy input, conduction will still dominate.

Oil shale must be heated to pyrolysis prior to significant drainage occurring. The following empirical relationship between oil shale's heat capacity, its temperature and Fischer Assay (FA) yield was developed by Shaw, 1947 [11].

$$C_p = 4186.8(0.172 + (0.067 + 0.00162FA) \times 10^{-3}T_R) \qquad (40)$$

where C_p is heat capacity [J/kg·K] above 77°F and $T_R$is absolute temperature [R].

An excellent study by Prats and O'Brian [12] determined transversely isotropic thermal properties for oil shale as functions of FA yield and temperature, using samples from the Piceance Creek basin and the Uinta basin in Utah. They determined room temperature oil shale thermal conductivities (W/m·K) to be

$$\begin{aligned} \lambda_H(75°F) &= 1.7307[1.2299\exp(-0.01840FA)] \\ \lambda_G(75°F) &= 1.7307[1.1276\exp(-0.01843\ FA)] \\ \lambda_V(75°F) &= 1.7307[1.0338\exp(-0.01846\ \mathrm{FA})] \end{aligned} \qquad (41)$$

where λ_H is horizontal conductivity, λ_V is vertical conductivity, and λ_G is the geometric

mean of them both.

Prats and O'Brian (ibid.) also developed correlations showing how thermal properties change as samples were heated well into pyrolysis [800°F, (427 °C)]; as a result, these correlations are considered general enough to cover the entire pyrolysis process. The time and temperature dependent mechanical properties were tested numerical per Fig. 4 The three correlations are compared in Fig. 5 for 25 gal/ton FA oil shale.

$$\begin{aligned}
\lambda_H(T_F) &= \lambda_H(75°F)\begin{pmatrix}1 - 1.0932\times10^{-4}[\mathrm{T_F}-75]\\ -4.1949\times10^{-7}[\mathrm{T_F}-75]^2\end{pmatrix}\\
\lambda_G(T_F) &= \lambda_G(75°F)\begin{pmatrix}1 - 1.149\times10^{-4}(\mathrm{T_F}-75)\\ -3.6667\times10^{-7}(\mathrm{T_F}-75)^2\end{pmatrix}\\
\lambda_V(T_F) &= \lambda_V(75°F)\begin{pmatrix}1 - 1.1948\times10^{-4}(\mathrm{T_F}-75)\\ -3.1271\times10^{-7}(\mathrm{T_F}-75)^2\end{pmatrix}
\end{aligned} \tag{42}$$

2.4 Pyrolysis Kinetics Model

Choosing an appropriate pyrolysis model for oil shale is not a trivial task. First, the rate of reaction depends on both heating rate and temperature. Second the FLAC3D™ is not designed to handle either multiphase flow or kinetics. Therefore, simplifying assumptions must be made to allow for reasonable calculation time. Third, pyrolysis kinetic rate laws are generally determined via the thermo-gravimetric analysis method [29]–[31]. While this will not affect the initial reaction rate (pyrolysis is a pseudo-homogeneous reaction), the residence time of reacted material may be significantly longer. Unless it can be drained, much of the oil produced during *in situ* pyrolysis will eventually decompose into natural gas and coke.

Pyrolysis is not a single reaction, but a cascade of thermal decomposition reactions affecting thousands of species at different rates. Simple kinetics models may be deceptive because some components of oil shale will react at much lower temperatures

than others. On the other hand, computational cost must be kept in check because heterogeneous reactions add geometric complexity to reservoir simulation. *Every species must be solved for every reaction at every zone in the system at every time step. Once the new weight fractions are calculated, porosity, permeability, fluid density, compressibility, and pore pressure also need to be reevaluated for the same conditions.* For analyzing subsidence, little extra insight is expected by introducing more components or reactions than necessary to resolve forces.

This study models pyrolysis using four components and two reactions to minimize computational cost, while still catching the most important poroelastic aspects of the system. A basic kinetics model by Braun and Burnham [32] for Type II shales[5] was adapted. H:C ratios for Green River pyrolysis components were adapted from Bauman et al. [33], and weighted for 4 components using molar averaging of combined components. Component properties can be seen in Table 1.

Fractional yield of oil was estimated using Fischer Assay data from Skyline for 25 gal/ton shale. The remaining coefficients were determined via a mass balance for carbon and

hydrogen. The plausibility of this approach was validated by comparison with more complex models developed by Burnham and Braun [35]. As in other models, the stoichiometric coefficients are only approximations, and should not be construed as strong theoretical values.

Oil shale pyrolysis is an endothermic reaction, but literature enumerating the heat requirements is surprisingly sparse. Perhaps this is because heat of reaction depends on the chosen kinetic model and pseudo-components; nevertheless, nearly all references to

[5] Green River oil shale is Type II shale or lacustrine, meaning "from lake beds."

the heat of pyrolysis go back to only a few sources. These are Burnham and Braun [24], Youtsos et al. [36] and Camp [34] and Yang and Sohn's [37].

Burnham and Braun's models [32] are most frequently used as the basis for heats of reaction at different temperatures [9], [33], [36]; but the papers don't actually have heats of reaction recorded. Youtsos et al. appear to provide higher estimates of the heat of kerogen decomposition relative to other studies.

Camp's studies do not differentiate between stages of pyrolysis, while Yang and Sohn's investigation was on whole oil shale and includes mineral reactions. As a compromise, Camp's estimate for pyrolysis enthalpy was used for the kerogen decomposition reaction, and Braun and Burnham's estimate was used for oil degradation in Table 2. The model was tested in MATLAB numerically for a zone 5 m away from the heater well, per Fig. 6, using the heating rate predicted for heating a rectangular slab.

Several authors have suggested using the isoconversional method [30] to better capture the chemical kinetics of oil shale pyrolysis, but it was unclear how to implement it numerically. Studies also suggest that *in situ* pressures over 6.9 MPa (1000 psi) may reduce base pyrolysis temperatures [38], but this will not likely be encountered in this model.

2.5 Component Models

Three levels of component properties are considered in this model of *in situ* oil shale pyrolysis, as seen in Fig. 7. At the highest level are bulk properties, which are determined by a weighted average of the fluid and solid phase properties. The fluid and solid phase properties are likewise a volumetric average of their respective components. The fluid phase consists of a high-temperature, high-pressure solution of pseudo-

components gas and oil. The gas is modeled after propane, while the oil is based on shale oil recovered using Skyline 16 well data [39]. The solid phase is considered a uniform mixture of coke (or char), kerogen (which would include bitumen) and minerals (modeled as dolomite).

2.5.1 Oil Compressibility

Finding an appropriate model for the bulk modulus of shale oil requires accounting for wide changes in pressure, temperature, and composition. Unfortunately, transforming oil composition renders most commonly used correlations invalid. To illustrate the challenge, one of the most widespread and robust correlations for determining changes in oil density with temperature and pressure was developed by M.B. Standing [40]. At constant temperature, the overall fluid density (oil+gas) (lb/ft^3) changes with pressure as

$$\Delta\rho_T = (0.167 + 16.181 * 10^{-0.0425\,\rho_{pL}})\left(\frac{P}{1000}\right) - 0.01(0.299 + 263.10^{-0.0603\,\rho_{pL}})\left(\frac{P}{1000}\right)^2 \quad (43)$$

and changes with temperature at atmospheric pressure by

$$\rho_p = \left[0.0133 + 152.4\left(\rho_{pL} + \Delta\rho_T\right)^{-2.45}\right](T - 60) - \left[8.1 \times 10^{-6} - 0.0622 * 10^{-0.0764\left(\rho_{pL}+\Delta\rho_T\right)}\right](T - 60)^2 \quad (44)$$

The apparent liquid densities of natural gases can fairly well represented by Katz chart,

$$\rho_{pL} = 38.52 * 10^{-0.00326\,^\circ API} + (94.75 - 33.93 \log {}^\circ API) \log \gamma_g \quad (45)$$

where γ_g is the gas specific gravity when dissolved in oil.

Unfortunately, these correlations require defining gas-oil ratios and oil bubble-point pressure. Neither of these properties can be deduced for a two-component oil-gas system. Additionally, Equations 43 and 44 are incompatible with Biot's model for

consolidation because kinetics treats gas and oil separately.

A reasonable model was therefore developed in Equation 46 by combining a robust correlation by McCain et al., 1988, [41] with a minimum oil modulus, to avoid unphysical compressibility.

Biot's theory of consolidation [14] assumes an elastic linear relationship between

$$K_1 = \min\left(K_{1,0}, \quad \frac{e^{7.114} P_{psi}^{1.294}}{T_R^{0.981} API^{0.770} \gamma_g^{0.446}}\right) \tag{46}$$

stress and strain, defined on the assumption that those strains are small. Using Biot's correlation requires establishing the relationship between porosity and compressibility. Biot makes no attempt in his original derivation to differentiate pore volume, saturation, or porosity.

$$\frac{1}{\phi M}\frac{\partial P}{\partial t} + \frac{\phi}{S}\frac{\partial S}{\partial t} + \frac{S}{\phi}\frac{\partial \phi}{\partial t} = -\frac{1}{\phi S}(\nabla \cdot \vec{q} + \nabla q_v) - \frac{\alpha}{\phi}\frac{\partial \epsilon}{\partial t} + \beta\frac{\partial T}{\partial t} \tag{47}$$

If saturation is constant at unity, Equation 47 may be rewritten as

$$\frac{1}{M}\frac{\partial P}{\partial t} + \frac{\partial \phi}{\partial t} = -(\nabla \cdot \vec{q} + \nabla q_v) - \alpha\frac{\partial \epsilon}{\partial t} + \phi\beta\frac{\partial T}{\partial t} \tag{48}$$

Useful relations between porosity and compressibility for linear poroelastic solids were also derived by Zimmerman [42] for single-phase fluids, but were not ultimately adopted in this model.

2.6 Porosity and Permeability

Porosity in oil shale being heated to pyrolysis is not constant. Fig. 8 demonstrates how porosity can vary before, during, and after pyrolysis. The data were adapted from experimental work summarized by Cameron Engineers [43].

It is plausible to assign porosity based on a fit to Dineen's data, but this leads to

calculation errors in volume and mass balance. In this study, porosity was determined by explicitly calculating the volume fraction of fluid in each cell of the simulation. Assuming that all of the pores are filled with oil or gas (overall saturation of unity), porosity can be determined as follows. First, volume fractions of components are calculated from component mass fractions using following formula.

$$\chi_i = \frac{\frac{w_i}{\rho_i}}{\sum_{i=1}^{N=5} \frac{w_i}{\rho_i}} \tag{49}$$

where χ_i is a component's volume fraction, w_i is a component's weight fraction, K_i is the component's bulk modulus, and ρ_i is the component's density. Porosity is defined as the sum of the fluid volume fractions. The volume calculation determines the relative volume fractions of a material, given the bulk moduli of each component at the same pore pressure.

For numerical stability, and to maintain physically plausible scenarios, it was necessary to define both maximum and minimum porosities. Maximum porosity may be explained by visualizing a volume of pyrolyzing oil shale as a fixed-volume batch reactor. Initially, the system is almost completely solid. As kerogen decomposes, it generates oil and gas. The products are less dense than the reactants under a fixed pressure, but the system does not allow for isobaric volume expansion once all possible porosity is accounted for. For a container of fixed volume, where no leakage (or rupture) is allowed, the only way to maintain mass conservation is for the products to be compressed into the same space as the reactants. The produced fluid creates an excess pressure that will either result in strain in both the pore and bulk material, or drainage out of the shale. While a cell in oil shale can expand with the expanded pore pressure, the

real-world system can only expand so much before it becomes nonphysical.

There is also a lower limit to porosity, at which point flow in and out of a given volume of oil shale simply cannot continue. This accounts for irrecoverable fractions of petroleum and helps the simulation avoid dividing by zero in flow calculations.

Assuming that all components retain a linear stress-strain relationship, the porosity/pore pressure correction can be determined using the following relationship.

$$\text{if} \begin{cases} \phi < 0.01, & \Delta P_c = \dfrac{\phi_{Min} - \phi}{\sum \left(\frac{1}{K_i}\right)_f} \\ \phi_{Min} \le \phi \le \phi_{Max}, & \Delta P_c = 0 \\ \phi > \phi_{Max}, & \Delta P_c = \dfrac{\sum (\chi_i)_{\text{organic}} - \phi_{Max}}{\sum \left(\frac{1}{K_i}\right)_{\text{organic}}} \end{cases} \tag{50}$$

Modelling permeability is challenging. The Kozeny-Karman equation is inappropriate for oil shale, but a general paucity of better models suggests that it may have to do for this simulation.

$$\kappa = \frac{D_p^2 \phi^3}{150(1-\phi)^2} \tag{51}$$

where κ is the geometric mean permeability (m^2) and D_p is the pore diameter (5×10^{-5} m) [10].

Permeability in oil shale is highly anisotropic, but a compatible oil shale permeability was not available for the simulation. High temperatures may increase permeability, but this newly acquired permeability cannot be maintained without further pyrolyzing the sample. A number of empirical models have been developed for permeability based on oil shale aggregates [44], [45]. Future investigators may wish to investigate a whole-

block oil shale permeability model.

In practice, the addition of a permeability gradient to FLAC3D™ reduces the critical time step for a finite difference solution to microseconds. This, combined with the inability of the software to multithread fluid calculations makes convergence impossible if permeability is varied. This challenge may not be unique to FLAC3D™, however.

2.6.1 Kerogen Properties

Empirical models for oil shale generally consider the properties of the bulk material rather than those of the constituents. While it is possible estimate a micromechanical model for most components of oil shale, this has yet to be done for kerogen. For purposes of this study, kerogen is used as a broad term for the initial raw organic matter. It would also include bitumen and other very heavy organics. Kerogen has yet to be mechanically tested as an isolated component.

However, one may be able to use a thought experiment to infer characteristic features of Green River Kerogen, using oil shale's sensitivity to temperature. The inorganic fraction of oil shale is generally insensitive to temperature below about 1300°F (where nahcolite decomposes), but 20 gal/ton and richer oil shales lose 80% or more of their strength below 200°F [17]. Pyrolysis rates are insignificant for the time-scale of this simulation at temperatures much below 440°F. While kerogen may not be the dominant phase, it clearly acts as a binding agent in oil shale.

Kerogen's mechanical properties could therefore be approximated by those of oil shale before pyrolysis temperatures. Conveniently, oil shale has been tested at representative temperatures in the laboratory. The caveat to this approximation is that the bulk material properties of oil shale cannot be treated as kerogen once pyrolysis begins.

After pyrolysis begins, the kerogen approximation is lumped in with other solid phases by volume averaging the properties.

2.6.2 Fluid Bulk Modulus Calculation

Given that neither the typical shale oil bubble point pressure, nor the saturated gas-oil ratio are known, a correlation developed by McCain et al. [41] will have to suffice for approximating the fluid bulk modulus. The API gravity is 28°, based on results found from the Skyline coring data [39].

$$\mathrm{K_1} = \frac{6895\mathrm{e}^{7.114}\left(\frac{\mathrm{P_{eval}}}{6895}\right)^{1.394}}{\mathrm{T_R^{0.981}\,API^{0.770}\,\gamma_g^{0.446}}} \tag{52}$$

The gas modulus is calculated retroactively based on the real gas equation. Assuming that the z-factor remains constant over pyrolysis temperatures (500-600 K [440-620°F]), the equivalent gas bulk modulus may be approximated by

$$K_2 = P \tag{53}$$

Assuming that the fluid volumes are additive, the effective fluid modulus is found using the Voight estimate [46]. The normal relation must be divided by porosity, because the volume fractions are defined relative to bulk material properties.

$$K_f = \frac{1}{\phi}\left[\sum(\chi_i K_i)_f\right] \tag{54}$$

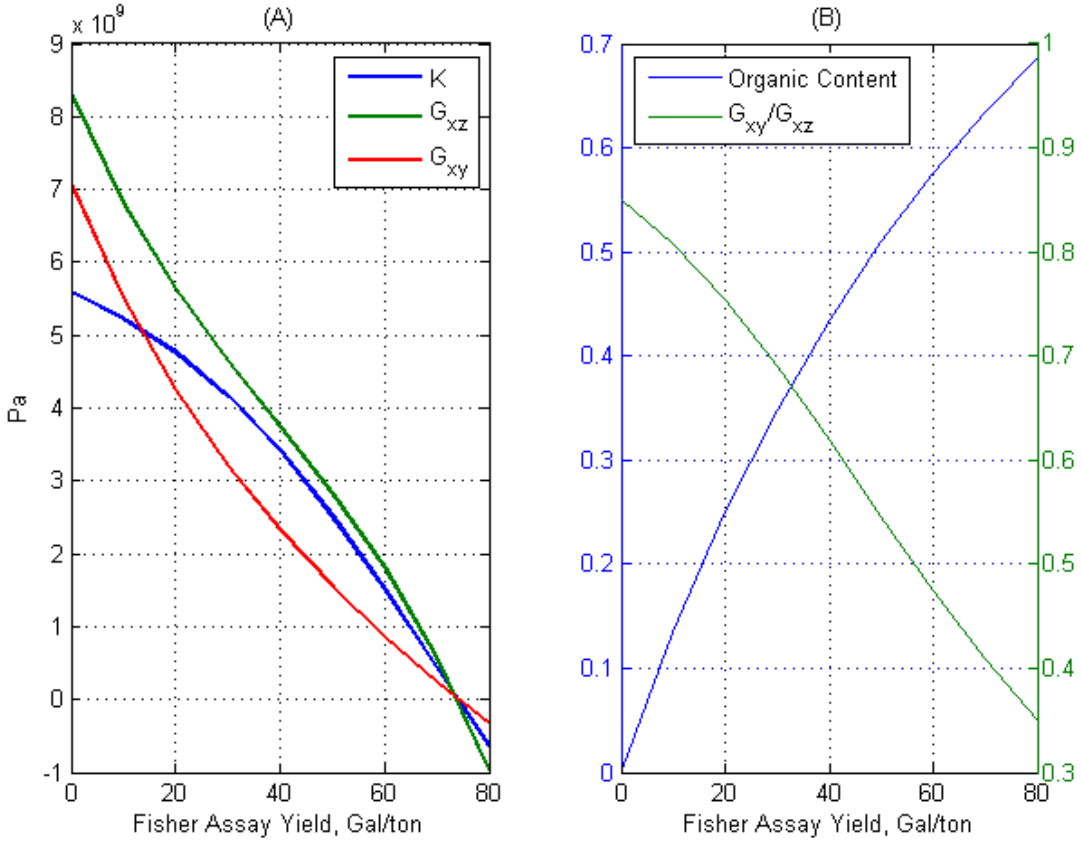

Fig. 1. A) Initial oil shale moduli predicted by Chong and Smith model. B) Organic content and shear anisotropy predicted by model.

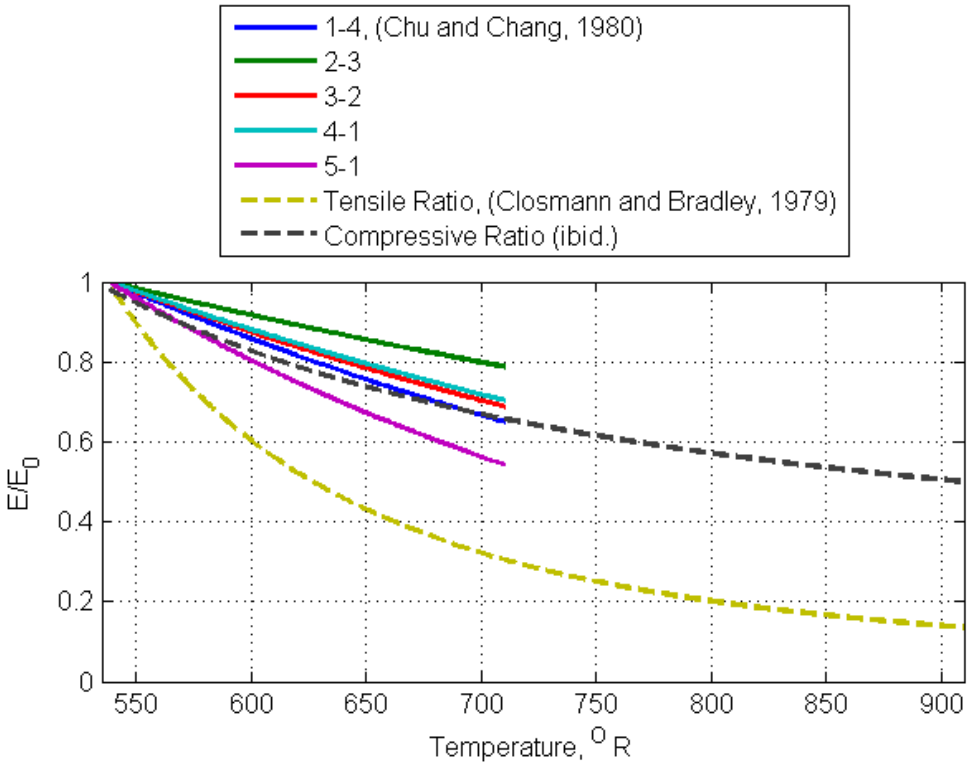

Fig. 2. Normalized comparison of several correlations showing how Young's modulus varies with temperature. The solid contours are the plotted results from Chu and Chang's [25] correlations while the dashed contours are the Closmann and Bradley model [17].

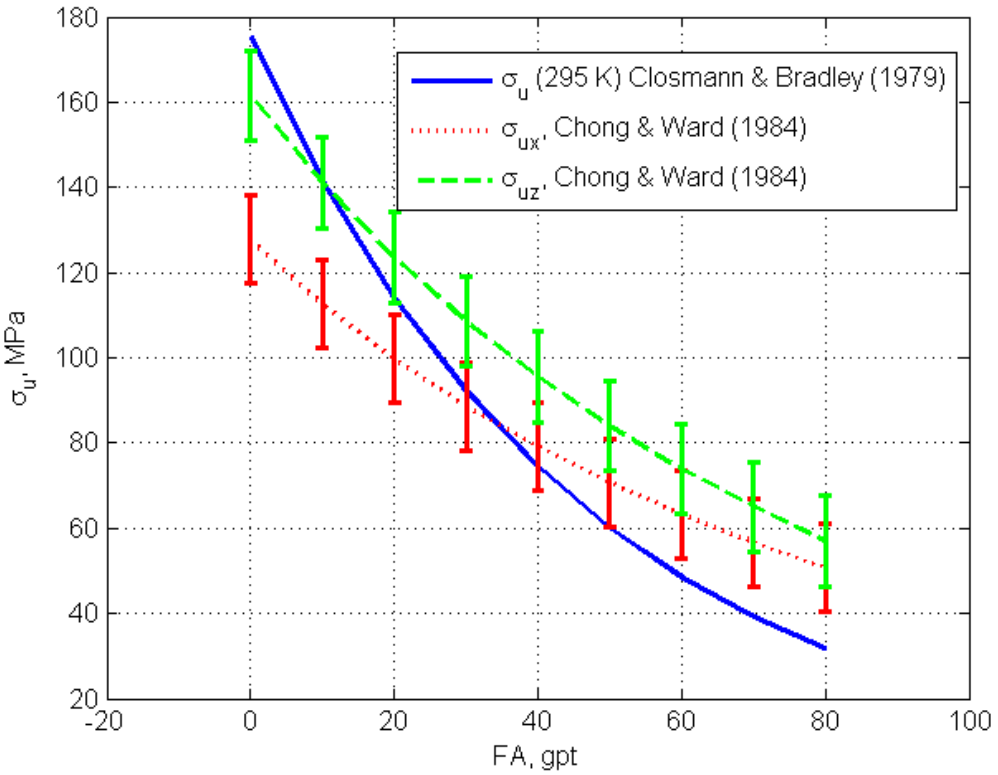

Fig. 3. Comparison of models for oil shale compressive strength between Closmann and Bradley, and Chong and Smith.

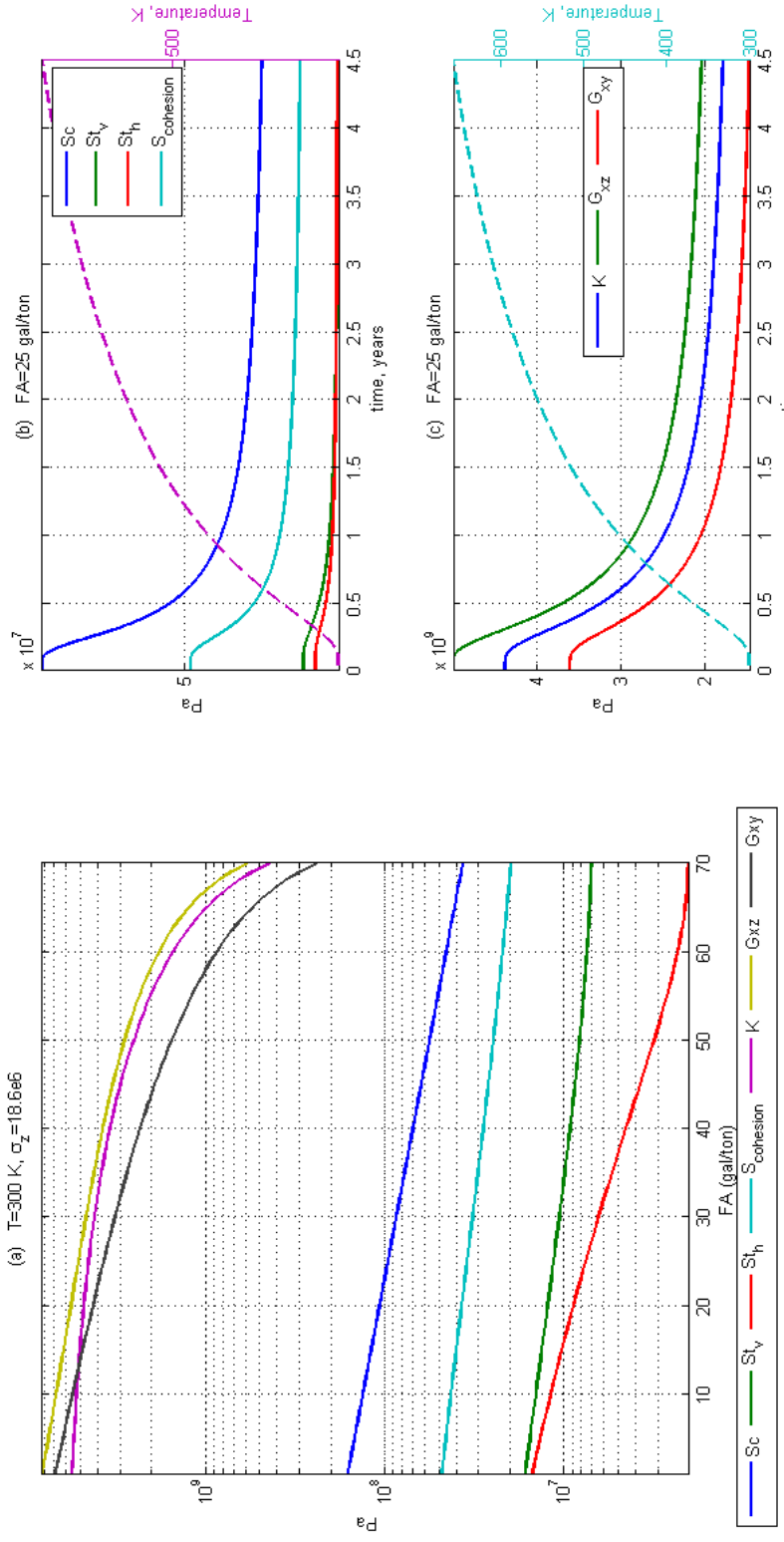

Fig. 4. Oil shale thermal model adapted from Closmann and Bradley, using Chong and Smith to initialize elastic properties.

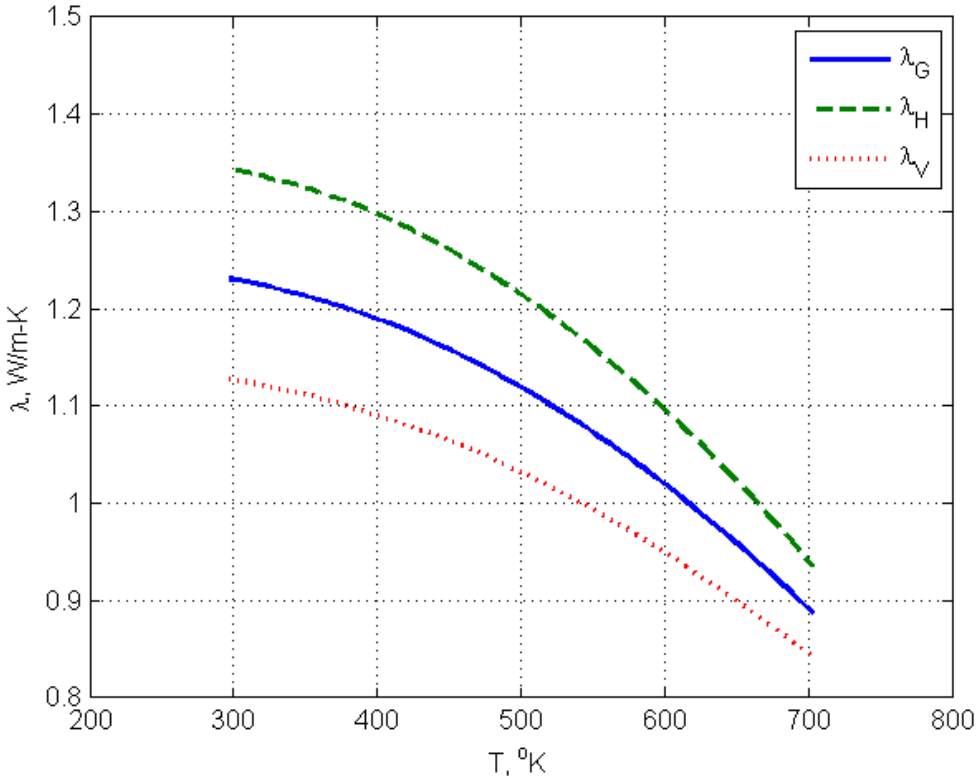

Fig. 5. Prats and O'Brian empirical model of thermal conductivities for 25 gal/ton FA oil shale conductivity as a function of temperature.

Table 1. Component chemical and mechanical properties.

Species	MW	H:C	Density (kg/m^3)	Bulk Modulus (Initial)
Oil	368.7	1.52	910	2.92 MPa
Gas	41.33	2.41	39[6]	2.68 MPa[7]
Coke	12.44	0.357	2200[8]	34.0 GPa
Kerogen	670	1.5	1050	13.79 GPa[9]
Minerals (Dolomite)	N/A	N/A	2750	60 GPa

Table 2. Pyrolysis model.

Reaction (mass basis)	Rate Constant Equations $k_j = A_j \sum_i f_{ji} \exp\left(\frac{E_{ji}}{RT}\right)$
$\underbrace{CH_{1.5}}_{kerogen} \rightarrow_{k_1} 0.669\ \underbrace{CH_{1.52}}_{oil} + 0.178\ \underbrace{CH_{2.41}}_{gas} + 0.153\ \underbrace{CH_{0.357}}_{coke}$	$A_1 = 1 \times 10^{13}\ (s^{-1})$ $f_1 = [0.05 \quad 0.20 \quad 0.50 \quad 0.20 \quad 0.05]$ $E_1 = [49\ 50\ 51\ 52\ 53]\ (kcal/mol * K)$ $\Delta H_{R1} = 370\ kJ/kg$ [34]
$\underbrace{CH_{1.52}}_{oil} \rightarrow_{k_2} 0.566\ \underbrace{CH_{2.41}}_{gas} + 0.434\ \underbrace{CH_{0.357}}_{coke}$	$A_2 = 1 \times 10^{12}, \qquad f_2 = 1$ $E_2 = 54\ \ kcal/(mol * K)$ $\Delta H_{R2} = 126\ kJ/kg$[32]

[6] Approximating the gas as propane at 4.8 MPa and 600 K, about the middle of pyrolysis, McCain [57].
[7] Gas compressibility is considered equivalent with the average pore pressure between time steps.
[8] Density of solid graphite (necessary because porosity is handled separately).
[9] Value at room temperature.

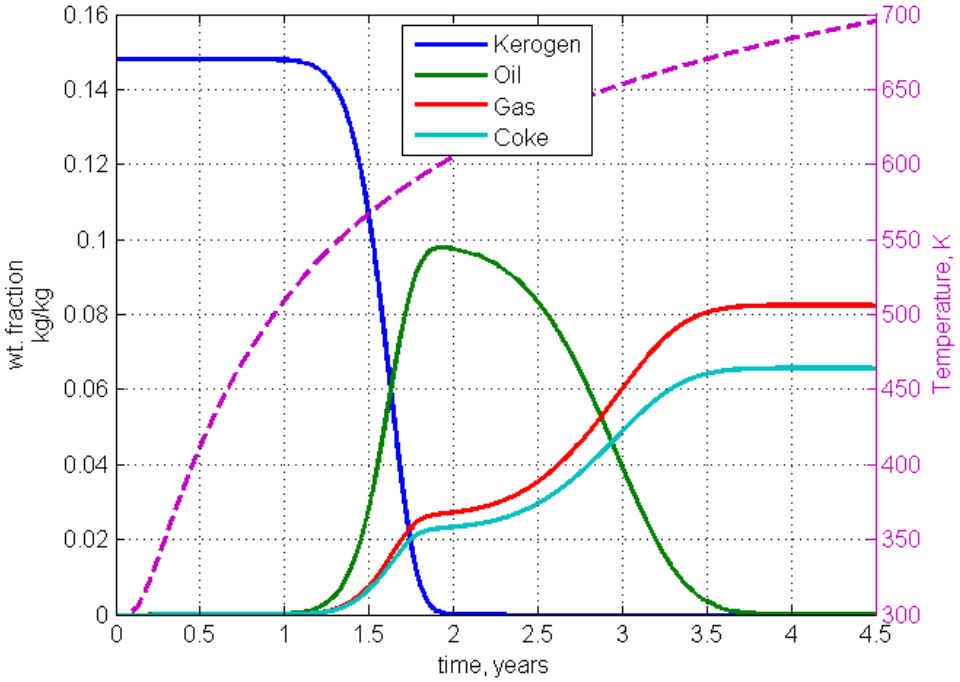

Fig. 6. Nonisothermal kinetics for a position 5 m from the heater (700 K), assuming no fluid advection.

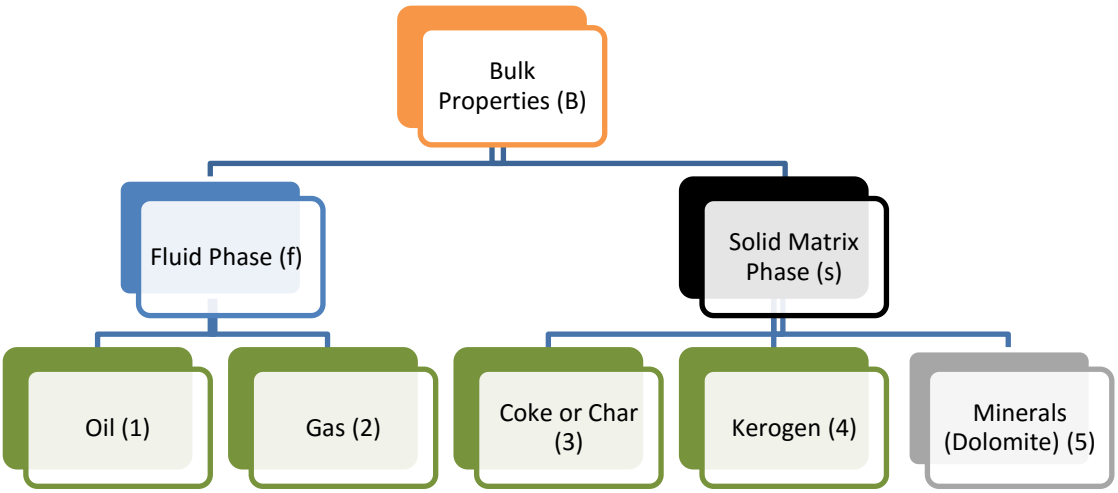

Fig. 7. Hierarchy of material properties.

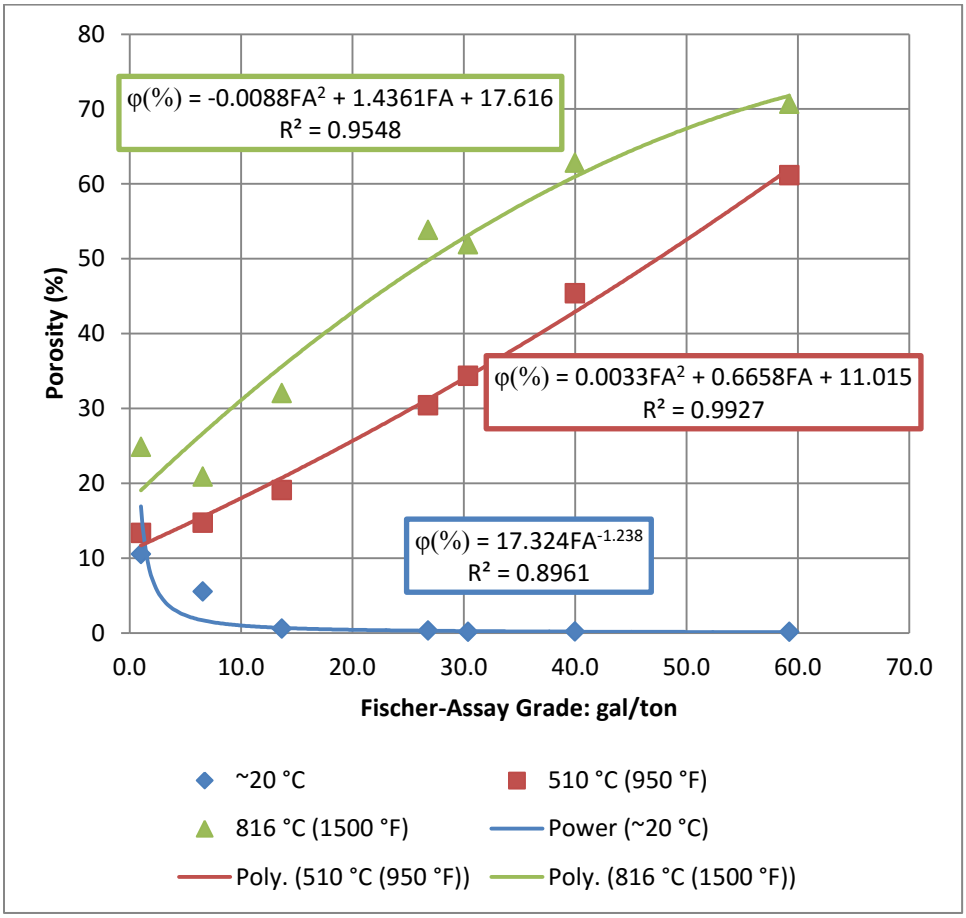

Fig. 8. Porosity of various grades of oil shale at several temperatures.

CHAPTER 3

BOUNDARY CONDITIONS AND IMPLEMENTATION

3.1 Geometry and Structural Boundary Conditions

As seen in Fig. 9, the geometry chosen is a small region of the Mahogany zone, which is 4 x 4 x 6 m (13.1 x 13.1 x 19.7 ft.) The individual cells are initially cubes at one meter to a side. The heat injection well and production well are placed at (0, 0) and (4, 4), respectively. The simulated region, shown in Fig. 10, represents a quadrant of a larger proposed *in situ* program, not unlike pilot projects by Shell Oil [2].

The surface x-y boundaries of the simulated region are fixed due to symmetry with the other quadrants. Interior cells may still deform in x and y. The bottom surface at $z = 0$ is also fixed, to prevent rigid body motion. All external boundary deformation is therefore vertical.

3.1.1 Fluid and Heat Transfer Boundary Conditions

The symmetry used to define boundary conditions in this problem is seen in Fig. 10. The simulated region is one of four quadrants for a single production well. Since symmetrical heat and fluid dynamics exist in all other quadrants (one quadrant is shown in Fig. 10), no fluid or heat transfer passes through the x-y boundaries of the geometry shown in that figure. The top and bottom of the geometry are also impervious to transport phenomena, but this is not a reflection of expected reality.

The heating well is represented by a line of fixed temperature along x-y coordinates (0,0). Initial temperatures in zones along the heater line are averaged assuming a 12-in diameter heater well. No material enters or exits the system from the heater well.

While it is not unheard of for surface oil shale retorts to call for temperatures well over 1000°F, *in situ* heating must be done at lower temperatures to promote due to the long residence time of produced fluids. Greater temperatures reduce the time to heat through the well, but also reduce the amount of oil produced in pyrolysis. For this simulation, the heater temperature was set to 620°F (600 K). Once the cells near the production well have reached 440°F, fluid drainage is allowed in the production well. The production well is represented by zones bordering x-y coordinates (4,4). Fluids may leave the geometry by leakage from the production well when the zones have reached pyrolysis temperatures.

3.1.2 Alternative Heating Well Program (Inactive)

Code was written to modify the heater temperature depending on conditions at the production well. Although it was not active in the final implementation, the code represents one path a pyrolysis production plan might use in a commercial well. The heater is initially set at 620°F (600 K). Once the cells near the production well have reached 206°F (370 K), the heater temperature is gradually brought up to 800°F (700 K) at approximately[10] of 0.45°F (0.25 K) a day. Once the cells near the production well have reached 440°F and fluid begins draining, the heater would be brought back down to 620°F (600 K).

[10] Based on the default time-step size in the simulation, but this may be reduced by FLAC3D™ to ensure a stable numerical solution.

3.2 Initial Conditions and Driving Forces

The initial conditions are included in Table 3. The initial conditions include values based on measurements, averages, and computational expediency.

The overburden stress and pore pressure are estimates based on the average burial depth of the Mahogany zone. Oil shale richness is the average amount of oil that can be extracted from Mahogany Zone samples, using the Fischer Assay (FA) method. Fischer Assay should be considered a measuring stick, rather than a true indicator of the total oil that can be extracted. Temperature is based on a curve fit to actual Piceance Creek bottom-hole temperature data [47].

Porosity was set at 0.02 for numerical stability. The true initial porosity is likely much less (closer to 0.003, based on data summarized by Cameron Engineers [43]), but using extremely low values of porosity typically led to numerical instability. Permeability was set unrealistically large to aid faster solution time.

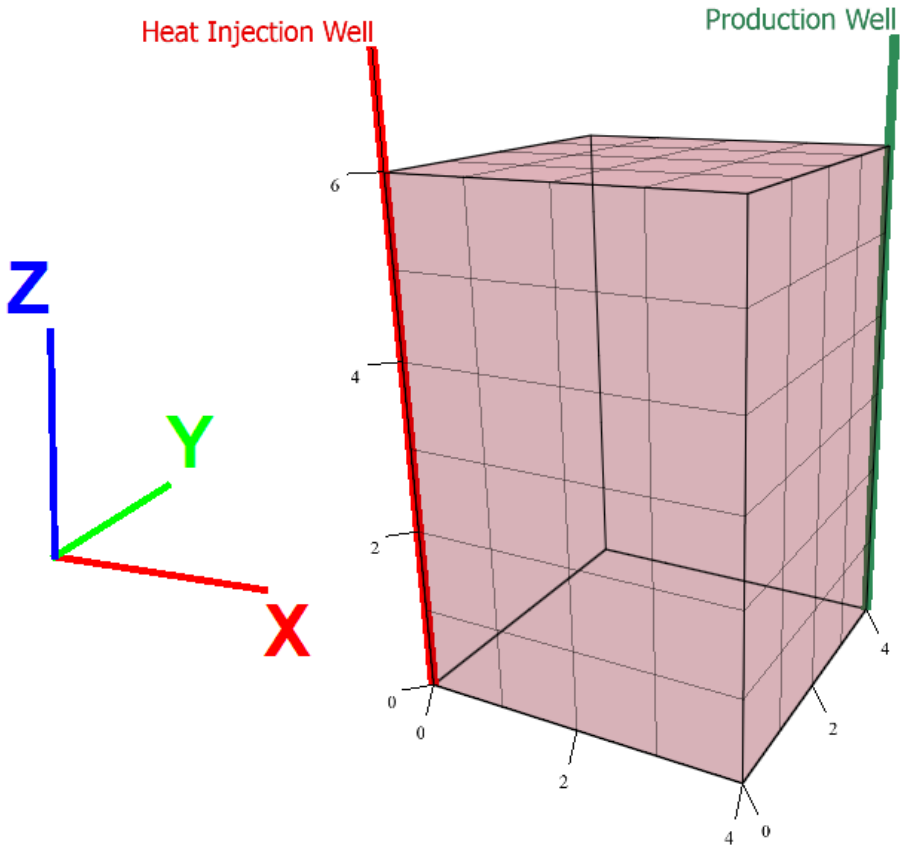

Fig. 9. Geometry of oil shale used in simulation. Measurements are in m.

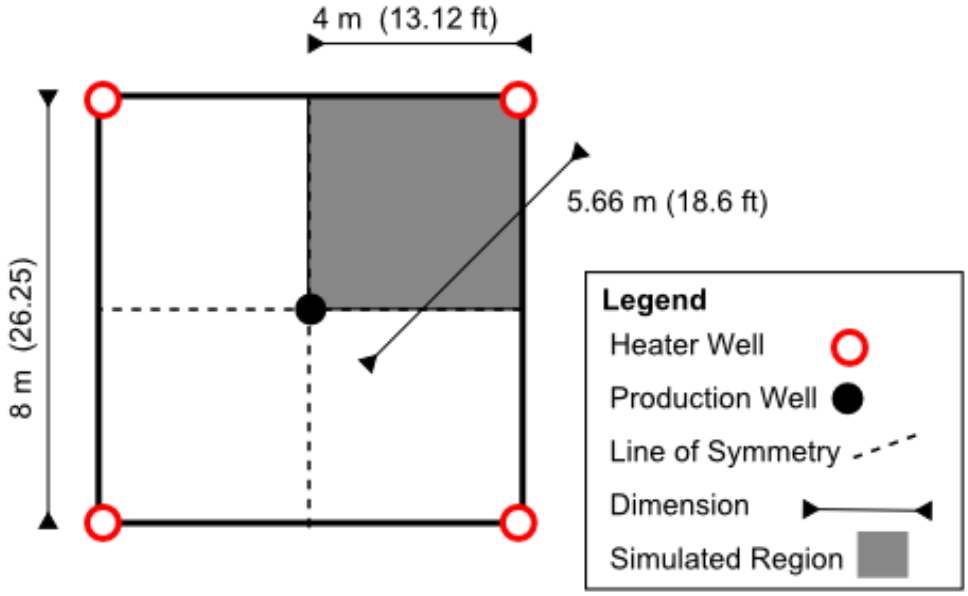

Fig. 10. Top-down schematic of geometry.

Table 3. Initial conditions of simulation.

Initial Condition	Value
Overburden Stress	942.7 psi (6.5 MPa)
Pore Pressure	394.5 psi (2.72 MPa) Geometry 388.7 psi (2.68 MPa) Out Well
Oil Shale Richness (Fischer Assay Yield)	25 gal/ton
Temperature	96°F (35.5 °C, 308.5 K) [47]
Porosity	0.02
Permeability (geometry)	4.94 mD $(5 \times 10^{-15}\ \mathrm{m}^2)$
Viscosity	0.2 cP (0.0002 Pa·s)

CHAPTER 4

RESULTS AND CONCLUSIONS

Few studies attempt to resolve subsidence while allowing for multiphase chemistry. There may not be an analytical solution to the problem, and numerical simulations are limited by software. While verification of the simulation would require a pilot scale test, individual models were validated using theoretical correlations.

4.1 Heat Transfer Validation Testing

The resulting simulation represents a highly nonlinear system. While we cannot verify the correctness of the complete model, it is still possible to test the correctness of the constitutive models in the system.

Nicholson [48] developed an analytical solution for heat transfer from a cylinder with a fixed temperature into an infinite medium. A numerical approximation was developed and plotted by Carslaw and Jaeger [49]. To validate heat transfer in the mesh, the following changes were made. The heater well in the simulation was usually represented by a line, but was expanded into a 1-m cylinder of constant temperature for validation. Because the cells are approximately 1-m blocks, an equivalent system had to be defined using geometry, per Fig. 11.

The pyrolysis simulation was run with all modules off except for heat transfer. The geometry was expanded to 15 m in the *x* and *y* directions to reduce boundary effects from

insulated walls. The temperature was tracked in at grid points where $x=y$ over timesteps of 2160 s (to better capture earlier Fourier numbers). The data were nondimensionalized as follows. Temperature results were nondimensionalized per Equation 55

$$\frac{T - T_0}{T_h - T_0} \tag{55}$$

where T_0 is the initial reservoir temperature and T_h is the heater well temperature.

The curves in Fig. 12 represent the heat transfer Fourier number[11] through the profile, as seen in Equation 56.

$$F_o = \lambda t/(\rho_B C_p r_h^2) \tag{56}$$

Transient heat transfer in the simulation compares well with Carslaw and Jaeger's work. Some of the early time inaccuracy may be due to temperature dependence of heat capacity and thermal conductivity. Thermal properties were calculated based on the average of the heater and baseline reservoir temperature (358°F). Additionally, the coarseness of the mesh and the insulated boundary conditions may contribute to errors. Time values were determined for the plotted Fourier numbers in Table 4 to aid interpretation of the thermal validation.

4.2 Full Simulation Results

Remembering Fig. 9 in Chapter 3, temperature, pressure, composition, and volumetric fraction data were tracked at several locations in the geometry, using a coordinate system with the heater well at the origin. While not all modules can be validated, the overall model may still be instructive of how the different forces interact.

[11] The Fourier number is the ratio of conductive heat transfer to heat storage rate.

The temperature history at several coordinates (m) in the model geometry is represented in Fig. 13. At approximately the 3-year mark, the results are visibly skewed by the insulated boundary conditions. These results are more representative of a large oil shale operation, with mirrored boundary conditions on each side of the system than what one would expect for a single-heater well operation. Oil shale's low thermal diffusivity results in a significant temperature gradient between the heating and production wells.

The pressure profile history seen in Fig. 14 is somewhat surprising. Due to the author's choice in permeability,[12] there is very little difference between the pressure development at the heater and the production well in the first two years. Early-time fluid results in a massive pressure increase because the fluid cannot escape the geometry. This is because permeability at the production well is essentially nonexistent. Fracturing might be predicted for this pressure, but no mass was left in the pseudo-fracture module at the conclusion of the simulation.

4.2.1 Composition Results

Volume fractions, shown in Fig. 15, were calculated for each component because porosity and other important mechanical properties are volumetrically averaged. Volumetric fractions are not as straightforward to calculate as mass fractions because volume is not strictly a preserved property. Even though ideal mixtures are assumed, each component is still subject to compression or expansion due to the relative compressibility of species. Additionally, the author had to implement several functions to ensure that volume fractions remained realistic.

[12] The assigned permeability was the highest value the software could give a stable solution for, in an attempt to test drainage. A more realistic value of permeability is approximately 5 orders of magnitude smaller.

The most valuable information in Fig. 15 is the production and drainage of fluids in key locations of the geometry. The volume fractions of oil (χ_1) and gas (χ_2) demonstrate how porosity develops over time (assuming 100% saturation of fluids), and may be used to help validate fluid transport. The nonreactive mineral fraction (χ_5), while not plotted, plays a critical role to ensure that porosity remains semirealistic in the simulation. To concern mass and avoid unrealistic compression of solid components, porosity has both minimum and maximum values. If porosity goes below 0.01, the simulation halts transport of fluid out the affected cell. If porosity goes above the initial organic fraction ($1 - \chi_5$), the fluids are compressed down to a more representative fraction (and a corrected pore pressure is calculated). The author has since discovered that this pressure correction was not actually assigned to zones. The density and volumetric corrections were implemented without also assigning the pressure correction. This error likely affected the expansion or compression of each cell at it adapted to pressure changes.

The correction to porosity shows as a sharp change in the volumetric fractions of each species. While the correction may be too stiff, choosing a smoother correction was beyond the scope of this study. Volume and density are interdependent. Both are modified by changes in stress and fluid flow; therefore, they could not be solved simultaneously by the author.

The mass fractions of each organic component are plotted in Fig. 16. Per the chosen reaction model adapted from the Burnham and Braun [1], oil is an intermediate product of pyrolysis. Porosity is increased by the pyrolysis of kerogen into oil and gas, but the reaction model also predicts that most of the oil will further decompose into gas and char.

Fig. 16 also shows that multicomponent fluid is moving through the reservoir. Because FLAC3D™ was not intended for multicomponent fluid movement, an in-house set of functions was developed in FISH (the coding language in FLAC3D™) to enable this functionality. Gas transport w_2 is the most direct evidence that the module is functional. Gas is an end product, so it can only decrease in the simulation through fracture loss and cell-to-cell drainage. No fluid was lost in the fractures in the final implementation.

A rich set of variables is behind varying curves seen oil and gas mass over time as one moves from the heater well (0,0) to the production well (4,4). The oil mass fraction w_1 rises and falls most dramatically near the heater due to rapid heating. The central (2,2) and production (4,4) cells only vary in temperature from each other by about 10 degrees, per Fig. 13, but their respective component profiles in Fig. 16 still vary considerably. While it is unclear how much oil moves cell to cell in the simulation, the gas transport in Fig. 15 was confirmed to be draining from the production well (4, 4).

Drainage is limited in the central cells, and does not appear to be a major factor at the heater well. This is most likely the result of a bug. Safeguards were created in the pyrolysis program to avoid letting mass or volume fractions go below zero due to mass flux or chemical reactions. If the oil mass fraction actually goes to zero, the safeguards unintentionally halt all movement of species in or out of a cell by changing the reaction time-step to zero. This may explain why oil and gas movement would stop in the production and center cells when the oil fraction goes to zero.

A minor amount of heave was observed in the simulation, per Fig. 17. While improvements are required in the drainage model, this situation is certainly possible. As

kerogen decomposes into fluids, there is an increase in pressure and porosity. The relative compressibility of the products and their drainage rate could result in either swelling or compaction. In this particular implementation, the opposing pressure-volumetric interactions mostly cancelled out each other.

A module was written to handle the potential for fracture formation in the geometry, but was not activated in the final implementation of the simulation. This approach to handling fractures may be of assistance to later researchers who wish to address the potential. Future studies seeking to simulate oil shale pyrolysis *in situ* need to account for the formation and transmissibility of fractures in oil shale undergoing pyrolysis.

Fractures could greatly aid heat or mass transfer through the material. Oil shale is such an excellent thermal insulator that even minute amounts of flow would result in a major improvement on heat transfer, as well as helping to produce oil.

4.3 Opportunities for Future Research

The model could be improved by a better understanding of pressure-volume behavior of the system during pyrolysis. This system assumed that volumes were additive and that all mixed properties met an ideal model. Future investigators might consider implementing more complex models, to improve pressure-volume calculation accuracy.

Previous models of oil shale often struggle to account for the large material transformation that occurs during pyrolysis. Empirically developed oil shale mechanics models encountered by the author are unable to account for failure modes after pyrolysis is initiated.

4.3.1 Challenges of Simulating *in situ* Pyrolysis

Future researchers may seek to improve or validate the proposed approach to problems of in- situ pyrolysis. This model allows for changes in porosity and makes mechanical properties dependent on composition, deformation of the rock, and fluid drainage. Additionally, modules were implemented to try to account for fracturing and volume sources due to fluid generation. Biot's linear model for consolidation, as implemented in FLAC3D™ was designed with a single-phase fluid in mind with unchanging properties, so liquid and gas components were approximated as a single "fluid" phase.

A robust simulation of *in situ* pyrolysis, including deformation, is not for the faint of heart. Linear approximations of nonlinear systems generally assume that the system stays within a small range of the average answer. This assumption fails spectacularly with oil shale, because the system goes through extremes that will challenge every numerical method to represent them. The porosity goes from zero to as much as 30-40% for richer oil shales. Changes in permeability are also known to be dramatic (but were not included in this study due to model and software limitations).The mechanical strength goes from about 3.8 MPa to almost zero, and elastic properties follow suit. The fluid phase bulk modulus goes from 5 MPa to 100 kPa, depending on the liquid-gas composition. Difficulty in representing oil shale subsidence will be a problem for every simulation. The challenges encountered in this investigation are not unique to FLAC3D™.

4.3.2 Variable Permeability and Phase Behavior

Variable permeability cannot be effectively modeled in FLAC3D™. Indeed this limitation may be a problem for other software packages, as flow must be able to resolve for variable transmissivity in adjacent cells that also have pressure gradients.

The study of oil shale production requires a permeability model that includes a dependence on FA richness, extent of pyrolysis, pressure, and temperature. Other investigators agree that this model would be very difficult to develop due to limitations in hardware and detection capability at *in situ* pyrolysis conditions.

4.4 Conclusions

The author has proposed a method of developing a stable simulation of *in situ* oil shale pyrolysis. The proposed oil shale mechanics model (while imperfect) allows for changes in porosity, composition, temperature, strength, and elasticity while allowing for fluid drainage. The hybrid model was made by incorporating Chong and Smith's robust empirical oil shale mechanics with Closmann and Bradley's thermally dependent correlations for subpyrolysis oil shale. Subsidence and fluid drainage were then implemented with Biot's linear poroelasticity model. Changes in porosity and mechanical properties were determined by using ideal mixture rules by volume. The gas and liquid phases were combined into a single fluid phase, which yields a saturation of 100%. The porosity is defined by the fluid volume fraction of the system.

The kinetics model is also a hybrid, combining a model for Type I oil shale by Burnham and Braun [32]with molecular weights adapted from Bauman and Deo [50]for Type II oil shale (which includes Green River) into a 4-organic component system. The yields were estimated using experimental data from Skyline Fischer Assay [39].

This model represents the first known attempt to account for oil shale's subsidence potential. No significant subsidence or heave was observed in this simulation, due to a balance of volume and pressure interactions. In the attempt, this work encountered and overcame many potential pitfalls of multiphysics problems in rock mechanics.

The program atlas and code available in the appendices demonstrate methods of adding new physics modules to FLAC3D™. This investigation also provides an example of how to include poroelastic effects and subsidence into an *in situ* pyrolysis simulation, while addressing many of the potential hazards of such an implementation. In this study, several useful formulae were independently derived. These and discussions of variables that could not be included in the simulation are found in the Appendices.

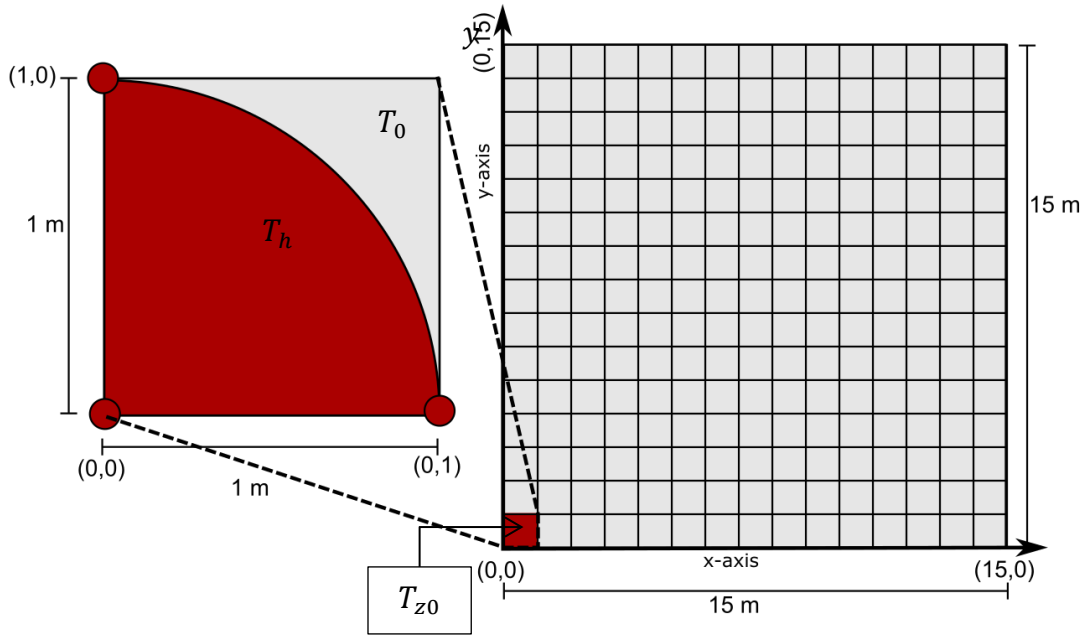

Fig. 11. Thermal validation geometry.

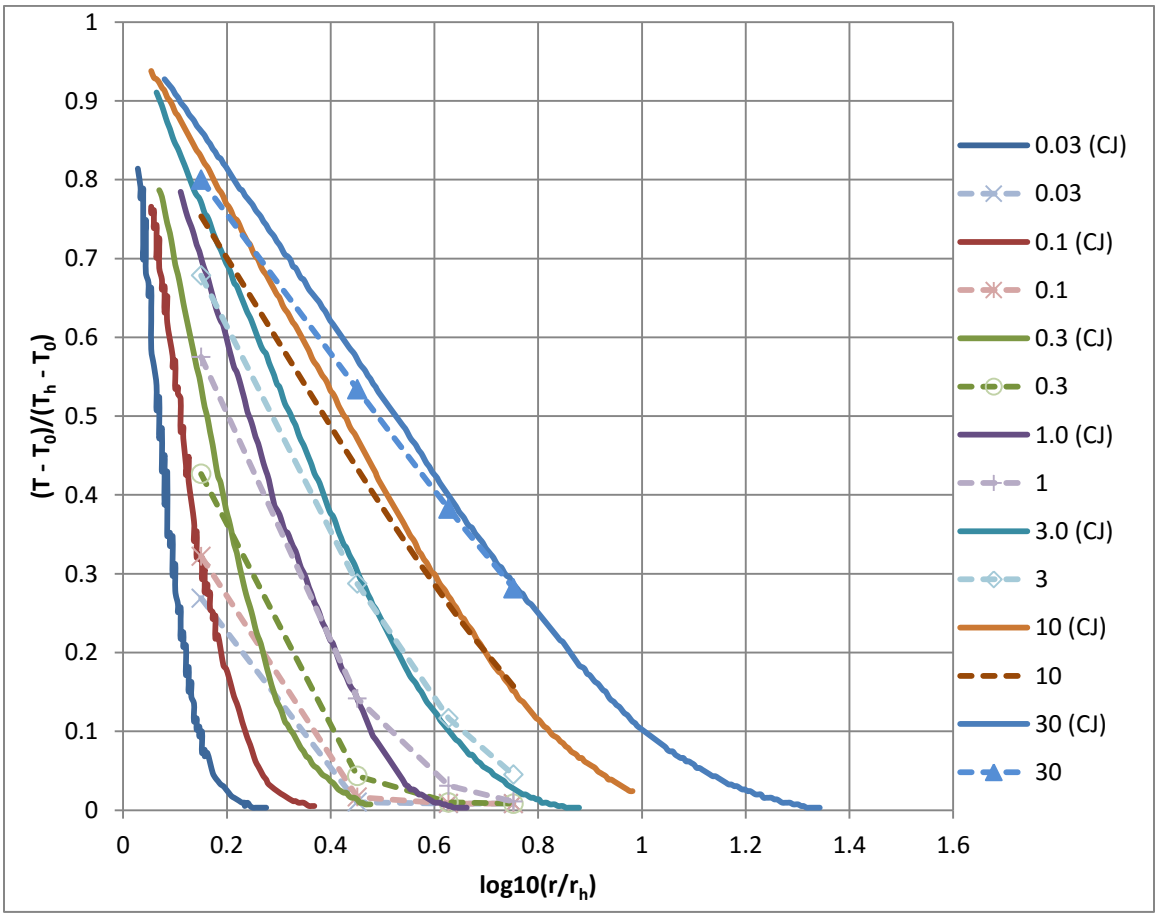

Fig. 12. Dimensionless temperature profile over dimensionless distance from the heater for different values of the Fourier number.

Table 4. Fourier numbers and equivalent time.

	Approximate Time		
Fo	s	days	years
0.03	6.11E+04	0.71	0.002
0.1	2.04E+05	2.36	0.006
0.3	6.11E+05	7.08	0.019
1	2.04E+06	23.6	0.065
3	6.11E+06	70.8	0.194
10	2.04E+07	236	0.646
30	6.11E+07	708	1.939

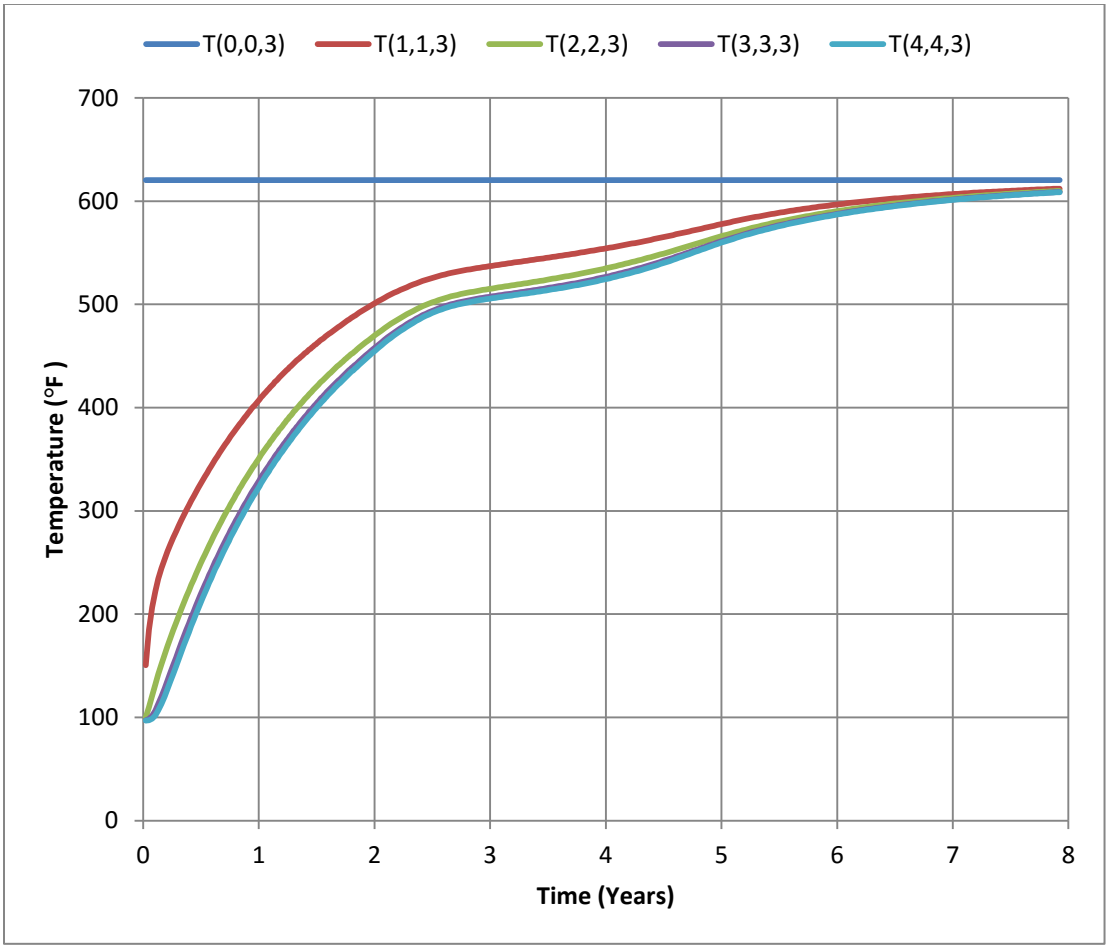

Fig. 13. Thermal history/profile of oil shale at several coordinates (measured in m), relative to the heater well (0,0).

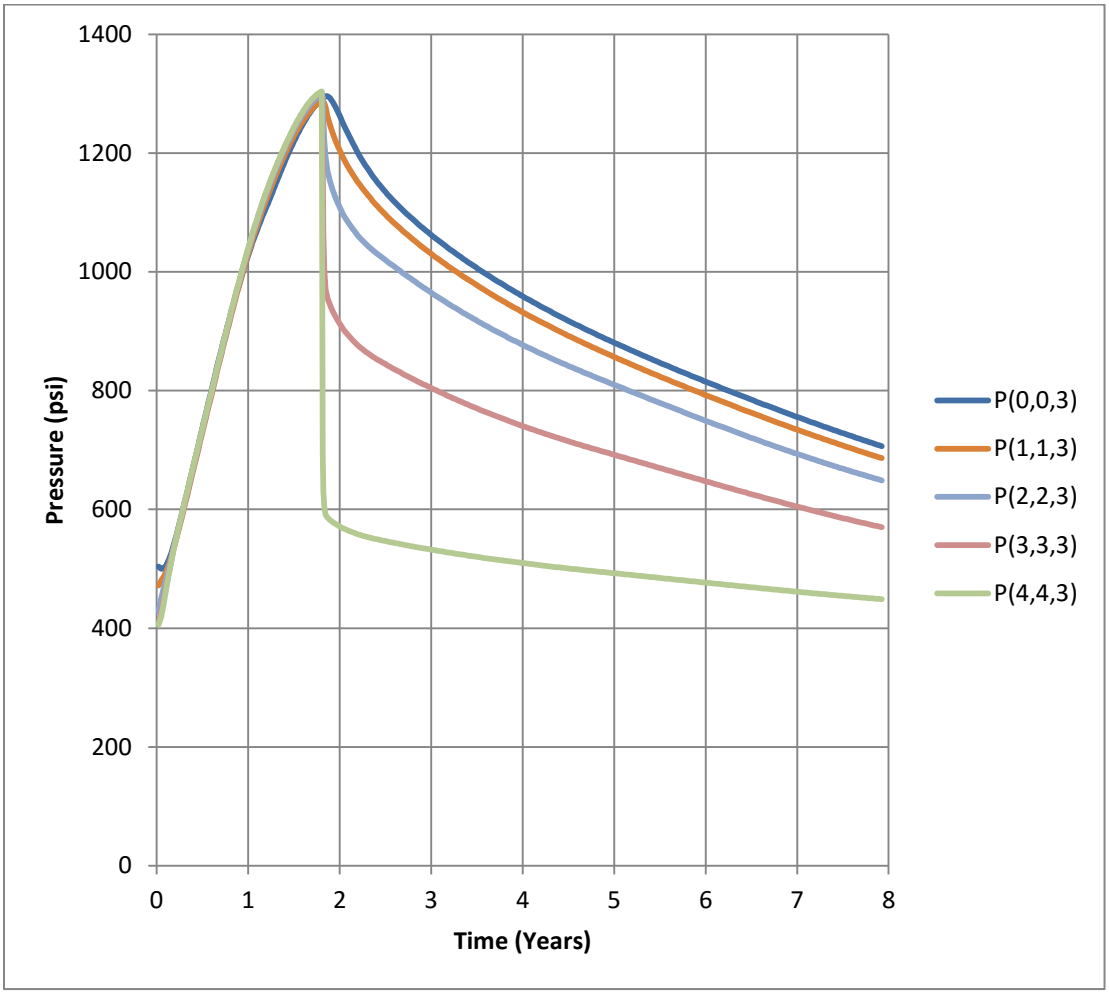

Fig. 14. Pressure history at at several coordinates (measured in m), relative to the heater well (0,0).

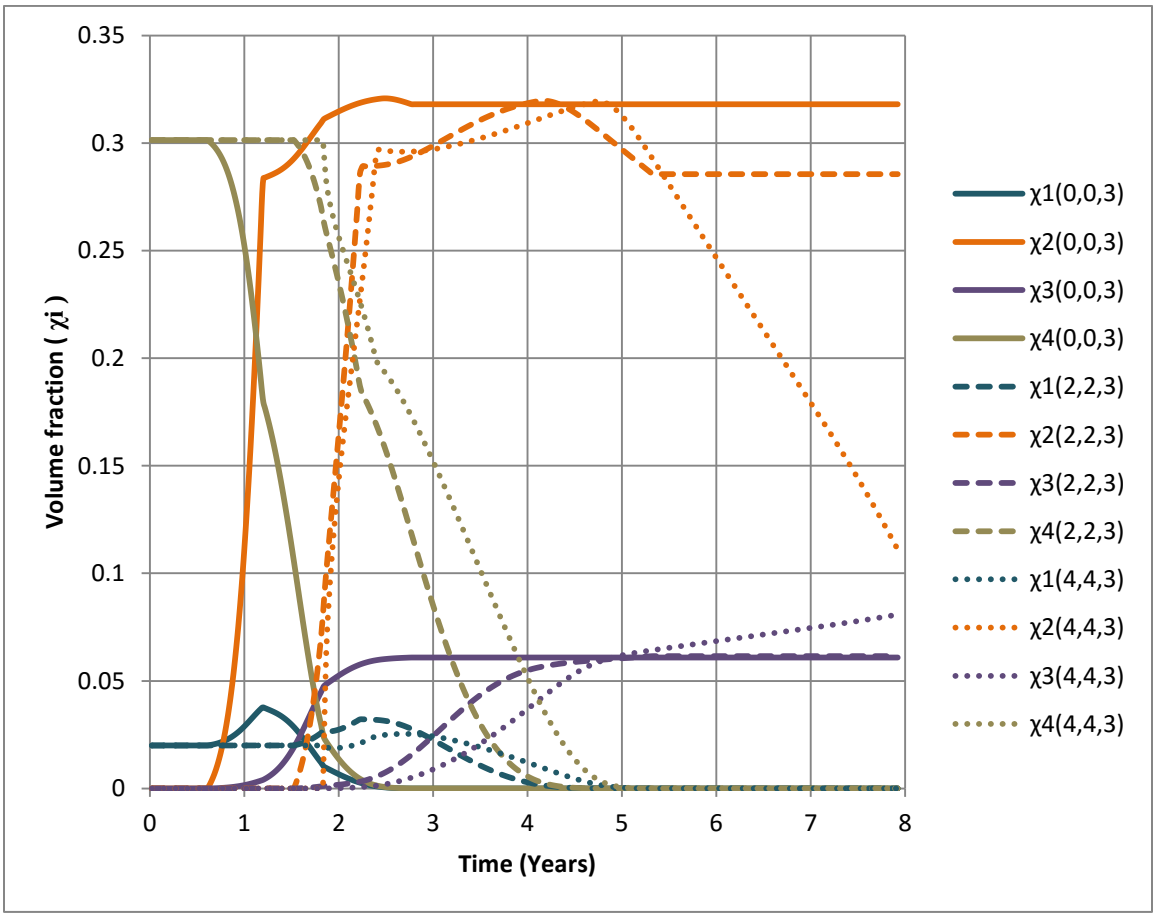

Fig. 15. Composition at center of geometry, by volume fraction. χ_1 is oil, χ_2 is gas, χ_3 is coke, χ_4 is kerogen.

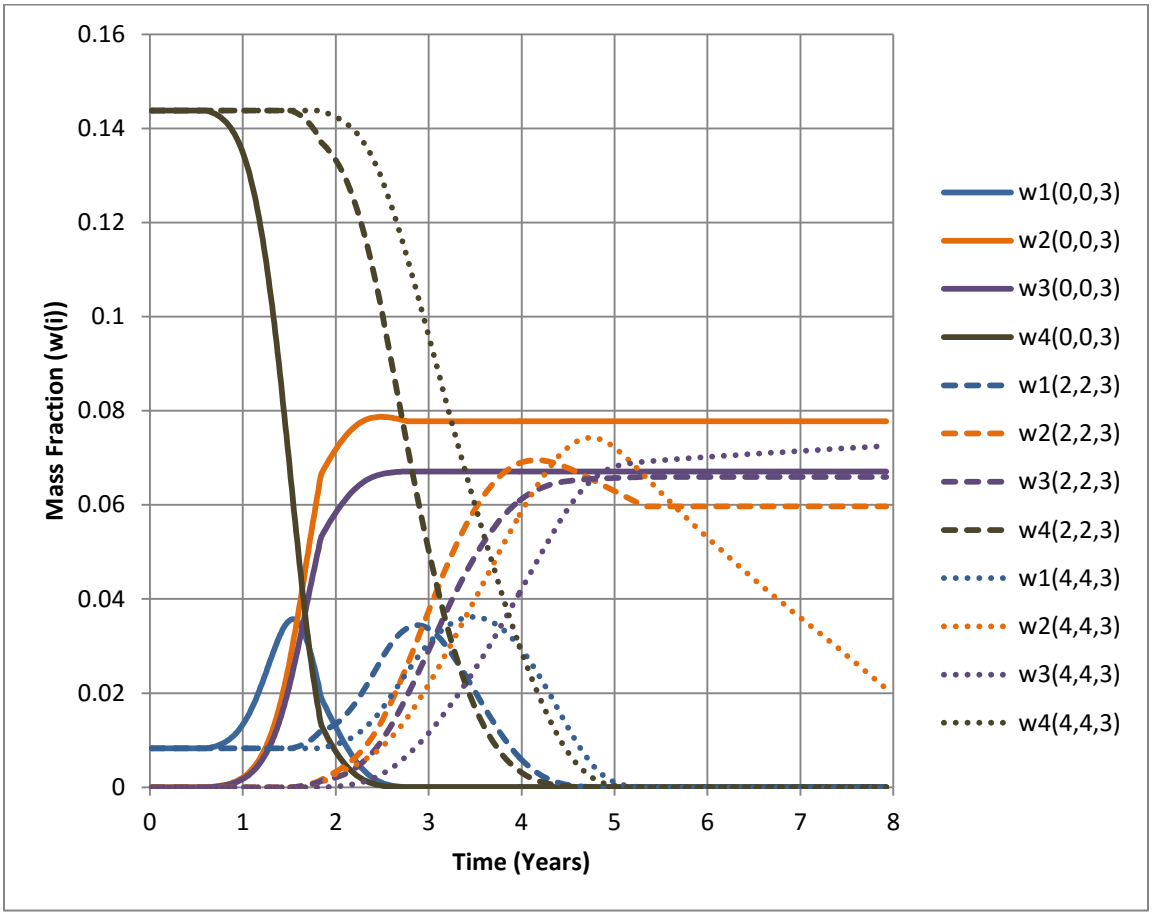

Fig. 16. Mass fraction history at coordinates relative to the heater well. w_1 is oil w_2 is gas, w_3 is char and w_4 is kerogen.

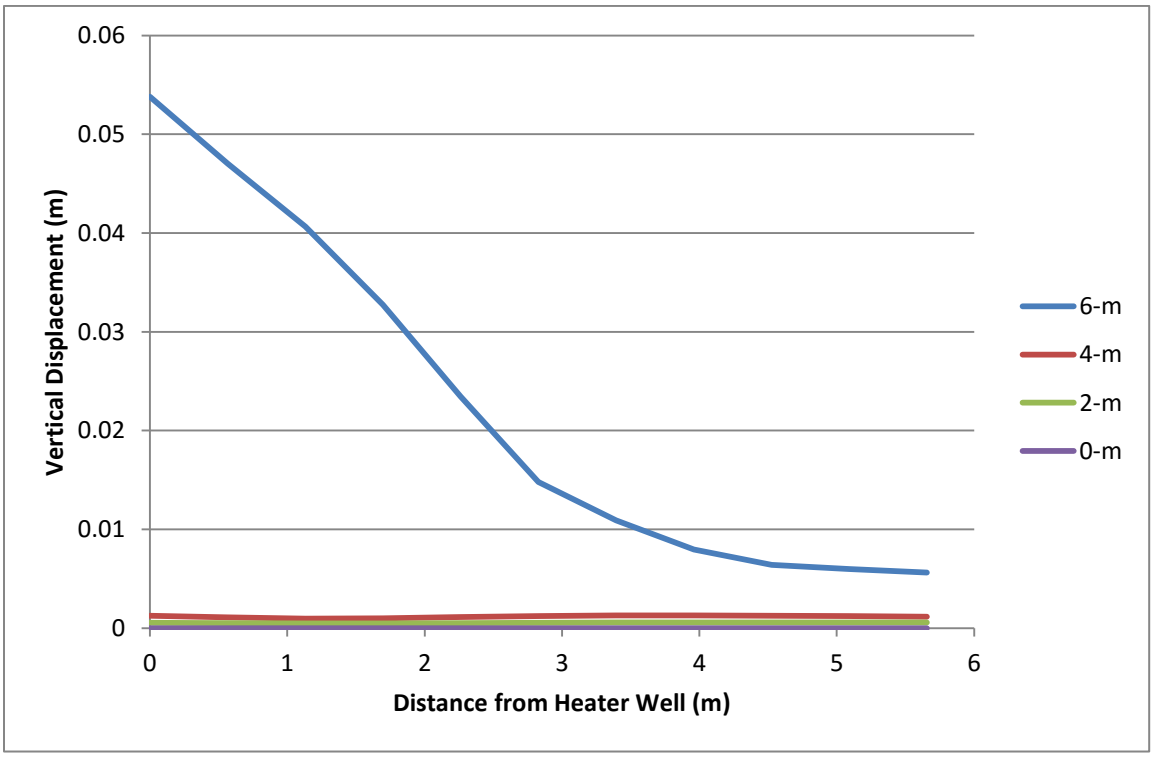

Fig. 17. Heave or subsidence (in m) of oil shale between the heater and production wells at the conclusion of pyrolysis and drainage, taken at every 2 m vertically from the deepest (0 m) to the most shallow (6 m) layers of the geometry.

APPENDIX A

FLAC3D SIMULATION PROGRAM ATLAS

A series of program maps and flowcharts was developed to ease analysis of the methods used to code this simulation. The actual code, written in FISH, can be found in Appendix B.

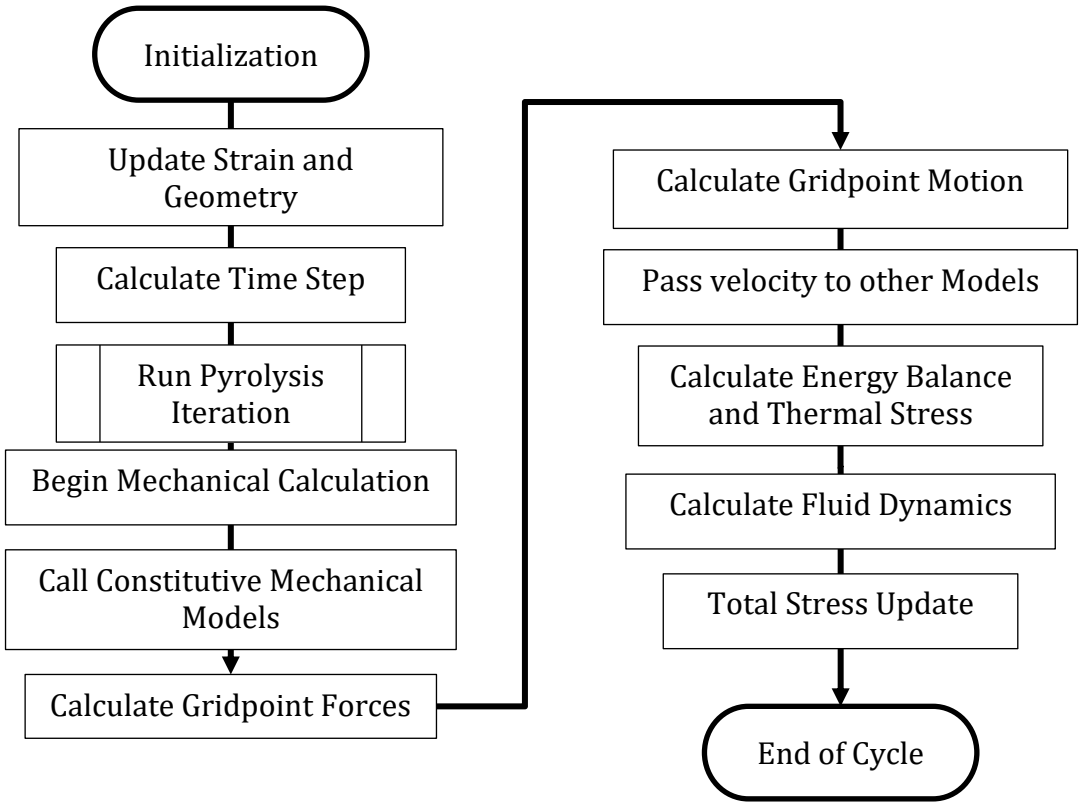

Fig. 18. FLAC3D™ calculation flowchart.

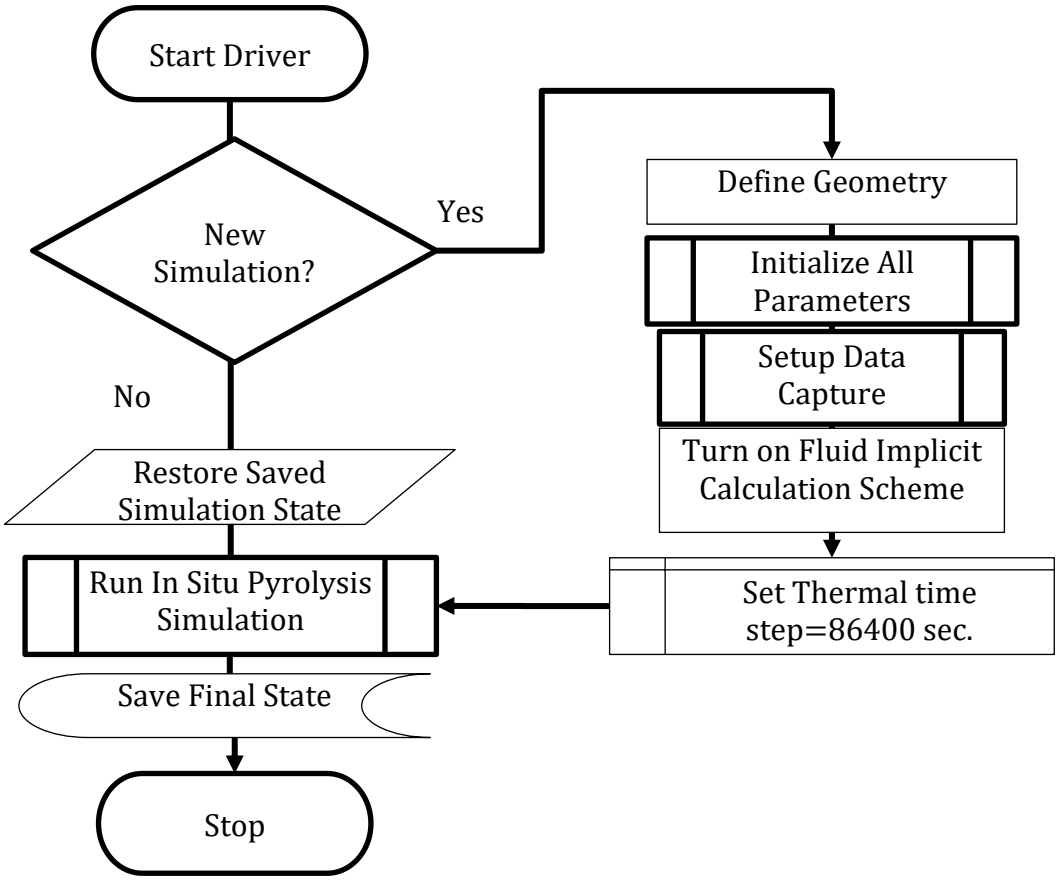

Fig. 19. Simulation driver flowchart.

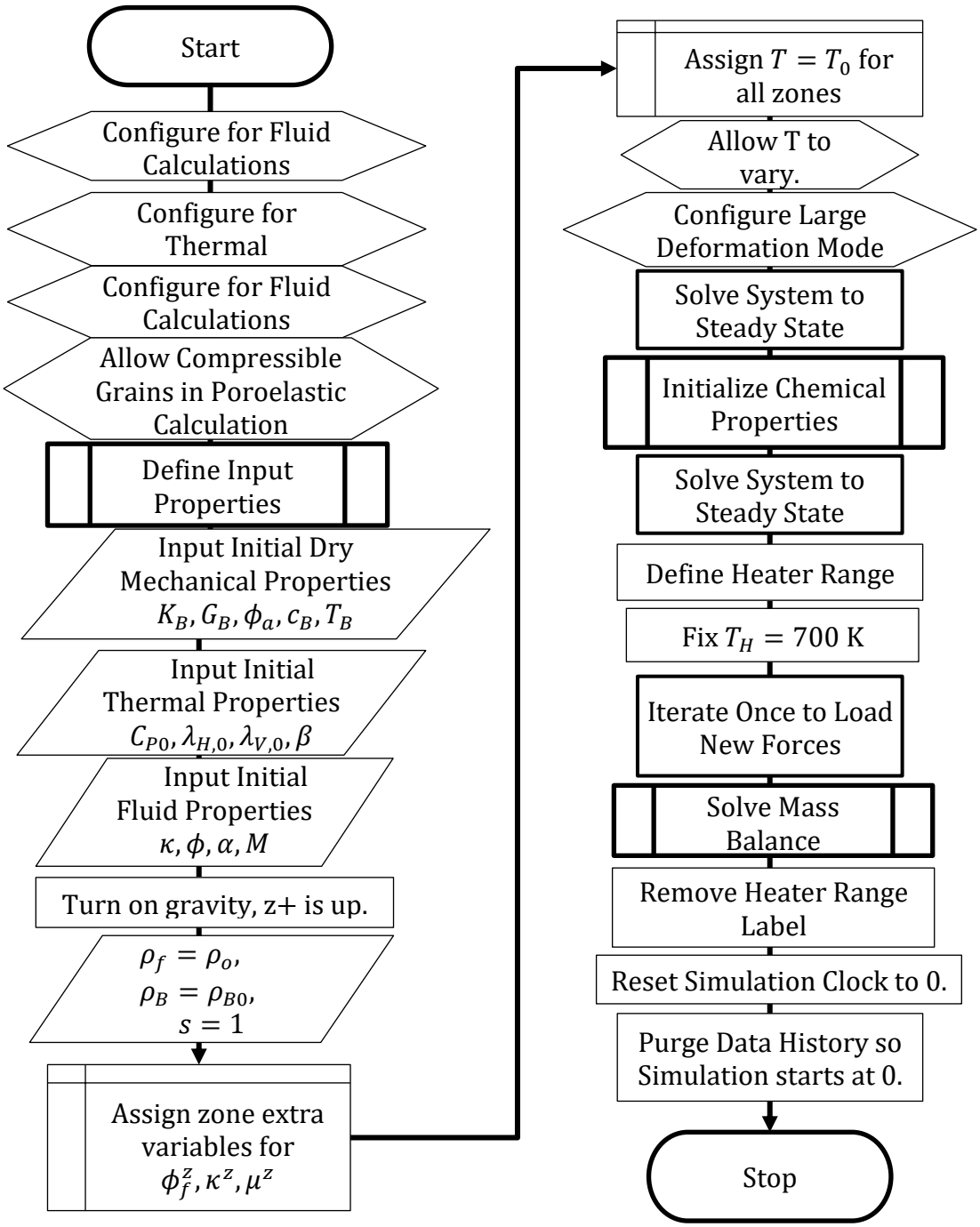

Fig. 20. Initialization flowchart.

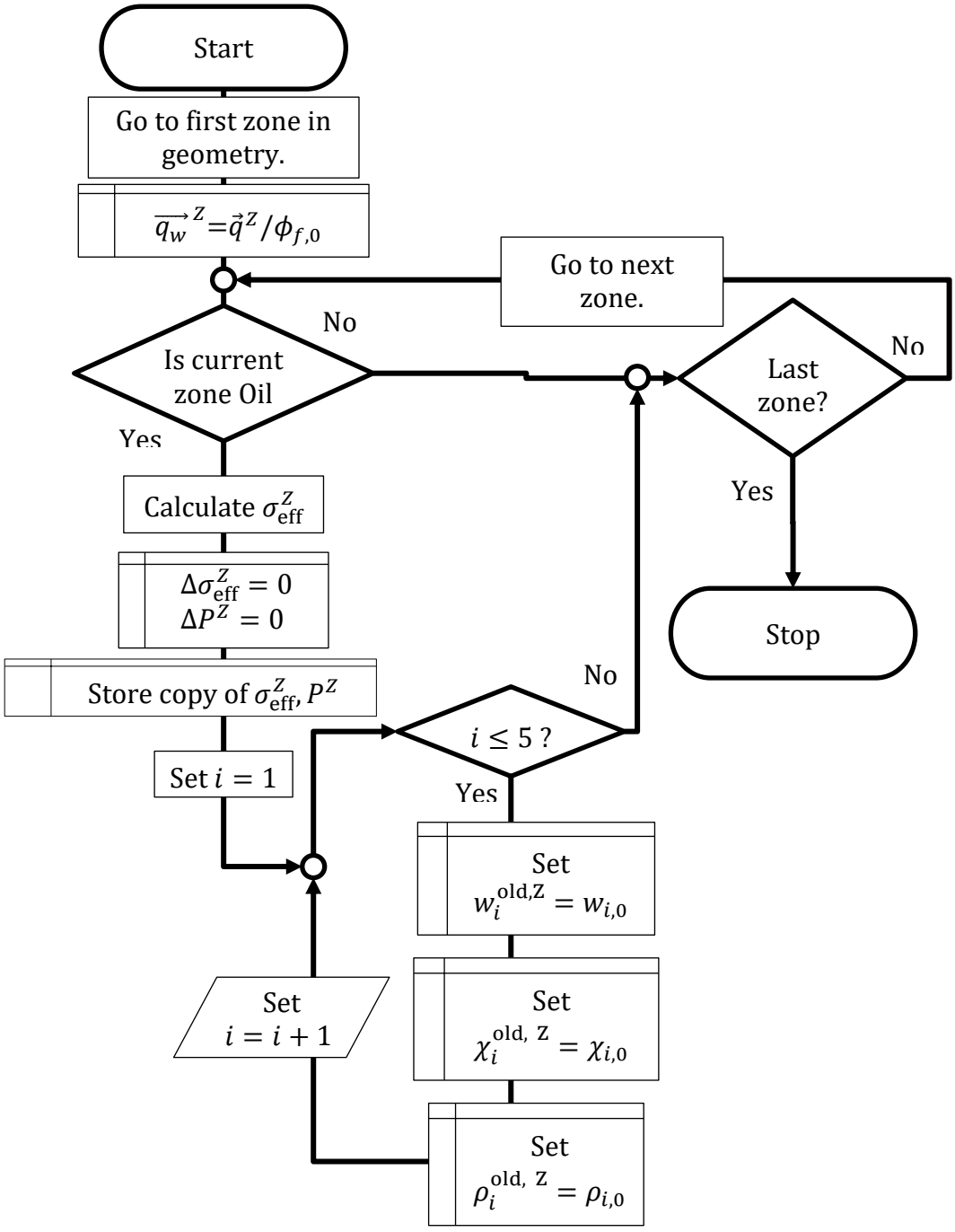

Fig. 21. Initialize chemical properties flowchart.

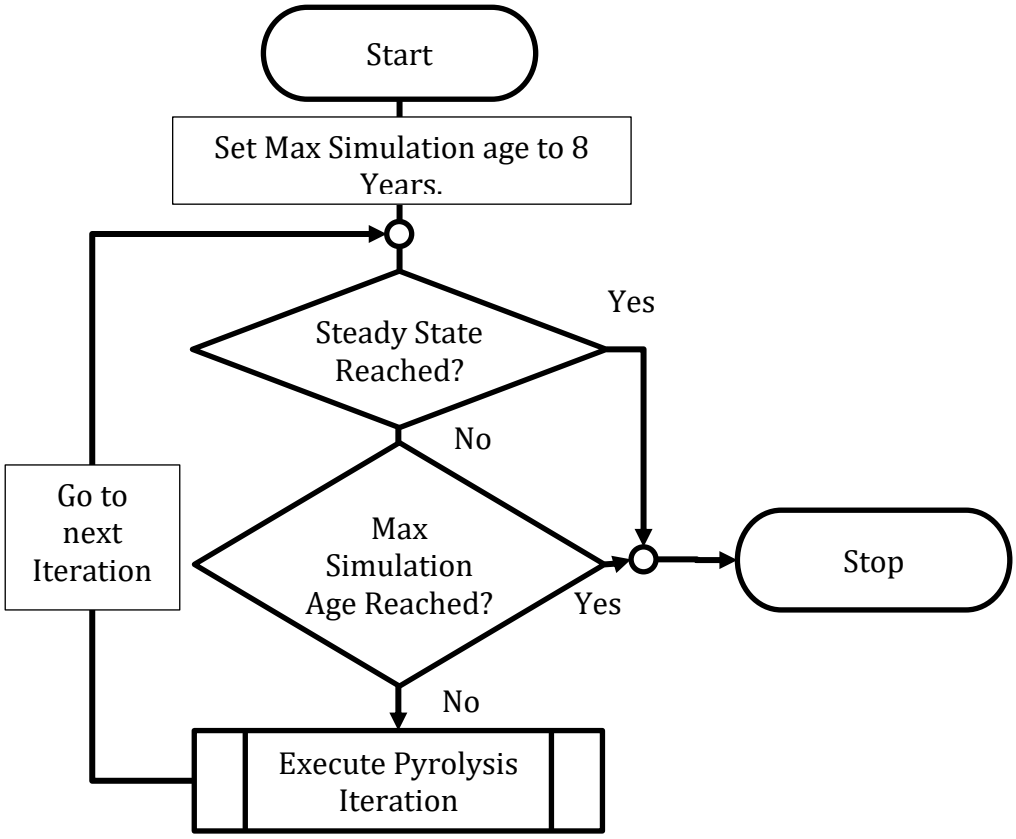

Fig. 22. Pyrolysis program: outer loop.

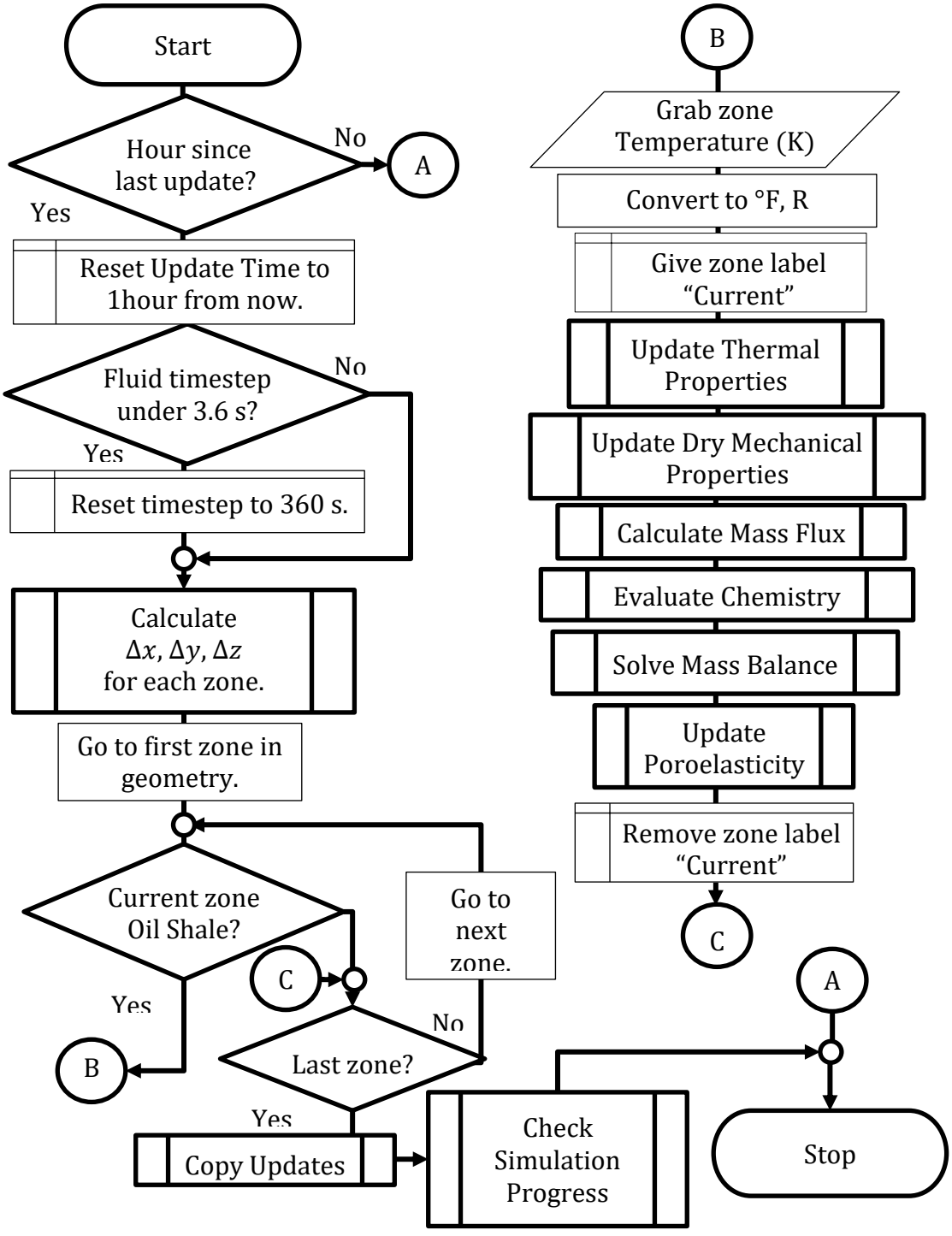

Fig. 23. Pyrolysis program: iteration flowchart.

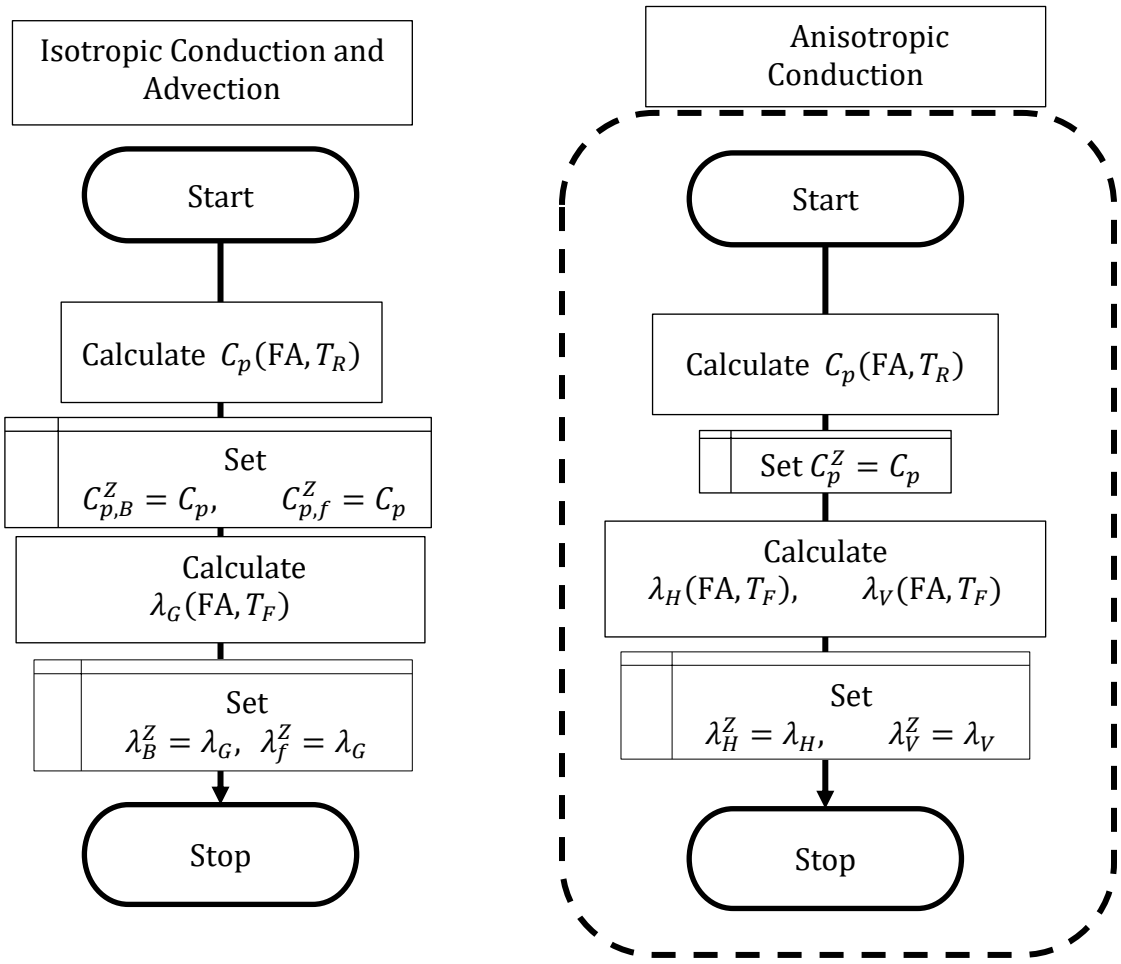

Fig. 24. Pyrolysis program: thermal properties update flowchart.

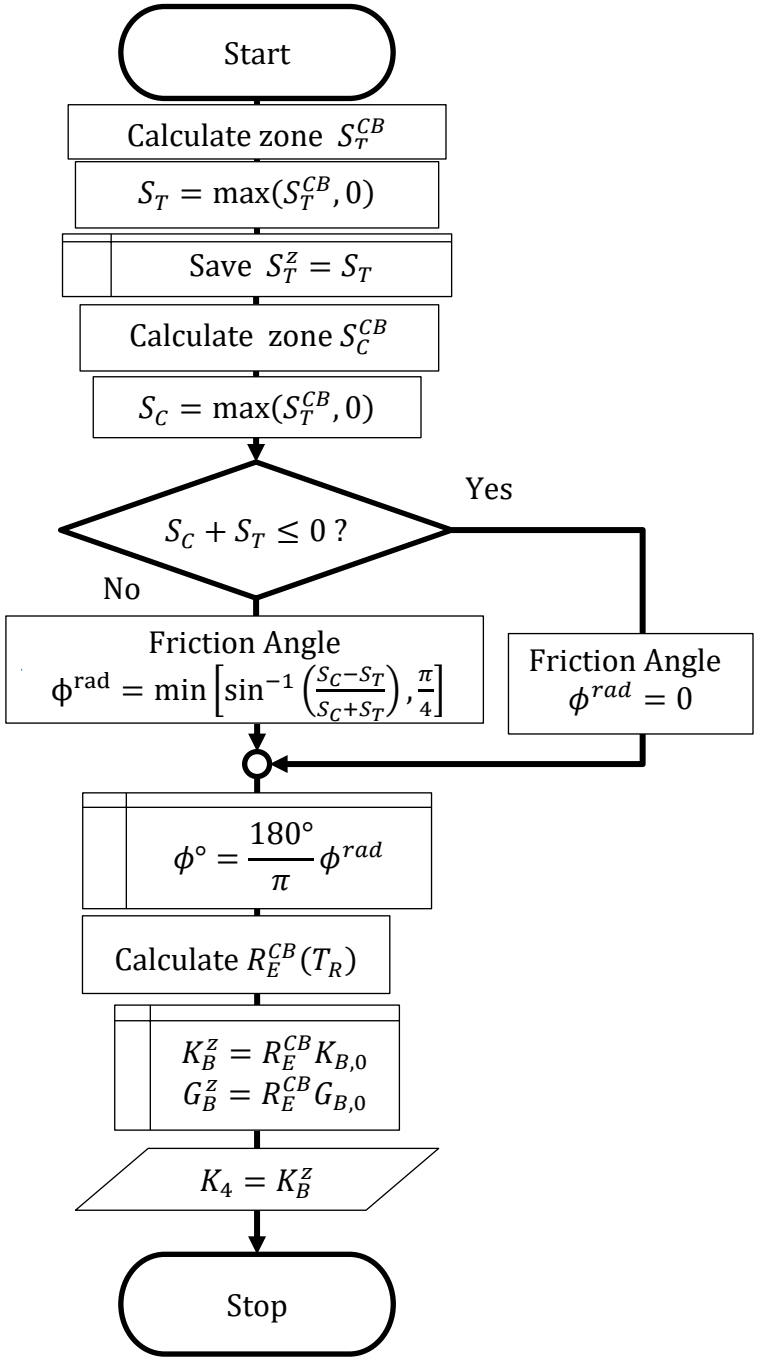

Fig. 25. Pyrolysis program: dry mechanical properties update flowchart.

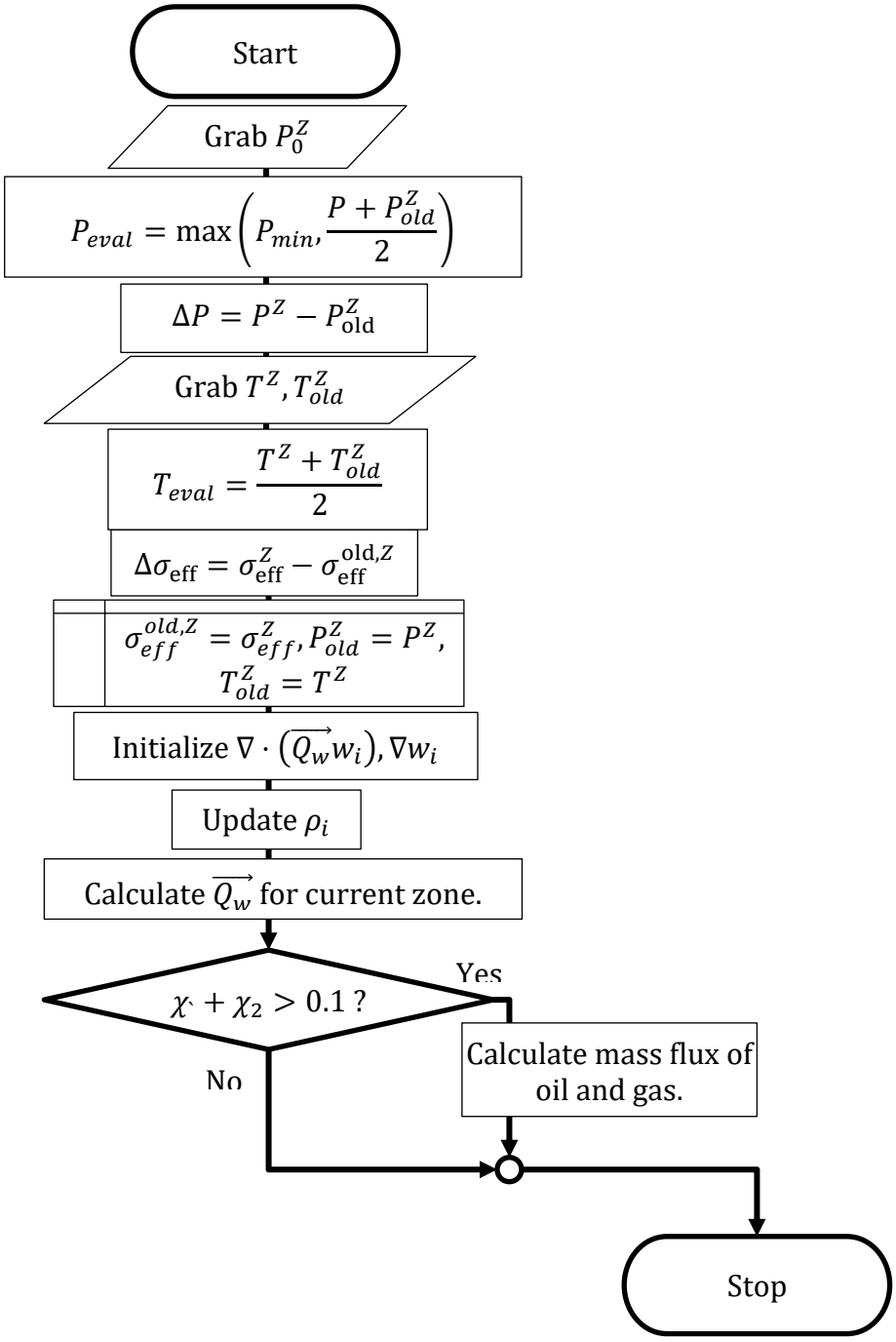

Fig. 26. Pyrolysis program: mass flux calculation flowchart.

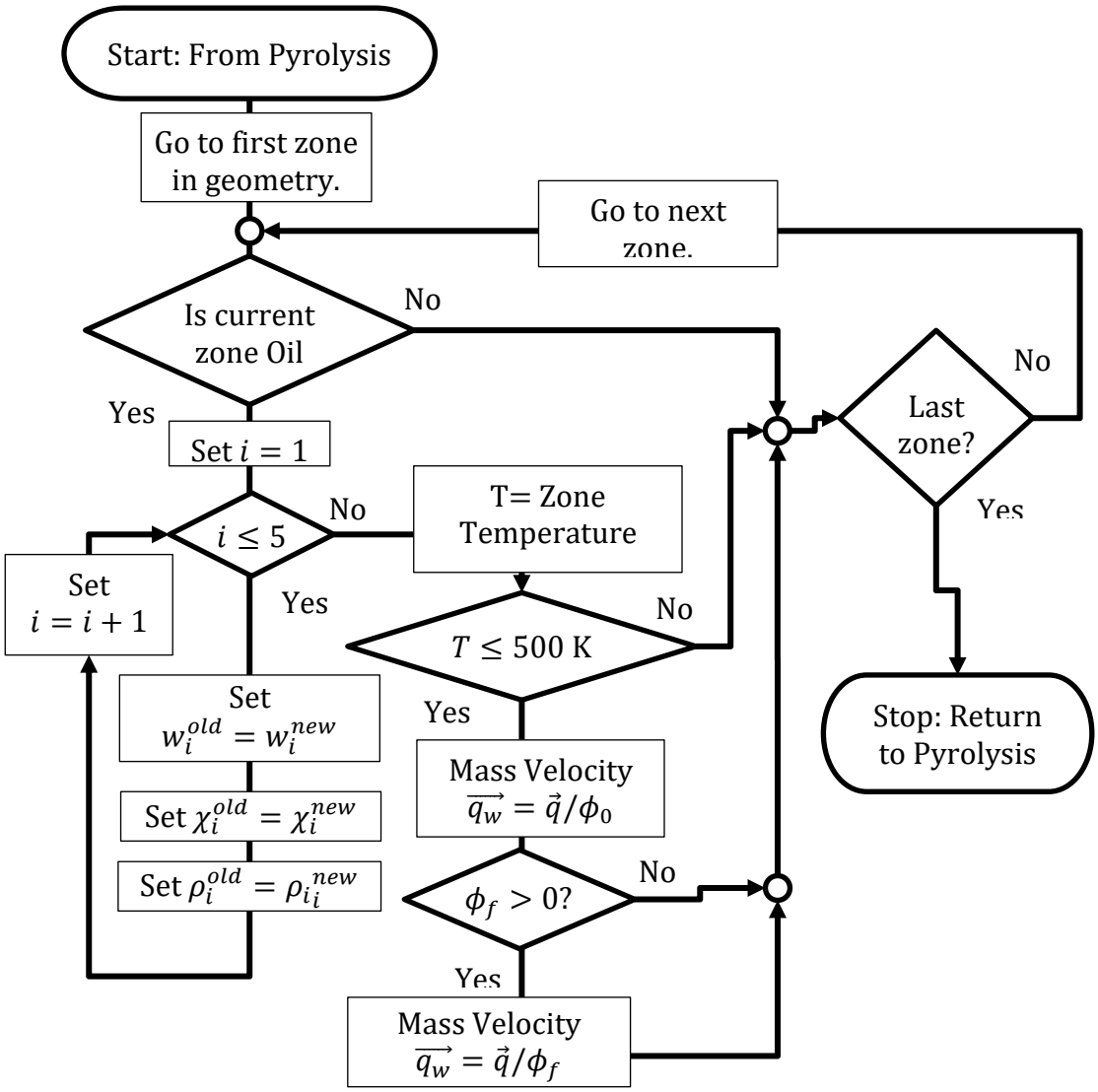

Fig. 27. Pyrolysis program: copy properties flowchart.

APPENDIX B

PYROLYSIS SIMULATION CODE

B.1 Driver

```
;;---Driver----
; OS_driver; File name.
; The driver is the master module of the simulation program.

new


; The zone_checker function was designed to ensure that custom geometry-dependent
calculations were pointed to the correct
; references.
define zone_checker
loop foreach zpnt z_list
if z_isgroup(zpnt,'Oilshale')=1
z_group(zpnt,2)='Current'
command
pause 0.2;
end_command
loop i (1,6)
z_facegroup(zpnt,i,2)=string(i)
end_loop
z_group(zpnt,2)='Done'
end_if
end_loop
end

define startup
command

call OS1_geom.f3dat suppress
; The Geometry Module generates the zones and groups in the simulation.
```

```
call OS2_initialize.f3dat suppress
;The Initialize Module calculates and assigns all initial properties and boundary
conditions to the geometry.
; Essential functions are also defined for use in the rest of the program

call OS3_hist_setup.f3dat suppress
; The History Setup Module records key data for evaluating the simulation results.
set fluid implicit on
set thermal dt 86400


end_command
end

@startup
;@zone_checker
;restore os_middle.sav ; In case of an interruption, the simulation can restore to a save-
point.
call OS4_pyrolyze.f3dat suppress ; The Pyrolyse program updates properties due to
pyrolysis.
; It represents the main body of the simulation.


save os_drainage.sav;@zone_checker


;;;--End Driver----
```

B.2 Geometry Module

```
;OS1_geom
;----Geometry Module----------
define geo1 ;Set Geometric Parameters here.
global x_size=4 ; m, size of oil shale reservoir
global y_size=4
global z_size=6
dy=1
dz=y_size
dx=y_size*z_size
moreDense = 2 ;Refining the grid by moreDense times in each direction.
ht=1.0
zt=1.0

end
```

```
@geo1
gen zone brick ... ; create the geometry
size @x_size @y_size @z_size ratio 1 1 1 ;...; x, y, z size of system (m) and ratio

; Densify only interior zones to speed calculation.
define densingzones
xs=0
ys=1
loop while ys < y_size
if xs < x_size
command
group zone Inside slot 3 range x( @xs [xs+1]) y(@ys @y_size)
end_command
end_if
xs=xs+1
ys=ys+1
end_loop
ht=0.5*ht
command
gen zone densify range group Inside nsegment @moreDense 1 @moreDense
attach face range z 0 @z_size
group zone Inside remove
end_command
end

;@densingzones
group zone OilShale range z 0 @z_size
group gp Heater slot 4 range x 0 tol 0.1 y 0 tol 0.1
group zone Production slot 4 range x [x_size-1] @x_size y [y_size-1] @y_size


fix x range x @x_size tol 0.01
fix y range y 0 tol 0.01
fix x range x 0 tol 0.01
fix y range y @y_size tol 0.01
fix z range z -0.01 0.01

return

;End Geometry
```

B.3 Initialization of Properties and Boundary Conditions

```
;; Initialize Module
;OS2_initialize


;-----Model Choices and Input Properties ------

; Pre-defined function for determining average effective stress
define CalcEffStress
eff_stress= (z_sig1(zpnt)+z_sig2(zpnt)+z_sig3(zpnt))/3+z_flprop(zpnt,'biot_c')*P
end


; The following functions, delta_xj and CDS, were defined so that mass transfer of oil
and gas from cell to cell
; could be calculated correctly.


define delta_xj(zpnt)
;This custom function gathers and stores geometric data from each cell in the geometry.
Because FLAC3D allows deformation, it's necessary to
; update this information every time mass flow is calculated.
xc=z_xcen(zpnt)
yc=z_ycen(zpnt)
zc=z_zcen(zpnt)


; z_faceextra(zpnt,#,1) is the distance between the center of this zone, and one of the 6
next to it (in or out of geometry).
; z_faceextra(zpnt,#,2) is the position of the adjacent cell on the # face. If the # face is on
the edge of the simulated region
; the distance position of the edge face is used instead.
; ip, jp, kp are respectively the x, y and z position of cells in the geometry.
; Delta x
if x_size=1
z_faceextra(zpnt,3,1)=1 ; If the system is only 1 cell in this dimention,dX is automatically
1 m.
z_faceextra(zpnt,4,1)=1


z_faceextra(zpnt,3,2)=0 ;
z_faceextra(zpnt,4,2)=1 ;
else
if ip=1
xp=z_xcen(z_join(zpnt,4))
```

```
z_faceextra(zpnt,3,1) = xp-xc
z_faceextra(zpnt,4,2) = 0 ; Notice, no 2 property for if ip is not 1. (For x and y, this will always be 0.)
else
xm=z_xcen(z_join(zpnt,3))
z_faceextra(zpnt,3,1)=xc-xm
if ip=x_size
z_faceextra(zpnt,4,1)=xc-xm
end_if
end_if
end_if
xt=(z_faceextra(zpnt,3,1)+z_faceextra(zpnt,4,1))/2

;Delta y
if y_size=1
z_faceextra(zpnt,6,1)=1
z_faceextra(zpnt,5,1)=1

z_faceextra(zpnt,6,2)=0
z_faceextra(zpnt,5,2)=1
else
if jp=1
yp=z_ycen(z_join(zpnt,5))
z_faceextra(zpnt,6,1)=yp-yc
z_faceextra(zpnt,6,2)=0
else
ym=z_ycen(z_join(zpnt,6))
z_faceextra(zpnt,6,1)=yc-ym
z_faceextra(zpnt,6,2)=ym ;
if jp=y_size
z_faceextra(zpnt,5,1)=yc-ym
z_faceextra(zpnt,5,2)=y_size ; If the cell is on a boundary, the 2 spot is used for the boundary position.
; If the adjacent cell is defined in the geometry, it points to the CENTER of that cell.
end_if
end_if
end_if

;Delta z
if z_size=1
z_faceextra(zpnt,1,1)=1
z_faceextra(zpnt,2,1)=1
z_faceextra(zpnt,1,2)=0
z_faceextra(zpnt,2,2)=1
else
if kp=1
```

```
zp=z_zcen(z_join(zpnt,2))
z_faceextra(zpnt,1,1)=zp-zc
z_faceextra(zpnt,1,2)=0
else
zm=z_zcen(z_join(zpnt,1))
z_faceextra(zpnt,1,1) = zc-zm
z_faceextra(zpnt,1,2)=zm

if kp=z_size
z_faceextra(zpnt,2,1)=zc-zm
end_if
end_if
end_if
;dz=zp-zm

zone_position
end

define zone_position ;Moves the flux and gradient calculations through geometry,
ensuring proper boundary
; conditions are applied.
ip=ip+1
if ip>x_size
; ii=out(string(ip)+'>'+string(x_size)) ;Output text used for debugging.
ip=1
jp=jp+1
if jp>y_size
jp=1
ip=1
kp=kp+1
end_if
end_if
;ii=out('Position= '+string(ip)+','+string(jp)+','+string(kp)) ; Displays position of current
cell in geometry.
end
; Arguably, this could be 2 different functions.
define CDS(var) ; Definition for the Central Difference Scheme
; Grab the centroid of the current zone "zpnt".
xc=z_xcen(zpnt)
yc=z_ycen(zpnt)
zc=z_zcen(zpnt)
dxj=get_array(6) ; Define an array to contain the distances to the 6 adjacent cell
centroids.

loop j(1,6)
dxj(j)=z_faceextra(zpnt,j,1)
```

```
end_loop

if var='w'
wj=get_array(6)
dwdx=get_array(3)

wc=z_extra(zpnt,10+i)
loop j (1,3)
; j=1=x's, j=2=y's, j=3=z's
caseof j
case 1
cz=ip
fm=3
fp=4
zm=3
zp=4
bc=xc
bcM=x_size
case 2
cz=jp
fm=6
fp=5
zm=6
zp=5
bc=yc
bcM=y_size
case 3
cz=kp
fm=1
fp=2
zm=1
zp=2
bc=zc
bcM=z_size
end_case
if bcM=0
dwdx(j)=0
else
if cz=1 ; If this is the first zone (cz could be x, y or z)
wj(fm)=z_extra(zpnt,10+i) ;w(j-1,t)=w(j,t-1) If on the minus boundary, use centroid w
from last timestep.
else
wj(fm)=z_extra(z_join(zpnt,fm),10+1) ; Otherwise, the mass fraction of the zone -1 is
simply the mass fraction of the previous zone.
end_if
```

```
if cz=bcM ;Handling boundaries depends on where the pointer is at the z+ boundary, or the x+ and y+ boundaries, respectively.
; As well as whether or not the producton well is flowing. (If in production mode, the gradient should consider x+ and y+ w's to be zero.
;if producing=1
; if j=3
wj(fp)=z_extra(zpnt,10+i)
; else
; wj(fp)=0
else
wj(fp)=z_extra(z_join(zpnt,fp),10+i)
end_if

dwdx(j)=( wj(zp)*dxj(zm)^2 - wj(zm)*dxj(zp)^2 + wc*(dxj(zp)^2-dxj(zm)^2) )/( dxj(zp)*dxj(zm)*(dxj(zm)+dxj(zp)) )
end_if
end_loop
grad_w(i)=vector(dwdx(1),dwdx(2),dwdx(3))
ii=lose_array(dwdx)
ii=lose_array(wj)
else if var='Qw'
div_Qw=0
Qcv=z_extra(zpnt,42)
Qj=get_array(6)
loop j (1,3)
; Boundary Conditions for Qw. Assuming 0 flow at most boundaries.
;
caseof j ; Initially, this is very similar to the dxj model. The difference is that this handles vectors.
case 1
bc=xc
cz=ip
bcM=x_size
Qc=xcomp(Qcv)
minf=3
maxf=4
zm=3
zp=4
case 2
bc=yc
cz=jp
bcM=y_size
Qc=ycomp(Qcv)
minf=6
maxf=5
zm=6
```

```
zp=5
case 3
bc=zc
cz=kp
bcM=z_size
Qc=zcomp(Qcv)
minf=1
maxf=2
zm=1
zp=2
end_case
if cz>1
Qchiec=z_extra(z_join(zpnt,minf),42)
; This statement represents flow of material to/from fractures.
; It grabs the flow from the minus cell in each case.
caseof j
case 1
Qj(minf)=xcomp(Qchiec)
case 2
Qj(minf)=ycomp(Qchiec)
case 3
Qj(minf)=zcomp(Qchiec)
end_case
; else if cz=1.
; if producing=1 ;Should not affect the minus cell.
; if z_isgroup(zpnt,'Production')=1 ; If the well is producing, and the pointer is on the
production well.
;Vers. A ; Qj(minf)=Qc ; But Qj(minf) This wouldn't apply at x=0, y=0 conditions unless
the pointer is at a z-boundary.
; ; They should not be anything but zero anyway.
; end_if
; else
; Qj(minf)=-Qc
; end_if
end_if

if cz<bcM
Qchiec=z_extra(z_join(zpnt,maxf),42) ; The meaning of Qchiec goes to adjacent flow
vector on +face of current cell.
caseof j
case 1
Qj(maxf)=xcomp(Qchiec)
case 2
Qj(maxf)=ycomp(Qchiec)
case 3
Qj(maxf)=zcomp(Qchiec)
```

```
end_case
else
if producing=1
if z_isgroup(zpnt,'Production')=1
Qj(maxf)=Qc
end_if
else
Qj(maxf)=-Qc
end_if
end_if
; CDS (Central Difference scheme) for calculating for Volumetric Flux
div_Qw=div_Qw+ ( Qj(zp)*dxj(zm)^2 - Qj(zm)*dxj(zp)^2 + Qc*(dxj(zp)^2-dxj(zm)^2)
)/( dxj(zp)*dxj(zm)*(dxj(zm)+dxj(zp)) )
end_loop
ii=lose_array(Qj)
end_if
ii=lose_array(dxj)
end

; Early in development, there was a plan to vary oil shale richness (to better simulate
actual Mahogany Zone in Green River oil shale).
define variableFA
loop i (1,z_size)
if i<z_size/10.0;
FA=5.0;
else if i<z_size/5.0
FA=10.0;
else if i<z_size/4.0
FA=25.0;
else if i<z_size/3.0
FA=50.0;
else if i<z_size/2.0
FA=25.0;
else if i<2*z_size/3.0
FA=10.0;
else
FA=0.0;
end_if

chi(4)=(FA*1.649)/(FA+111.8)
w(4)=(chi(4)*rhoi(4)) / ( rhoi(5) - chi(4)*(rhoi(5)-rhoi(4)) )
end_loop
end

define mech_initialization
```

```
;Strategy: Initialize variables using Chong and Smith, 1984. Then update for temperature
with
; Closmann and Bradley (including the Young's modulus).
;
argument T_k
argument _sz
argument _sx
T_F=(T_k-273.15)*1.8+32;
T_R=T_F+459.67


_sux=(127.73-112.15*chi(4))*1e6 ; Underscore notation used to avoid confusion with
later stress calculations.
_suz=(161.60-154.15*chi(4))*1e6
_Sxl=_sx/_sux
_Szl=_sz/_suz
_nzx= -0.04419 + 0.385*chi(4) +0.645*_Szl
_nxy= -0.03307 +0.333*chi(4) + 0.480*_Sxl
_Ex=(10.45 -17.4*chi(4) + 38.4*_Sxl -51.9*chi(4)*_Sxl - 18.83*_Sxl^4)*1e9
_Ez=(12.34 -21.96*chi(4)+ 74.61*_Szl -0.682*chi(4)*_Szl-9.869*_Szl^4)*1e9

osbulk= (_Ex*_Ez)/( 2*_Ez*(1-_nxy) + _Ex*(1-4*_nzx) ) ; My derivation.
osshear=(_Ex*_Ez)/( _Ez +_Ex*(1+2*_nzx) )
;shearxy=_Ex/(2*(1+_nzx))

;---Closmann and Bradley Initialization

; Tensile Strength (Closmann and Bradley, 1973)
St=(-288 + 7.79e8/(T_R^2)-19.3e3*FA/T_R+0.229*FA^2)*6.9848e3 ;
if St<0 then
St=0 ; Tensile Strength in Pa
end_if
ostens=St

; Compressive Strength
Sc=(3.48e5*T_F^(-0.615)*exp(-0.0214*FA))*6.9848e3
;dum=out('Sc_psi='+string(Sc_psi))
if Sc< 0 then
Sc=0
end_if
;
;--Friction Angle (Take advantage of relations used in Mohr-Coloumb failure.
if (Sc+St)<=0 then
rfric=0
else
rfric=asin((Sc-St)/(Sc+St))
```

```
if rfric/degrad > 45 then
rfric= 45*degrad
end_if
end_if
;ii=out(Sc)
osfric=rfric/degrad ;Better to assign in layers, or into individual zones?
oscohes=Sc*(1-sin(rfric)) / (2*cos(rfric))

;---- Update compressibilities (Based on Young's modulus change, Closmann and
Bradley, 1979)
Rc=0.1888*exp(886/T_R) ; (0.1888) Max T_R =1620 R
osbulk= Rc*osbulk
osshear=Rc*osshear

K_i(4)=osbulk ; On the other hand, they are updated for every zone, so this could work.

end

define biot_nums
argument phi ; oil shale porosity.
argument Kf
argument K
argument Ks
alpha=1-K/Ks
if alpha > 1
alpha=1
else if alpha < (3*phif/(2+phif))
alpha = 3*phif/(2+phif)
end_if

M = Kf/(phi+(alpha-phi)*(1-alpha)*Kf/K)
end

define input_props



; Driving Forces and Miscellaneous Inputs
doom_message=string('Something made the timestep crash!') ; Error message for if the
simulation goes unstable in execution.
; Component Properties
; Each component array is arranged such that {oil(1), gas(2), coke(3), kerogen(4),
minerals(5)}
; This choice was made to ease division of solid of fluid components.

; Component densities
```

```
rhoi=get_array(5);
rhoi(1)=910.0 ; kg/m^3, oil (Skyline FA Analysis)
rhoi(2)=37.0; kg/m^3, gas (McCain relations for Propane at 4.8e6 Pa, 600 K.)
rhoi(3)=2200.0; kg/m^3, coke (density of solid graphite)
rhoi(4)=1050.0; kg/m^3, kerogen, (J. Smith relations).
rhoi(5)=2750.0; kg/m^3, minerals, (J. Smith relations).
API=141.5/(rhoi(1)/1000.0)-131.5


;--Gas Parameters
MWg=41.33 ;These Should be predefined in Initial.
_R=8314.0 ;Gas constant in Metric Units, Pa-m^2/kmol-K
_z=0.95 ;Gas compressibility at pyrolysis T and P.

sg_g=MWg/28.97
Ps=1.01e5 ; Pa, standard Pressure
Ts=288.7 ; K, standard T used in calcs (60 F)
;; Fluid Moduli (Solid moduli are handled separately.

K_i=get_array(5);
K1o=2.92e6;
K_i(1)=2.92e6; Pa, for oil. McCain, pg. 523
K_i(2)=2.68e6; Pa, McCain Props for Propane at in situ conditions. (Based on 1/P)
K_i(3)= 34e9; Pa, for Coke (Graphite value)
K_i(4)=1.37e10; for Kerogen (Based on ambient oil shale properties.
K_i(5)=60e9; for Minerals (Approximated as Dolomite)


; Initial rock composition.
chi=get_array(5)
w=get_array(5)
;variableFA ; Optional function execution to vary the shale richness.


FA=25; gal/ton
osporos=0.17324*FA^(-1.238) ; Dinneen Porosity.
chi(1)=0.02; Oil volume, also the initial porosity. The Dineen porosity is more accurate,
but leads to unstable calculation.
chi(2)=0.0
chi(3)=0
chi(4)=FA*1.649/(FA+111.8);
chi(5)=1-chi(4)-chi(3)-chi(2)- chi(1);

;
; Initial Mass calculation, used to check that mass is neither created nor destroyed in the
simulation.
```

```
Mm=chi(5)*rhoi(5)*z_volume(z_near(0,0,0))
;chi(4)=1-0.34
;chi(5)=0.02
rho_b=0
rho_s=0
rho_f=0
;Calculate Phase and bulk density at each cell.
loop i (1,5)
rho_b=rho_b+chi(i)*rhoi(i)
if i<=2
rho_f=rho_f+chi(i)*rhoi(i)
else
rho_s=rho_s+chi(i)*rhoi(i)
end_if
ii=out('chi('+string(i)+') = '+string(chi(i)))
end_loop

Mzo=rho_b*z_volume(z_near(0,0,0)) ; Initial Mass in each cell.
Mm=chi(5)*rhoi(5)*z_volume(z_near(0,0,0)) ; Initial Mineral Mass
Mo=Mzo-Mm ; Initial Organic Mass

rho_f=rho_f/(chi(1)+chi(2))
loop i (1,5)
w(i)=chi(i)*rhoi(i)/rho_b

ii=out('w('+string(i)+') = '+string(w(i)))
end_loop

; Define initial Permeability

perm0=5e-15; m2/s This is significantly higher than the real permeability, but makes the
calculation much easier.
bc_kmu=perm0/.0002
;perm0=0
phiMax=1-chi(5) ; Maximum porosity is assumed to be the initial organic fraction of
each cell.


ii=out("chi(kerogen) ="+string(chi(4))) ; Displays a message with the initial kerogen
volume fraction.
ii=out("w(kerogen) ="+string(w(4))) ; Displays a message with initial kerogen mass
fraction.

; Boundary Conditions
global ini_T=308.5 ; K, (35.5 C, 96 F)
global T_heater=600 ; K, (627 C)
```

```
mu=0.0002 ; Pa·s, viscosity
G=1e7

global bc_pp=2.68e6 ; 300 m deep well.

global bc_kmu = perm0
global grad_S=9.81*rho_s ; Solid Gradient
global grad_F=-9.81*rho_f

;Force Boundary Conditions, AMSO

global overburden = -6.5e6 ; Pa overburden. (2209 kg/m^3, 300 m deep)
global os_pp=9.81*304.8*rho_f; Pa, pore pressure at 300 m
ii=out(os_pp)
; Mechanical Props Defined from AMSO Data
mech_initialization(ini_T,-overburden,-overburden/sqrt(2))
biot_nums(chi(1),K_i(1),K_i(4),K_i(4))

; Temperature dependent thermal properties, from several models.


; Granted the effect will be small, but the less shocks in my Sim, the better.
global cond_H0=1.7307*1.2299*exp(-0.01840*FA)*(1-1.0932e-4 *(T_F-75)-4.1949e-
7*(T_F-75)^2) ;Prats and O'Brian, 1975
global cond_V0=1.7307*1.0338*exp(-0.01846*FA)*(1-1.1948e-4 *(T_F-75)-3.1271e-
7*(T_F-75)^2) ; Derived from Pratz and O'Brian, 1975
global cond_G0=1.7307*1.1275*exp(-0.01843*FA)*(1-1.149e-4 *(T_F-75)-3.6667e-
7*(T_F-75)^2)
global Cp0=(0.172+(0.067+0.00162*FA)*1e-3*T_R)*4186.8; J/kg-K - Calculated using
Shaw, 1947.
global osthex=67e-6; microstrain
global checkpoint=0 ; Lets us know when we've heated through the shale.
global savepoint=1e4; So that the simulation can be restarted if needed.

; -------Pyrolysis Parameters------
R=1.987e-3; kcal/mol-K

dw=get_array(5)
grad_w=get_array(5)
div_Qww=get_array(5)
dwRx=get_array(5)

; Miscellaneous constants
svm=vector(1,1,1)
deltat=2160
update_time=0
```

```
t_fluids=0
heatSwitch=18*3600
fluidSwitch=86400
dt_crit=1e14

; Rxn 1: Kerogen Decomposition.
E1=get_array(5) ;kcal/mol
loop i (1,5)
E1(i)=48+i
end_loop

f1=get_array(5) ; Distribution function.
f1(1)=0.05,
f1(2)=0.2,
f1(3)=0.5,
f1(4)=0.2,
f1(5)=0.05;

A1=1e13
Hrx1=370e3; J/kg kerogen decomposed.

; Rxn 2: Oil Decomposition.
E2=get_array(1)
E2(1)=48;
f2=get_array(1)
f2(1)=1.0;
A2=1e12;
Hrx2=127e3; J/kg oil decomposed.

; Pyrolysis reaction coefficients
Ai=get_array( 2,4)
; Rxn 1 coefficients.
Ai(1,1)=0.669; Oil
Ai(1,2)=0.178; gas
Ai(1,3)=0.153; coke
Ai(1,4)= -1.0; kerogen

; Rxn 2:
Ai(2,1)=-1.0;
Ai(2,2)=0.566;
Ai(2,3)=0.434;
Ai(2,4)=0.0;

end
```

```
define initial_ChemProps ; Assign the initial Chemical properties to each cell in the
geometry.
loop foreach zpnt z_list
z_extra(zpnt,42)=z_q(zpnt)/(chi(1)+chi(2))
if z_isgroup(zpnt,'OilShale')=1
CalcEffStress
d_eff=0
dP=0 ;eff_str-z_extra(zpnt,1)
z_extra(zpnt,1)=eff_str

z_extra(zpnt,7)=z_temp(zpnt)
z_extra(zpnt,8)=z_pp(zpnt)
;Qw.

loop i (1,5)
z_extra(zpnt,10+i)=w(i)
z_extra(zpnt,15+i)=w(i)
z_extra(zpnt,20+i)=chi(i)
z_extra(zpnt,25+i)=chi(i)
z_extra(zpnt,30+i)=rhoi(i)
z_extra(zpnt,35+i)=rhoi(i)
end_loop
end_if
end_loop
end

; Start of Initialize Execution.

config thermal ;Enable thermodynamics model.
config fluid ; Enable the fluid dynamics model.


@input_props ;Implement properties used in all calculations.

; Assigns properties (recognized by the base software by default) to the geometry.
model mech mohr th_ani fl_iso range group OilShale
prop bulk=@osbulk shear=@osshear fric @osfric coh = @oscohes tens = @ostens ...
;Mechanical properties.
tk1=@cond_H0 tk2=@cond_H0 tk3=@cond_V0 spec @Cp0 ... ; Thermal Properties.
perm=@perm0 porosity=[chi(1)+chi(2)] u_th=@osthex biot_c=@alpha ... ; Fluid
properties
range group OilShale

set fluid on ; Activate the fluid solution and biot deformation models, respectively.
set fluid biot on
ini biot_m= @M ftens=0 range group OilShale;
```

```
; Activate gravity, and assign densities and other forces for the bulk and the fluid phases.
set gravity 0 0 -9.81
ini density @rho_s fdensity=[rho_f] sat=1 range group OilShale;mineral density kg/m^3

apply szz = @overburden ;grad (0,0,@grad_S)
ini pp = @os_pp grad (0,0,@grad_F) range group OilShale ; Apply stress and pore
pressure to geometry.
free pp

initial zextra 2 =[chi(1)+chi(2)] zextra 3=@perm0 zextra 4=@rho_s zextra 5=@rho_f
zextra 6=@rho_b range group OilShale ;Initialize phif,perm,mu.

initial t @ini_T ; initial temperature (K)
initial t [(1-0.25*pi*0.15^2)*ini_T + 0.25*pi*0.15^2*T_heater] range x 0 1 y 0 1 ;
Define heater as a 0.3 m well in cells (0,0,z).
free t ; Allow the temperature to change.

set large ; Allow large deformation in the geometry.

solve ; Solve for steady state. This allows the geometry to adapt to the initial forces.
@initial_ChemProps ; Assign Chemical Properties.

solve
; Set the boundary temperature and apply overburden forces.

;group zone StartZones slot 3 range x 0 2 y 0 2 z [0.5*z_size] tol [z_size*0.2]
fix t @T_heater range group Heater

step 1;Initialize new conditions.
save os_initial_eq.sav

set fluid time=0 ; Time Set to 0.
set thermal time=0
his reset
set large
return

;--End Initialize Module
```

B.4 Setting Up History to Track Key Variables

```
; OS3_hist_setup
define initial_mass
local zmidpt=z_near(x_size/2.,y_size/2.,z_size/2.)
ini_mass=z_density(zmidpt)*z_volume(zmidpt) ;
```

```
ini_z=gp_zdisp(gp_near(x_size/2.,y_size/2.,z_size))
end

define oilfield_units ;Simulation calculations are in metric, but most inputs/output are in
US units.
local inpt=gp_near(0,0,z_size)
local outpt=gp_near(x_size,y_size,z_size)
local midpoint=gp_near(x_size/2.,y_size/2.,z_size/2.)
local zmidpt=z_near(x_size/2.,y_size/2.,z_size/2.)
local zheater=z_near(0,0,z_size/2.)
local zwell=z_near(x_size,z_size,z_size/2.)
local topcnt=gp_near(x_size/2.,y_size/2.,z_size)
; Converts seconds to days.
sim_time=thtime/(365*86400)
; The subscripts h, 1, 2, 3, 4, p respectively are locations relative to the heater well.
; Temperature and Pressure data are gathered.
T_h = gp_temp(gp_near(0,0,z_size/2.0))
T_1 = gp_temp(gp_near(1,1,z_size/2.0))
T_c = gp_temp(gp_near(2,2,z_size/2.))
T_2 = gp_temp(gp_near(2,2,z_size/2.))
T_3 = gp_temp(gp_near(3,3,z_size/2.0))
T_p = gp_temp(gp_near(5,5,z_size/2.0))
T_4 = gp_temp(gp_near(4,4,z_size/2.0))
dZi = -(gp_zdisp(inpt)-ini_z)
dZo = -(gp_zdisp(outpt)-ini_z)

P_h = gp_pp(gp_near(0,0,z_size/2.0))
P_1 = gp_pp(gp_near(1,1,z_size/2.0))
P_2 = gp_pp(gp_near(2,2,z_size/2.0))
P_3 = gp_pp(gp_near(3,3,z_size/2.0))
P_4 = gp_pp(gp_near(4,4,z_size/2.0))
P_c = gp_pp(gp_near(2,2,z_size/2.))
P_p = gp_pp(gp_near(5,5,z_size/2.0))

phi_grab= z_extra(zmidpt,2) ;
masscheck=(z_extra(zmidpt,50));

caseof units ; Function for converting SI values into metric or US.
case 1 ;C, MPa, m
T_h=(T_h-273.1)
T_c=(T_c-273.1)
T_p=(T_p-273.1)
T_1=(T_1-273.1)
T_2=(T_2-273.1)
T_3=(T_3-273.1)
T_4=(T_4-273.1)
```

```
P_h=P_h*1e-6;
P_c=P_c*1e-6;
P_p=P_p*1e-6;

case 2 ;F, ft, psi

T_h=(T_h-273.15)*1.8+32
T_c=(T_c-273.15)*1.8+32
T_p=(T_p-273.15)*1.8+32
T_1=(T_1-273.15)*1.8+32
T_2=(T_2-273.1)*1.8+32
T_3=(T_3-273.1)*1.8+32
T_4=(T_4-273.1)*1.8+32

P_h=P_h/6895;
P_c=P_c/6895;
P_p=P_p/6895;
P_1=P_1/6895
P_2=P_2/6895
P_3=P_3/6895
P_4=P_4/6895

end_case
end

define kinetics_track ; Collects data on the mass and volumetric composition at key
locations in the geometry.
local zsource=z_near(0,0,z_size/2)
local zmidpt=z_near(2,2,z_size/2)
local zsink=z_near(4,4,z_size/2)

wt10=z_extra(zsource,11)
wt20=z_extra(zsource,12)
wt30=z_extra(zsource,13)
wt40=z_extra(zsource,14)
wt50=z_extra(zsource,15)

chi10=z_extra(zsource,21)
chi20=z_extra(zsource,22)
chi30=z_extra(zsource,23)
chi40=z_extra(zsource,24)
chi50=z_extra(zsource,25)

wt12=z_extra(zmidpt,11)
```

```
wt22=z_extra(zmidpt,12)
wt32=z_extra(zmidpt,13)
wt42=z_extra(zmidpt,14)
wt52=z_extra(zmidpt,15)

chi12=z_extra(zmidpt,21)
chi22=z_extra(zmidpt,22)
chi32=z_extra(zmidpt,23)
chi42=z_extra(zmidpt,24)
chi52=z_extra(zmidpt,25)

wt14=z_extra(zsink,11)
wt24=z_extra(zsink,12)
wt34=z_extra(zsink,13)
wt44=z_extra(zsink,14)
wt54=z_extra(zsink,15)

chi14=z_extra(zsink,21)
chi24=z_extra(zsink,22)
chi34=z_extra(zsink,23)
chi44=z_extra(zsink,24)
chi54=z_extra(zsink,25)

stepsize=fldt
end

@initial_mass
; The following code adds each of the previously defined variables to recorded history of
the simulation.
set @units=2
his add fish oilfield_units
his add fish T_h
his add fish T_c
his add fish T_p
his add fish P_h
his add fish P_c
his add fish P_p
his add fish dZi
his add fish dZo
his add fish sim_time
his add fish masscheck
his add fish phi_grab
his add fish kinetics_track
his add fish wt10
his add fish wt20
his add fish wt30
```

```
his add fish wt40
his add fish wt50
his add fish chi10
his add fish chi20
his add fish chi30
his add fish chi40
his add fish chi50
his add fish wt12
his add fish wt22
his add fish wt32
his add fish wt42
his add fish wt52
his add fish chi12
his add fish chi22
his add fish chi32
his add fish chi42
his add fish chi52
his add fish wt14
his add fish wt24
his add fish wt34
his add fish wt44
his add fish wt54
his add fish chi14
his add fish chi24
his add fish chi34
his add fish chi44
his add fish chi54

his add fish stepsize ; Used to help debug the code.
his add fish T_1
his add fish T_2
his add fish T_3
his add fish T_4
his add fish P_1
his add fish P_2
his add fish P_3
his add fish P_4

set hist_rep 10 ; Gather data every ten time-steps into the simulation.
label (0,0,[1.2*z_size]), end (0 0 0), arrow off ...
text 'Heat Injection Well'
label (@x_size,@y_size,[1.2*z_size]), end (@x_size,@y_size,0) arrow off ...
text 'Production Well'
    return
```

B.5 Pyrolysis Program

```
    ; OS4_pyrolyze
define initial_mass
local zmidpt=z_near(x_size/2.,y_size/2.,z_size/2.)
ini_mass=z_density(zmidpt)*z_volume(zmidpt) ;

ini_z=gp_zdisp(gp_near(x_size/2.,y_size/2.,z_size))
end

define oilfield_units ;Simulation calculations are in metric, but most inputs/output are in
US units.
local inpt=gp_near(0,0,z_size)
local outpt=gp_near(x_size,y_size,z_size)
local midpoint=gp_near(x_size/2.,y_size/2.,z_size/2.)
local zmidpt=z_near(x_size/2.,y_size/2.,z_size/2.)
local zheater=z_near(0,0,z_size/2.)
local zwell=z_near(x_size,z_size,z_size/2.)
local topcnt=gp_near(x_size/2.,y_size/2.,z_size)
; Converts seconds to days.
sim_time=thtime/(365*86400)
; The subscripts h, 1, 2, 3, 4, p respectively are locations relative to the heater well.
; Temperature and Pressure data are gathered.
T_h = gp_temp(gp_near(0,0,z_size/2.0))
T_1 = gp_temp(gp_near(1,1,z_size/2.0))
T_c = gp_temp(gp_near(2,2,z_size/2.))
T_2 = gp_temp(gp_near(2,2,z_size/2.))
T_3 = gp_temp(gp_near(3,3,z_size/2.0))
T_p = gp_temp(gp_near(5,5,z_size/2.0))
T_4 = gp_temp(gp_near(4,4,z_size/2.0))
dZi = -(gp_zdisp(inpt)-ini_z)
dZo = -(gp_zdisp(outpt)-ini_z)

P_h = gp_pp(gp_near(0,0,z_size/2.0))
P_1 = gp_pp(gp_near(1,1,z_size/2.0))
P_2 = gp_pp(gp_near(2,2,z_size/2.0))
P_3 = gp_pp(gp_near(3,3,z_size/2.0))
P_4 = gp_pp(gp_near(4,4,z_size/2.0))
P_c = gp_pp(gp_near(2,2,z_size/2.))
P_p = gp_pp(gp_near(5,5,z_size/2.0))

phi_grab= z_extra(zmidpt,2) ;
masscheck=(z_extra(zmidpt,50));

caseof units ; Function for converting SI values into metric or US.
case 1 ;C, MPa, m
```

```
T_h=(T_h-273.1)
T_c=(T_c-273.1)
T_p=(T_p-273.1)
T_1=(T_1-273.1)
T_2=(T_2-273.1)
T_3=(T_3-273.1)
T_4=(T_4-273.1)


P_h=P_h*1e-6;
P_c=P_c*1e-6;
P_p=P_p*1e-6;

case 2 ;F, ft, psi

T_h=(T_h-273.15)*1.8+32
T_c=(T_c-273.15)*1.8+32
T_p=(T_p-273.15)*1.8+32
T_1=(T_1-273.15)*1.8+32
T_2=(T_2-273.1)*1.8+32
T_3=(T_3-273.1)*1.8+32
T_4=(T_4-273.1)*1.8+32

P_h=P_h/6895;
P_c=P_c/6895;
P_p=P_p/6895;
P_1=P_1/6895
P_2=P_2/6895
P_3=P_3/6895
P_4=P_4/6895

end_case
end

define kinetics_track ; Collects data on the mass and volumetric composition at key
locations in the geometry.
local zsource=z_near(0,0,z_size/2)
local zmidpt=z_near(2,2,z_size/2)
local zsink=z_near(4,4,z_size/2)

wt10=z_extra(zsource,11)
wt20=z_extra(zsource,12)
wt30=z_extra(zsource,13)
wt40=z_extra(zsource,14)
wt50=z_extra(zsource,15)
```

```
chi10=z_extra(zsource,21)
chi20=z_extra(zsource,22)
chi30=z_extra(zsource,23)
chi40=z_extra(zsource,24)
chi50=z_extra(zsource,25)

wt12=z_extra(zmidpt,11)
wt22=z_extra(zmidpt,12)
wt32=z_extra(zmidpt,13)
wt42=z_extra(zmidpt,14)
wt52=z_extra(zmidpt,15)

chi12=z_extra(zmidpt,21)
chi22=z_extra(zmidpt,22)
chi32=z_extra(zmidpt,23)
chi42=z_extra(zmidpt,24)
chi52=z_extra(zmidpt,25)

wt14=z_extra(zsink,11)
wt24=z_extra(zsink,12)
wt34=z_extra(zsink,13)
wt44=z_extra(zsink,14)
wt54=z_extra(zsink,15)

chi14=z_extra(zsink,21)
chi24=z_extra(zsink,22)
chi34=z_extra(zsink,23)
chi44=z_extra(zsink,24)
chi54=z_extra(zsink,25)

stepsize=fldt
end



@initial_mass
; The following code adds each of the previously defined variables to recorded history of
the simulation.
set @units=2
his add fish oilfield_units
his add fish T_h
his add fish T_c
his add fish T_p
his add fish P_h
his add fish P_c
his add fish P_p
```

```
his add fish dZi
his add fish dZo
his add fish sim_time
his add fish masscheck
his add fish phi_grab
his add fish kinetics_track
his add fish wt10
his add fish wt20
his add fish wt30
his add fish wt40
his add fish wt50
his add fish chi10
his add fish chi20
his add fish chi30
his add fish chi40
his add fish chi50
his add fish wt12
his add fish wt22
his add fish wt32
his add fish wt42
his add fish wt52
his add fish chi12
his add fish chi22
his add fish chi32
his add fish chi42
his add fish chi52
his add fish wt14
his add fish wt24
his add fish wt34
his add fish wt44
his add fish wt54
his add fish chi14
his add fish chi24
his add fish chi34
his add fish chi44
his add fish chi54

his add fish stepsize ; Used to help debug the code.
his add fish T_1
his add fish T_2
his add fish T_3
his add fish T_4
his add fish P_1
his add fish P_2
his add fish P_3
his add fish P_4
```

```
set hist_rep 10 ; Gather data every ten time-steps into the simulation.
label (0,0,[1.2*z_size]), end (0 0 0), arrow off ...
text 'Heat Injection Well'
label (@x_size,@y_size,[1.2*z_size]), end (@x_size,@y_size,0) arrow off ...
text 'Production Well'
    return
```

APPENDIX C

APPROXIMATING ISOTROPIC ELASTIC MODULI FROM TRANSVERSELY ANISOTROPIC MODULI

Since FLAC3D™ assumes isotropy during plastic failure and poroelasticity, it is expedient to approximate "average" bulk and shear moduli. The following development is in generic Cartesian coordinates. Begin by adapting the inverse form of Hooke's Law for a transversely isotropic system, developed by Amadei [20]. Assuming that the plane of symmetry is in the 1-2 plane, the following notation may be used.

$$E = E_1 = E_2, \qquad E' = E_3, \qquad G = G_{12}, \qquad G' = G_{13} = G_{23}, \qquad \nu = \nu_{12}, \qquad \nu' = \nu_{13} = \nu_{23} \tag{57}$$

$$\begin{Bmatrix} \epsilon_{11}^e \\ \epsilon_{22}^e \\ \epsilon_{33}^e \\ 2\epsilon_{12}^e \\ 2\epsilon_{13}^e \\ 2\epsilon_{23}^e \end{Bmatrix} = \begin{bmatrix} \frac{1}{E} & -\frac{\nu}{E} & -\frac{\nu'}{E'} & & & \\ -\frac{\nu}{E} & \frac{1}{E} & -\frac{\nu'}{E'} & & & \\ -\frac{\nu'}{E} & -\frac{\nu'}{E} & \frac{1}{E'} & & & \\ & & & \frac{1}{G} & & \\ & & & & \frac{1}{G'} & \\ & & & & & \frac{1}{G'} \end{bmatrix} \begin{Bmatrix} \sigma_1 \\ \sigma_2 \\ \sigma_3 \\ \tau_{12} \\ \tau_{13} \\ \tau_{23} \end{Bmatrix} \tag{58}$$

Matrix multiplication is then used to solve each strain component.

$$\begin{aligned}
\epsilon_{11}^{e} &= \frac{1}{E}\sigma_1 - \frac{\nu}{\mathrm{E}}\sigma_2 - \frac{\nu'}{\mathrm{E}'}\sigma_3 \\
\epsilon_{22}^{e} &= -\frac{\nu}{E}\sigma_1 + \frac{1}{\mathrm{E}}\sigma_2 - \frac{\nu'}{\mathrm{E}'}\sigma_3 \\
\epsilon_{33}^{e} &= -\frac{\nu'}{E'}\sigma_1 - \frac{\nu'}{E'}\sigma_2 + \frac{1}{\mathrm{E}'}\sigma_3 \\
\epsilon_{12}^{e} = \frac{1}{2G}\tau_{12}, \qquad \epsilon_{13}^{e} &= \frac{1}{2G'}\tau_{13}, \qquad \epsilon_{23}^{e} = \frac{1}{2G'}\tau_{23}
\end{aligned} \tag{59}$$

Although an oil shale reservoir is technically anisotropic, it is still possible to derive a bulk modulus. This is justified using a thought experiment. If we take a sample of oil shale (or any other material) and subject it to uniaxial stress, we logically expect that the amount of strain would vary based on orientation of the sample. If we instead apply a hydrostatic pressure, such that $P = \sigma_1 = \sigma_2 = \sigma_3$, the principal strain relations can be greatly simplified.

$$\begin{aligned}
\epsilon_{11} = \epsilon_{22} &= \left(\frac{1-\nu}{E} - \frac{\nu'}{E'}\right)P \\
\epsilon_{33} &= \frac{1-2\nu'}{E'}P
\end{aligned} \tag{60}$$

While the isotropic relation used for defining a bulk modulus K in Equation 58 will not generally be true, consider the following.

$$\epsilon_{11} = \epsilon_{22} = \epsilon_{33} = \frac{\mathrm{P}}{3\mathrm{K}} \tag{61}$$

Assuming that the sample remains in the elastic region when placed under a uniform confining pressure, an anisotropic material will experience the same *volumetric strain* regardless of orientation. If it is valid to assume that $0 < (\nu, \nu') < 0.5$, the equivalent bulk modulus definition for *any* linearly elastic material under hydrostatic pressure is

$$\epsilon_v = \frac{P}{K}. \tag{62}$$

It is generally assumed that strains are small ($\epsilon \ll 1$) to avoid higher order terms. A

more rigorous definition for ϵ_v is

$$\epsilon_v = (\Delta\epsilon_{11} + \Delta\epsilon_{22} + \Delta\epsilon_{33}) + (\Delta\epsilon_{11}\Delta\epsilon_{22} + \Delta\epsilon_{11}\Delta\epsilon_{33} + \Delta\epsilon_{22}\Delta\epsilon_{33}) - \Delta\epsilon_{11}\Delta\epsilon_{22}\Delta\epsilon_{33} \tag{63}$$

What qualifies as small? Graphing the ratio of the simplified volumetric strain to the true volumetric strain shows that $\epsilon_{v,error} \cong \epsilon_{ave}$ for $\epsilon_{ave} \leq \sim 0.1$. Therefore, if linear elasticity holds for as large as a 10% reduction in the average length of the sample, any estimate for volumetric strain will be at most, about 10% off. This accuracy should be more than sufficient for estimating an equivalent bulk modulus.

The derivation proceeds from this point with the simplified volumetric strain assumption.

$$\begin{gathered} \epsilon_v = \epsilon_{11} + \epsilon_{22} + \epsilon_{33} = \left[2\left(\frac{1-\nu}{E} - \frac{\nu'}{E'}\right) + \frac{1-2\nu'}{E'}\right] P = \frac{P}{K} \\ \frac{2(1-\nu)}{E} + \frac{1-4\nu'}{E'} = \frac{1}{K} \\ \frac{2E'(1-\nu) + E(1-4\nu')}{EE'} = \frac{1}{K} \end{gathered} \tag{64}$$

The equivalent bulk modulus for a transversely isotropic material is therefore

$$K = \frac{EE'}{2E'(1-\nu) + E(1-4\nu')} \tag{65}$$

APPENDIX D

VARIABLE PERMEABILITY AND VISCOCITY IN OIL SHALE

D.1 Permeability

The simulation was unable to handle variable permeability, but several insights were gained from investigating the relationship between permeability and porosity.

The Kozeny-Carman equation is regularly used to relate porosity and permeability, but it was found to be inappropriate for oil shale [44]. There have been several studies investigating changing permeability of oil shale fragments [44], [45], [51], but the results are not transferable to competent material. Experimental data could not be found for relationships between permeability and porosity for oil shale undergoing pyrolysis. Developing a new permeability model was beyond the scope of this study. Lacking a more appropriate model, permeability κ (m^2) could be updated for each zone using the following form of the Kozeny-Carman equation, as suggested by Tiwari. [10]

$$\kappa = \frac{\phi^3 D_p^2}{150(1-\phi)^2} \mathrm{e}^{-\omega \Delta \sigma_{\mathrm{eff}}} \tag{66}$$

where ϕ is porosity $\Delta\sigma_{eff}$, is effective stress, ω is an experimentally determined term and D_p is pore diameter (50 μm).

D.2 Stress-dependent Porosity

During *in situ* pyrolysis and drainage, we expect significant changes in porosity due to fluid production, loss, and drainage. Porosity's stress dependence can be modeled by an exponential function, as suggested by Detournay and Chang [52], as well as Burnham and Braun [32]. If spherical pores are assumed, the porosity may be expressed as

$$\phi = \phi_0 \exp\left[-\frac{3(\bar{\sigma} - P)}{4(G - \Delta G_R)}\right], \tag{67}$$

where ϕ_0 is initial porosity, $\Delta\phi_r$ is the porosity change due to reactions, $\bar{\sigma}$ is the mean confining stress, P is pore pressure, G is the initial shear modulus, and ΔG_R is the change in shear modulus due to reactions.

D.3 Shale Oil and Gas Fluid Viscosity

Representing viscosity change through pyrolysis is complicated. Viscosity is significantly affected by changes to the oil-gas mixture as well as temperature, and pressure. The specific properties of shale oil are dependent on pyrolysis conditions (temperature, pressure, storage time), so one cannot simply look up formation properties. As an alternative, one can use correlations to estimate appropriate values for oil and gas viscosities separately and then use volumetric averaging.

For the gas phase, the correlations of Lee et al. [53] were used to determine viscosity μ_g (Pa·s).

$$\mu_g = 0.001(\mathcal{K}_1 \exp(X\rho_g^Y)) \tag{68}$$

where

$$\rho_g = \frac{PM_g}{zRT} \tag{69}$$

$$\mathcal{K}_1 = \frac{\left(9.4 \times 10^{-4} + 2M_g \times 10^{-6}\right) T_R^{1.5}}{209 + 19M_g + T_R} \tag{70}$$

$$X = 3.5 + \frac{986}{T_R} + 0.01M_g \tag{71}$$

$$Y = 2.4 - 0.2X \tag{72}$$

In Equations 68-72, ρ_g is density (g/cm^3), T_R is temperature (°R), M_g is the molecular mass of the gas (41.33 g/mol), and μ_g is viscosity (Pa·s).

Oil viscosity is estimated by adapting an empirical correlation developed by Ng and Egbogah [54].

$$\log(\log(\mu_o + 1)) = 1.8653 - 0.025086API - 0.5644\log(T_F) \tag{73}$$

Where μ_o is oil viscosity (mPa·s), and T_F is temperature (°F). Equation 71 correlates well with experimental results found by Seitzer and Lovell [55] for Utah shale oil, as well as various retort processes summarized by Baughman [43]. A molecular correlation by Bird, Stewart, and Lightfoot [56] was also considered, but it underpredicts oil viscosity by a factor of 10.

$$\mu_o = \frac{N_A \hbar \rho_o}{M_o} \exp\left(\frac{3.8T_b}{T}\right) \tag{74}$$

where μ_o is oil viscosity (mPa·s), N_A is Avogadro's number (6.022×10^{23}), $\hbar$ is Plank's constant (6.626×10^{-34} J·s), ρ_o is oil density (kg/m^3), and M_o is the shale oil's pseudo-molecular weight (368.7 kg/kmol). The T_b chosen was 685 K, approximating the oil as a large alkane (C26). The overall fluid viscosity is a volumetric average of the oil and gas components.

$$\mu = \mu_o \phi_o + \mu_g \phi_g \tag{75}$$

REFERENCES

[1] R. L. Braun and A. K. Burnham, "Math. model of oil generation, degradation, and expulsion," *Energy*, vol. 4, no. 2, pp. 132–146, 1990.

[2] T. Fowler and H. Vinegar, "Oil shale ICP-Colorado field pilots," *SPE West. Reg. Meet.*, 2009.

[3] J. R. Dyni, "Oil shale," in *2010 Survey of Energy Resources*, I. Iancu, A. W. Clarke, and J. A. Trinnaman, Eds. London: World Energy Council, 2010, pp. 93–122.

[4] P. M. Crawford, K. Biglarbigi, A. R. Dammer, and E. Knaus, "Advances in world oil shale prod. technologies," in *Proceedings of SPE Annual Technical Conference and Exhibition*, 2008, pp. 1–11.

[5] V. Rajaram, J. S. Long, and K. K. Bhattacharyya, "Geotechnical considerations, mine design Federal Oil Shale Tract C-a, Colorado," in *The 18th U.S. Symp. on Rock Mechanics*, 1977, no. 3, pp. 1–6.

[6] RedLeaf Res. Inc., "EcoShale technology." [Online]. Available: http://www.redleafinc.com/ecoshaletechnology. [Accessed: 16-Apr-2016].

[7] Gulf Oil Corporation and Standard Oil (Indiana), "Detailed development plan, Tract C-a," in *Rio Blanco Oil Shale Project*, 1976.

[8] A. Andrews, "Oil Shale: History, Incentives, and Policy," Congressional Research Service, RL33359, 2006.

[9] J. Bauman, "Significant parameter identification and characterization of complex *in situ* reservoir simulations," Ph.D. dissertation, Dept. Chemical Eng., Univ. Utah, Salt Lake City, 2012.

[10] P. Tiwari, "Oil shale pyrolysis: benchscale experimental studies and modeling," Ph.D. dissertation, Dept. Chemical Eng., Univ. Utah, Salt Lake City, 2012.

[11] R. J. Shaw, "Specific heat of Colorado oil shale," US Dept. of the Interior, Bureau of Mines, Vol. 4151, 1947.

[12] M. Prats and S. M. O'Brian, "The thermal conductivity and diffusivity of Green River oil shales," *J. Pet. Technol.*, vol. 27, no. 1, pp. 97–106, Apr. 1975.

[13] W. Voight, "Über die Beziehung zwischen den beiden elastischen Konstanten eines isotropen Körper [On the relationship between the two elastic constants of an isotropic body]," *Wied, Ann.*, vol. 38, pp. 573–587, 1889.

[14] M. A. Biot, "General theory of three-dimensional consolidation," *J. Appl. Phys.*, vol. 12, no. 2, pp. 155–164, 1941.

[15] K. P. Chong and J. W. Smith, "Mechanical characterization of oil shale," in *Mechanics of Oil Shale*, K. P. Chong and J. W. Smith, Eds. London: Elsevier Ltd, 1984, pp. 165–228.

[16] M. Cleary, "Some deformation and fracture characteristics of oil shale," in *19th US Symp. on Rock Mechanics*, 1978, pp. 72–82.

[17] P. J. Closmann and W. B. Bradley, "The effect of temperature on tensile and compressive strengths and Young's Modulus of oil shale. SPE 6734," *Soc. Pet. Eng. J.*, vol. 267, pp. 301–312, 1979.

[18] J. W. Smith, "Theoretical relationship between density and oil yield for oil shales," US Dept. of the Interior, Bureau of Mines, Vol. 7248, 1969.

[19] K. Chong, K. Uenishi, A. C. Munari, and J. W. Smith, "Three dimensional characterization of the mechanical properties of oil shale," in *20th U.S. Symp. on Rock Mechanics*, 1979, pp. 369–380.

[20] B. Amadei, "Importance of anisotropy when estimating and measuring *in situ* stresses in rock," *Int. J. Rock Mech. Min. Sci. Geomech. Abstr.*, vol. 33, no. 3, pp. 293–325, Apr. 1996.

[21] J. W. Smith and K. P. Chong, "Introduction to mechanics of oil shale," in *Mechanics of Oil Shale*, 1st ed., K. P. Chong and J. W. Smith, Eds. New York: Elsevier Applied Science Publishers, 1984, pp. 1–42.

[22] P. R. Tisot, "Alterations in structure and physical properties of Green River oil shale by thermal treatment," *J. Chem. Eng. Data*, vol. 12, no. 3, pp. 405–411, 1967.

[23] K. Rajeshwar, R. Nottenburg, and J. Dubow, "Review thermophysical properties of oil shales," *J. Mater. Sci.*, vol. 14, pp. 2025–2052, 1979.

[24] F. E. W. Duvall, H. Y. Sohn, and C. H. Pitt, "Physical behaviour of oil shale at various temperatures and compressive loads," *Fuel*, vol. 64, no. 7, pp. 938–940, 1985.

[25] M. Chu and N. Chang, "Uniaxial creep of oil shale under elevated temperatures," in *ARMA*, 1980, no. 1966, pp. 207–216.

[26] T. Mraz, J. DuBow, and K. Rajeshwar, "Acoustic wave propagation in oil shale: 2.

Modelling," *Fuel*, vol. 62, no. 12, pp. 1462–1467, 1983.

[27] F. Tong, L. Jing, and R. W. Zimmerman, "A fully coupled thermo-hydro-mechanical model for simulating multiphase flow, deformation and heat transfer in buffer material and rock masses," *Int. J. Rock Mech. Min. Sci.*, vol. 47, no. 2, pp. 205–217, Feb. 2010.

[28] R. J. Miller, F.-D. Wang, T. Sladek, and C. Young, "The effects of *in situ* retorting on oil shale pillars," US Dept. of the Interior, Bureau of Mines, Golden, IR Contract H026203, 1979.

[29] J. L. Hillier and T. H. Fletcher, "Pyrolysis kinetics of a Green River oil shale using a pressurized TGA," *Energy & Fuels*, vol. 25, no. 1, pp. 232–239, Jan. 2011.

[30] P. Tiwari and M. Deo, "Compositional and kinetic analysis of oil shale pyrolysis using TGA–MS," *Fuel*, vol. 94, pp. 333–341, Apr. 2012.

[31] S. Li and C. Yue, "Study of different kinetic models for oil shale pyrolysis," *Fuel Process. Technol.*, vol. 85, no. 1, pp. 51–61, Jan. 2004.

[32] R. L. Braun and A. K. Burnham, "PMOD : a flexible model of oil and gas generation, cracking, and expulsion," *Org. Geochem.*, vol. 19, no. 1–3, pp. 161–172, 1992.

[33] J. H. Bauman, C. Huang, M. R. Gani, and M. D. Deo, "Modeling of the in-situ production of oil from oil shale," in *Oil Shale: A Solution to the Liquid Fuel Dilemma*, A. M. Harstein and O. Ogunsola, Eds. Washington, D.C.: Amer. Chem. Soc., 2010, pp. 137–140.

[34] D. W. Camp, "Oil shale heat-capacity relations and heats of pyrolysis and dehydration," in *Oil Shale Symp.*, 1987.

[35] R. L. Braun and A. K. Burnham, "Chemical reaction model for oil and gas generation from Type I and Type II kerogen," Lawrence Livermore Nat. Lab., Livermore, CA, UCRL-ID-114143, 1993.

[36] M. S. K. Youtsos, R. S. Cant, and E. Mastorakos, "Simulations of thermal upgrading methods for oil shale reservoirs, SPE 163338," in *SPE Kuwait Int. Pet. Conf. and Exhib.*, 2012.

[37] H. Yang and H. Sohn, "Mathematical analysis of the effect of retorting pressure on oil yield and rate of oil generation from oil shale," *Ind. Eng. Chem. Process*, no. 24, pp. 274–280, 1985.

[38] G. W. Thomas, "Some effects of overburden pressure on oil shale during underground retorting, SPE 1272," *Soc. Pet. Eng. J.*, pp. 1–8, 1966.

[39] M. Vanden Berg, "Core Center News: Skyline 16 Green River formation core –

world class lacustrine teaching tool," *Utah Geo. Survey*, 2015. [Online]. Available: http://geology.utah.gov/map-pub/survey-notes/core-center-news/lacustrine-teaching-tool/.

[40] M. B. Standing, *Volumetric and Phase Behavior of Oil Field Hydrocarbon Systems*. Dallas: Soc. of Pet. Eng. of AIME, 1977.

[41] J. McCain, W.D., J. B. Rollins, and A. J. Villena, "The coefficient of isothermal compressibility of black oils at pressures below the bubble point," *SPE Form. Eval.*, vol. 3, no. 3, pp. 659–662, 1988.

[42] R. W. Zimmerman, "Compressiblities and effective stress coefficients for linear elastic porous solids: lower bounds and results for the case of randomly distributed spheroidal pores," in *Issues in Rock Mechanics*, 1986, pp. 712–719.

[43] Cameron Engineers Inc., "US oil shale," in *U.S. Oil Shale, U.S. Coal, Oil Sands: Synthetic Fuels Data Handbook*, 2nd ed., G. L. Baughman, Ed. Denver, Colorado, USA: Cameron Engineers, Inc., 1978.

[44] D. Trimmer and H. C. Heard, "Compaction and permeability of oil-shale aggregates at high temperatures," *Soc. Pet. Eng. J.*, vol. 20, no. 2, pp. 95–104, 1980.

[45] P. R. Tisot and H. W. Sohns, "Structural response of rich Green River oil shales to heat and stress and its relationship to induced permeability," *J. Chem. Eng. Data*, vol. 15, no. 3, pp. 425–434, 1970.

[46] R. Hill, "The elastic behaviour of a crystalline aggregate," *Proc. Phys. Soc. Sect. A*, vol. 65, no. 5-A, pp. 349–354, 1952.

[47] P. Morgan and B. Scott, "Bottom-hole temperature data from the Piceance Basin, Colorado : indications for prospective sedimentary basin EGS resources," *GRC Trans.*, vol. 35, pp. 477–486, 2011.

[48] J. W. Nicholson, "A problem in the theory of heat conduction," in *Proc. of the Royal Soc. of London. Series A, Containing Papers of a Math. and Phys. Character*, 1921, vol. 100, no. 704, pp. 226–240.

[49] H. S. Carslaw and J. C. Jaeger, "The Laplace transformation," in *Conduction of Heat in Solids*, 2nd ed., New York, NY, USA, Clarendon Press, 1986, pp. 335–338.

[50] J. Bauman and M. Deo, "Simulation of a conceptualized combined pyrolysis, *in situ* combustion, and CO2 storage strategy for fuel production from Green River oil shale," *Energy & Fuels*, vol. 26, pp. 1731–1739, 2012.

[51] P. A. Sewell, N.-Y. Chang, and H.-Y. Ko, "Radial permeabilities of oil shale and coal," in *20th U.S. Symp. on Rock Mech.*, 1979, pp. 565–572.

[52] E. Detournay and A. H.-D. Cheng, “Fundamentals of poroelasticity,” in *Comp. Rock Eng.: Principles, Practice and Projects, v. 2*, 1st ed., J. A. Hudsen, E. T. Brown, C. Fairhurst, and E. Hoek, Eds. Tarrytown, New York, USA: Pergamon Press Ltd, 1993, pp. 113–171.

[53] A. L. Lee, M. H. Gonzalez, and B. E. Eakin, “The viscosity of natural gases,” *J. Pet. Technol.*, vol. 18, no. 08, pp. 997–1000, Apr. 2013.

[54] J. T. H. Ng and E. O. Egboga, “An improved temperature-viscosity correlation for crude oil systems, PN 83-34-32,” in *34th Annu. Tech. Meeting of the Pet. Soc. of CIM*, 1983.

[55] W. H. Seitzer and P. F. Lovell, “Flow properties of Utah shale oils,” *Soc. Pet. Eng. J.*, vol. 21, no. 6, pp. 679–686, 1981.

[56] R. B. Bird, W. E. Stewart, and E. N. Lightfood, “Viscosity and the mechanisms of momentum transport,” in *Transport Phenomena*, Rev. 2nd ed., Danvers, MA, USA, John Wiley and Sons, Inc., 2007, pp. 30–31.

[57] W. D. McCain, *The Properties of Petroleum Fluids*, 2nd ed., Tulsa, OK, USA, PennWell Corp.,1990.